The Development of an Inertia Estimation Method to Support Handling Quality Assessment

Tilbe Mutluay

Delft University of Technology

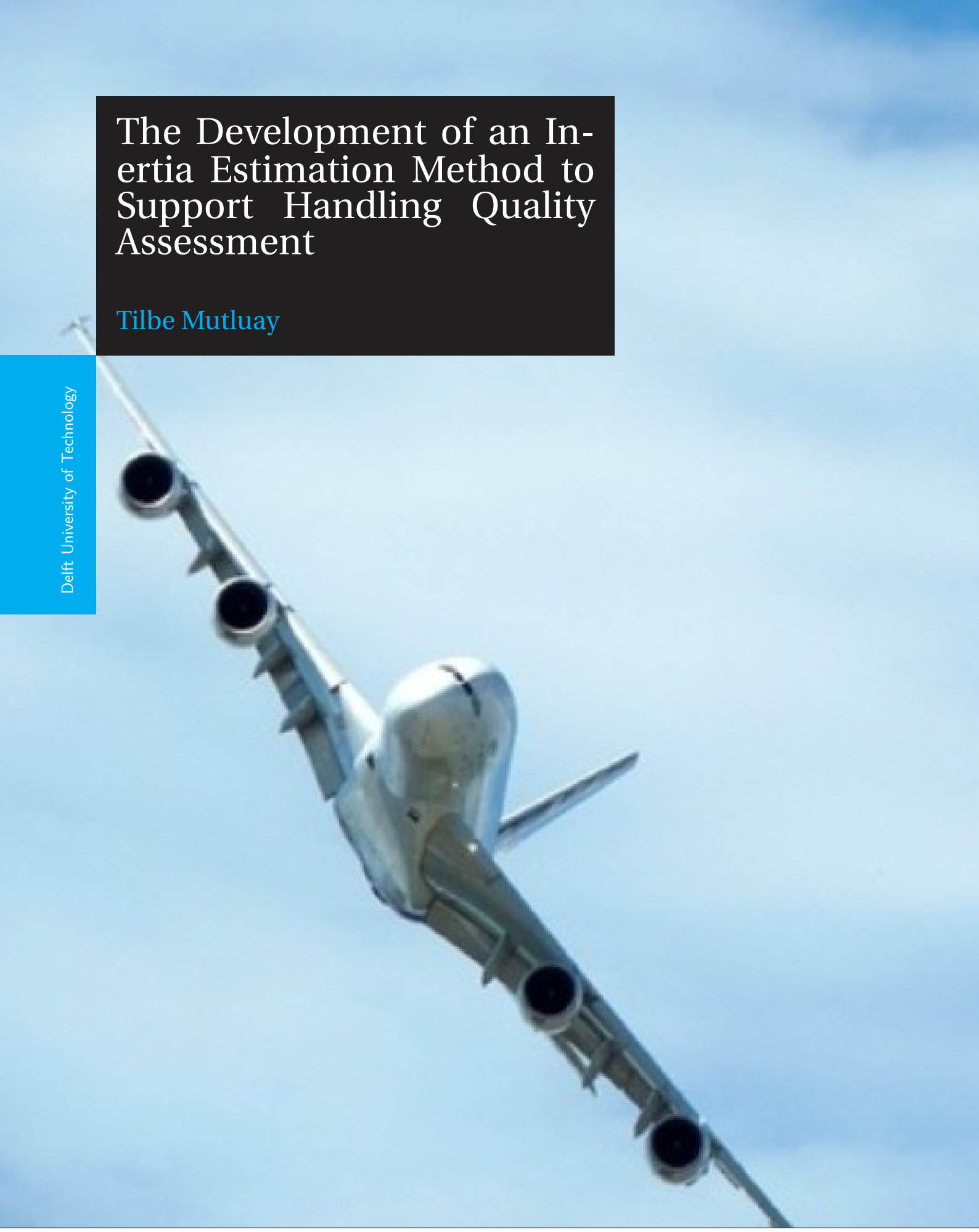

TU Delft Delft University of Technology

Challenge the future

THE DEVELOPMENT OF AN INERTIA ESTIMATION METHOD TO SUPPORT HANDLING QUALITY ASSESSMENT

by

Tilbe Mutluay

in partial fulfillment of the requirements for the degree of

Master of Science
in Aerospace Engineering

at the Delft University of Technology,
to be defended publicly on Tuesday September 29, 2015.

Student number:	4250397
Thesis registration number:	042#15#MT#FPP
Supervisor:	Dr. ir. R. Vos
Thesis committee:	Prof. dr. ir. L. Veldhuis
	Dr. ir. M. Voskuijl
	Dr. S. Hartjes

TU Delft Delft University of Technology

CONTENTS

ABSTRACT

Mass of an aircraft as well as distribution of it along the body are important concerns during the design process due to their significant influence on performance and inertia. Inertia of an aircraft has to be known in order to examine the handling qualities, which have a large effect on aircraft's design. However, due to the smeared properties of the structure and many of the system architectures, the calculation of inertia is non-trivial. Moreover, non-traditional aircraft designs might not be able to rely on existing empirical calculations. Hence, the main objective of this project is developing a rapid geometry based inertia estimation applicable for any aircraft configuration. In order to have a design sensitive method, the aircraft is divided into three categories namely bodies of revolution, lifting surfaces and point masses where components are grouped according to their shapes. Fuselage and nacelle components are categorized as bodies of revolution and their inertias are estimated in a similar fashion. Lifting surfaces include main wing, horizontal and vertical stabilizers. The rest of the aircraft components are assumed to be point masses. The implemented method is used in conventional, canard and three surface configurations. In order to examine their handling qualities, control and stability derivatives are also needed which is why a calculation method is implemented. Calculated inertia and derivatives of each configuration are used as input in a flight mechanics toolbox. Hence, the influence of configuration on aircraft's inertia and consequently on aircraft behavior has been able to examined in a rapid process.

ACKNOWLEDGEMENTS

This thesis is the last part of the invaluable time I had in master program at Aerospace Engineering at the Delft University of Technology. I would like to thank people who has given their full support during this time.

First of all, I would like to thank my supervisor Roelof Vos who guided me through the whole project with his new ideas and feedbacks. I would also like to thank Mark Voskuijl and Maurice Hoogreef for their support.

I would also like to thank my friends who have been there for me through the whole master program and the most difficult times during the thesis. I would like to thank my friends whom I studied bachelor with in Middle East Technical University for their full support from the application process till the end of the master. I would especially like to thank Sena Yazirli and Ilgaz Doga Okcu from Middle East Technical University who have supported me with new ideas even from far away. A special thanks to my friends from Delft University of Technology, Mustafa Can Karadayi, Javier Vargas Jimenez, Sercan Ertem and especially to Arda Caliskan, who made this project possible with exquisite discussions and his full support.

Finally, a very special thanks to my parents who have supported me in everything, have always believed in me and have made my dream come true.

NOMENCLATURE

γ	Dihedral angle
Λ	Sweep angle
λ	Taper ratio
Λ_{LE}	Leading edge sweep angle
A_{fus_i}	Cross-sectional area of fuselage at ith station
b	Span
c_r	Root chord
C_{D_α}	drag-due-to-angle-of-attack derivative
$C_{D_{\delta_c}}$	drag-due-to-canardcontrol derivative
$C_{D_{\delta_e}}$	drag-due-to-elevator derivative
C_{D_q}	drag-due-to-pitch-rate derivative
C_{L_α}	lift-due-to-angle-of-attack derivative
C_{l_β}	rolling-moment-due-to-sideslip derivative
$C_{l_{\delta_a}}$	rolling-moment-due-to-aileron derivative
$C_{L_{\delta_c}}$	lift-due-to-canardcontrol derivative
$C_{L_{\delta_e}}$	lift-due-to-elevator derivative
$C_{l_{\delta_r}}$	rolling-moment-due-to-rudder derivative
C_{l_p}	rolling-moment-due-to-roll-rate derivative
C_{L_q}	lift-due-to-pitch-rate derivative
C_{l_r}	rolling-moment-due-to-yaw-rate derivative
C_{m_α}	moment-due-to-angle-of-attack derivative
$C_{m_{\delta_c}}$	moment-due-to-canardcontrol derivative
$C_{m_{\delta_e}}$	moment-due-to-elevator derivative
C_{m_q}	moment-due-to-pitch-rate derivative
C_{n_β}	yawing-moment-due-to-sideslip derivative
$C_{n_{\delta_a}}$	yawing-moment-due-to-aileron derivative
$C_{n_{\delta_r}}$	yawing-moment-due-to-rudder derivative
C_{n_p}	yawing-moment-due-to-roll-rate derivative
C_{n_r}	yawing-moment-due-to-yaw-rate derivative
C_{y_β}	sideforce-due-to-sideslip derivative

$C_{y_{\delta a}}$	sideforce-due-to-aileron derivative
$C_{y_{\delta r}}$	sideforce-due-to-rudder derivative
C_{y_p}	sideforce-due-to-roll-rate derivative
C_{y_r}	sideforce-due-to-yaw-rate derivative
I_o	Centroidal inertia
I_{xx}	Rolling moment of inertia
I_{xy}	xy product of inertia
I_{xz}	xz product of inertia
I_{yy}	Pitching moment of inertia
I_{yz}	yz product of inertia
I_{zz}	Yawing moment of inertia
m	Mass
N_{st}	Number of station
pm	Point mass
s	Arc length between each fuselage lumped mass
t/c	Thickness-to-chord ratio
t_{r_w}	Airfoil thickness at wing root
t_{t_w}	Airfoil thickness at wing tip
W_f	Fuselage weight
W_i	Weight at ith station
X_{cg}	Aircraft center of gravity in x axis
x_{fs}	Front spar location in x direction
x_{ms}	Medium spar location in x direction
x_{rs}	Rear spar location in x direction
Y_{cg}	Aircraft center of gravity in y axis
y_{fus_1}	Fuselage outer point in y axis
y_{fus_2}	Fuselage center point in y axis
Z_{cg}	Aircraft center of gravity in z axis
z_{fus_1}	Fuselage top point in z axis
z_{fus_2}	Fuselage center point in z axis
z_{fus_3}	Fuselage bottom point in z axis

I

THESIS

1

INTRODUCTION

Performance analysis of an aircraft is mainly based on its mass, which is why it is the main concern during the design phase [1]. The distribution of the mass along the body is of importance as well since it determines the moment of inertia which consequently affects the dynamics of the body. Having the moment of inertia and stability and control derivatives, the handling characteristics of an aircraft can be examined.

Handling characteristics or handling qualities are defined in Ref. [2], as “those qualities or characteristics of an aircraft that govern the ease and precision with which a pilot is able to perform the tasks required in support of an aircraft role." In [3] the fundamental handling characteristics inside the operational flight envelope are summarized to be such that the airplane

- has sufficient control power to maintain steady state straight flight and maneuvering
- must be maneuverable between different flight conditions
- must have sufficient control power to accomplish transition from ground operations to airborne operations and vice versa

In other words, they express the airplane’s response and ability to achieve the required mission, either in a straight flight or a maneuver, with respect to the pilot control input. They should be examined during the conceptual design phase in order to have an adequate control surface sizing or to determine the complexity of the required flight control system [4].

Having said that inertia has to be known in order to examine the handling characteristics, it should be noted that due to the smeared properties of the structure and many of the system architectures, the calculation of inertia is non-trivial. Moreover despite the fact that majority of the commercial airplanes have a conventional configuration there is a trend towards non-traditional aircraft designs in the search for high efficiency. Hence, several methods that are proposed in the literature, which mostly rely on empirical calculations, may not be applicable on for every design especially for non-conventionals.

1.1. RESEARCH QUESTION AND THESIS GOAL

Considering the inadequacy of providing reliable estimation for unconventional designs, the method that is to be developed should be highly based on physics. It should take the geometry changes into account instead of relying on empirical methods. This leads to following goal of the project:

Develop a rapid geometry-based inertia estimation method applicable for different aircraft configurations which would accelerate the estimation of handling qualities in a conceptual design environment

In order to reach the project goal, following research question is to be solved:

How to estimate the inertial properties of conventional and unconventional configurations, as well as control and stability derivatives, to assess handling qualities during the conceptual design phase?

The sub-questions that will be answered to both help answering the main research question and subsequently help to achieve the goal of the thesis are:

- How accurate is the inertia estimation?
- How accurate is the control and stability derivatives estimation?
- How does the configuration affect the handling qualities?

1.2. REPORT STRUCTURE

The report consists of two parts which cover the main thesis and code documentation successively. The first part consists of 6 chapters. Chapter 2 gives a background information on aircraft dynamic behavior and its relation to inertia of the aircraft. Existing inertia estimation methods are briefly covered here. Furthermore, a brief explanation about handling quality assessment is given. In addition, a brief description of the design tool Initiator and the flight mechanics tool FMT are provided. In Chapter 3, the inertia estimation method, which is the main context of the thesis, is described. Besides that, implemented method of stability and control derivatives calculation and their use in calculation of aerodynamic forces and moments are briefly explained. Chapter 4 includes the validation of the work performed. Chapter 5 presents the results of the work on different aircraft configurations and highlight the arising differences in dynamic behavior due to change in the design. The thesis is concluded in Chapter 6. Recommendations for the further studies on the subject are presented in Chapter 7. The implementation of the work is explained in Part II. The overview of work flows in Initiator and in FMT are elaborated in Chapter 8 and Chapter 9 successively. The activity diagrams of calculations can be found here.

2

BACKGROUND

Background information on existing inertia, on handling qualities and on tools that are to be used for the purpose of the thesis are presented in this chapter.

2.1. EXISTING INERTIA ESTIMATION METHODS

Moment of inertia is defined as the measure of resistance of a body to angular acceleration about an axis of rotation. The mathematical expression of moment of inertia of a body is expressed as follows.

$$I = mr^2 + I_o \tag{2.1}$$

The first term in the equation represents the resistance of the body to rotation about the remote axis, while the latter represents the resistance to rotation of each component about its own axes. From this simple equation, it can be stated that inertia depends on the body shape, amount, and distribution of mass.

To begin with, the moment of inertia of an airplane is determined about its longitudinal, lateral and vertical axes which gives roll, pitch and yaw. The inertia matrix of the airplane with six independent moments of inertia can be written as

$$\begin{bmatrix} I_{xx} & I_{xy} & I_{xz} \\ I_{yx} & I_{yy} & I_{yz} \\ I_{zx} & I_{zy} & I_{zz} \end{bmatrix}$$

where the symmetric terms are equal. Moreover, in most aircraft configurations the airplane is symmetric about the XZ plane, which leads to the assumption of I_{xy} and I_{yz} are zero. However, care should be taken in the layout of the system and control elements as well as non-traditional designs such as skewed wings in which this assumption would be inaccurate.

Existing inertia estimation methods are often based on empirical data. [4] and [5] methods propose simple and feasible approaches for calculation of inertia where statistical data is used for correlation. It should be noted that since they are structured according to traditional aircraft configuration, geometrical approximations may fit to conventional configurations while they may introduce errors in unconventional ones. They cannot be reliable in every case as they do not take the geometry changes into account and rely on empirical methods.

A method which takes the geometry into account, is proposed in [6] in which the inertia is estimated by modeling the components as a series of lumped masses. The method includes two types of structure which are bodies of revolution and lifting surfaces. Former represents the fuselages, nacelles, etc. while the latter refers to wings, canards, etc. Modeling of the bodies of revolution is based on a series of cross sections, where the weight is distributed linearly between those cross sections along the body axis. Modeling of lifting surfaces is based on a series of planar lumped masses, where a linear weight distribution, with the slope proportional to the taper ratio, is assumed along the span. Similar to bodies of revolution, the variation is integrated along

the span in order to calculate the weight at predetermined number of spanwise sections. Calculated weight is dispersed along the chord. Presented lumped masses method is advantageous in terms of accuracy and independence on a database of similar aircraft.

2.2. EXAMINING HANDLING QUALITIES

Airplanes are classified according to US military specifications MIL-F-8785C with respect to their applications in aviation. They are categorized in four classes as below. [3]

Class I Small, light airplanes such as light utility, primary trainer etc.
Class II Medium weight, low-to-medium maneuverability airplanes such as heavy utility, reconnaissance, heavy attack etc.
Class III Large, heavy, low-to-medium maneuverability airplanes such as heavy transport heavy cargo, heavy bomber etc.
Class IV High maneuverability airplanes such as fighter, attack, tactical reconnaissance etc.

In addition this classification, handling quality requirements are classified according to flight phases. There are three flight phases that are defined.

Flight Phase Category A Non-terminal flight phase that requires rapid maneuvering, precision tracking or precise flight path control
Flight Phase Category B Non-terminal flight phase that is accomplished using gradual maneuvers and without precision tracking
Flight Phase Category C Terminal flight phase that is accomplished using gradual maneuvers, usually requiring accurate flight path control

Having defined the categories of airplanes and flight phases, the handling quality levels are given as follows

Level 1 Flying qualities clearly adequate for the mission Flight Phase
Level 2 Flying qualities adequate to accomplish the mission Flight Phase, but some increase in pilot workload or degradation in mission effectiveness, or both, exists.
Level 3 Flying qualities such that the airplane can be controlled safely, but pilot workload is excessive or mission effectiveness is inadequate, or both. Category A Flight Phases can be terminated safely, and Category B and C Flight Phases can be completed.

Here, it should be noted that aircraft must be designed to meet the Level 1 handling quality requirements in their normal operating state.

Handling qualities are examined with respect to longitudinal and lateral/directional requirements. Longitudinal handling quality requirements consider two modes which are phugoid and short period. Lateral/Directional handling qualities cover dynamics due to two axes of rotation and its cross-coupling effects. Three modes are related to lateral/directional dynamics, namely Dutch roll, spiral and roll modes [7].

LONGITUDINAL HANDLING QUALITIES

Phugoid mode is an oscillatory mode which is lightly damped and has a low frequency. Even though the period is not an important factor due to its length in phugoid mode, the damping is important. The requirement for phugoid damping for Flight Phase Category B is shown in Table 2.1

Table 2.1: Phugoid damping requirements

Level	Minimum ζ_{ph}
Level 1	0.04
Level 2	0
	Minimum T_{2ph}(sec)
Level 3	55

Short period mode can be defined as one of the oscillatory natural response of an aircraft to longitudinal perturbations. As the name suggests, it has a relatively short period and is usually heavily damped. There are defined limits for short period undamped natural frequency $\omega_{n_{sp}}$ and short period damping ratio ζ_{sp}. The requirements for short period undamped natural frequency is shown in Figure 2.1.

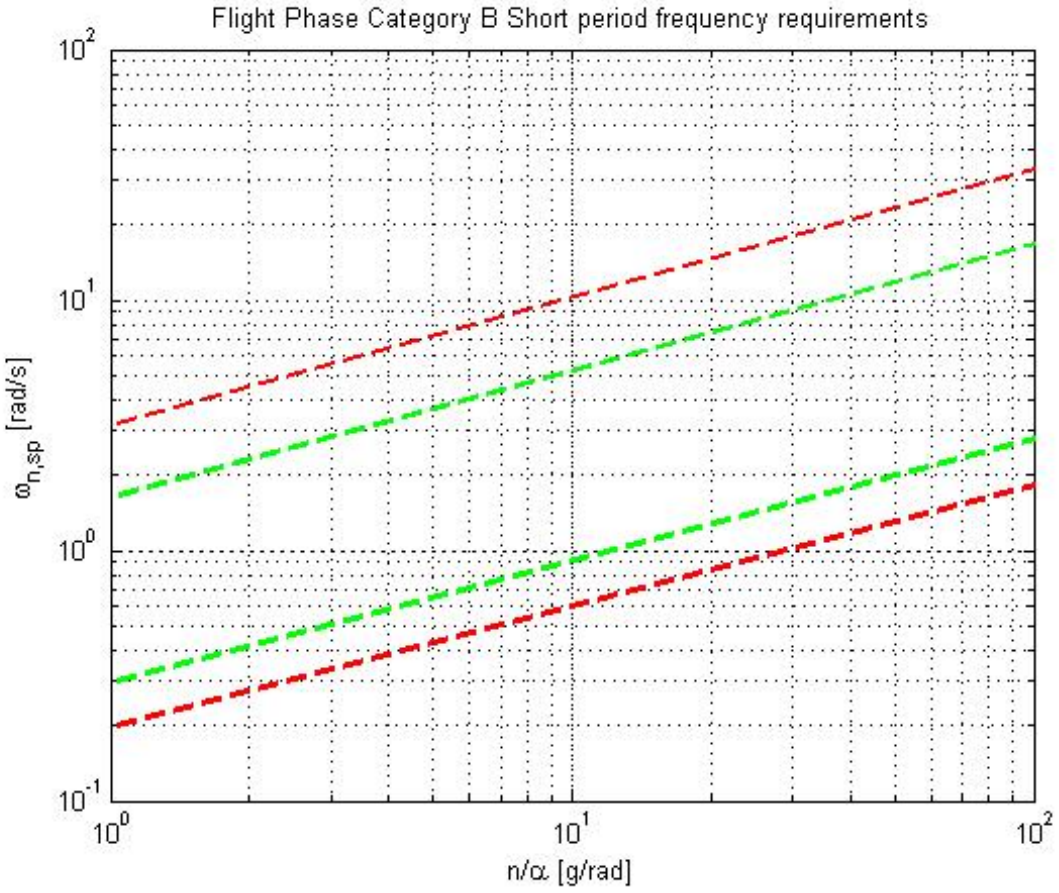

Figure 2.1: Short period undamped natural frequency requirement for Flight Phase Category B

The green and red borders in Figure 2.1, covers the Level 1 and Level 2 handling quality zones respectively. Outside the red borders the aircraft has Level 3 handling quality in terms of short period undamped natural frequency requirement.

The short period damping ratio limits for flight phase Category B are presented in Table 2.2.

Table 2.2: Short period damping ratio requirement for Flight Phase Category B

Level	Minimum ζ_{sp}	Maximum ζ_{sp}
Level 1	0.30	2.0
Level 2	0.20	2.0
Level 3	0.15	no max

Another parameter that is related to longitudinal handling qualities is the Control Anticipation Parameter (CAP). It is defined as the ratio of the instantaneous angular acceleration in pitch to acceleration sensitivity of the aircraft, where the acceleration sensitivity is the steady-state change in load factor. Mathematical derivation of CAP results in the ratio of undamped natural frequency square to load factor with respect to angle of attack [8]. It is indicated in the range of allowable values over the range of allowable short period damping ratios [3]. CAP is an important parameter giving a good indication on pilot's perception of the pitch and vertical accelerations. The requirements for CAP and short period damping ratio is shown in Figure 2.2. In the figure, the region surrounded by the green lines represents Level 1, while the area between that and blue lines represents Level 2. Level 3 is represented by the red lines.

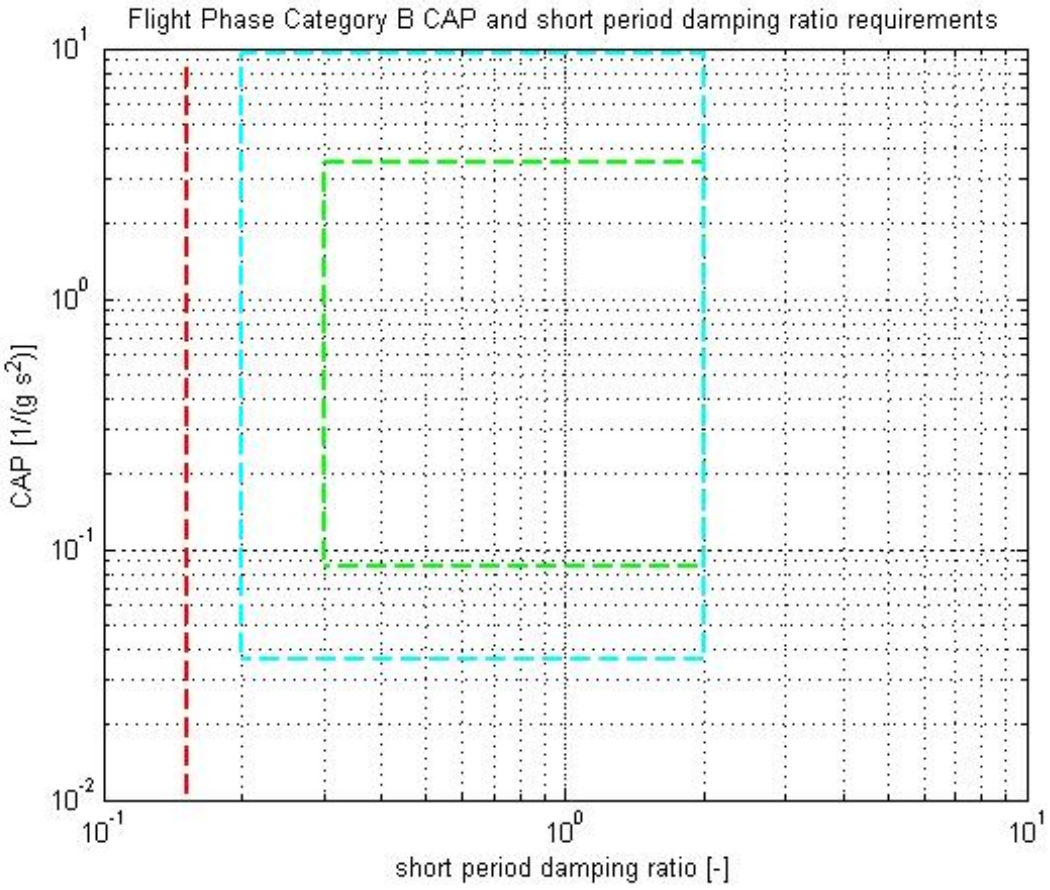

Figure 2.2: CAP and short period damping ratio requirements for Flight Phase Category B

LATERAL/DIRECTIONAL HANDLING QUALITIES

Dutch roll mode is one of the natural responses of the aircraft following lateral/directional perturbations. It is an oscillatory mode that is lightly damped and has a relatively short period.

Dutch roll frequency and damping ratio requirements for the category of case studies are shown in Table 2.3.

Table 2.3: Minimum Dutch roll undamped natural frequency and damping ratio requirements for Category B flight phase

Level	Min ζ_d	Min ω_{n_d}	Min $\zeta_d \omega_{n_d}$
Level 1	0.08	0.4	0.15
Level 2	0.02	0.4	0.05
Level 3	0	0.4	-

Spiral mode is one of the two exponential modes composing the natural response of the aircraft to lateral/directional perturbations. It can be either stable or unstable and even in unstable cases it does not introduce difficulty due to its long enough time constant [9].

The spiral mode handling quality is examined in terms of minimum time to double the amplitude. The requirements are shown in Table 2.4.

Table 2.4: Minimum time to double the amplitude in spiral mode

Level	Min T_{2s} (sec)
Level 1	20
Level 2	8
Level 3	4

Likewise the spiral mode, roll mode is an exponential mode of the natural response against lateral/directional perturbations, which mainly represents the rolling response.

Roll mode time constant T_r defines the roll response speed to a lateral control input. A small roll mode time constant indicates a rapid roll rate response while a large value signifies low reaction. The maximum allowable roll mode time constant is listed on Table 2.5.

Table 2.5: Maximum allowable roll mode time constant

Level	Maximum T_r (sec)
Level 1	1.4
Level 2	3.0
Level 3	10.0

2.3. TOOL DESCRIPTION

2.3.1. INITIATOR

Initiator is a Matlab based object-oriented program developed in TU Delft as a design optimization framework by Reno Elmendorp as his Master thesis [10]. The purpose of this framework is to find an optimum design for a number of aircraft configurations depending on the top-level requirements. Initiator consists of three main parts, namely controller object, geometry objects and modules, where all program flow is directed by the controller object. Aircraft object contains requirements for the specified mission(s), configuration and performance parameters and all parts which represent the aircraft geometry. Four module classes are available as Sizing, Analysis, Design, and Workflow. Preliminary sizing is performed with respect to top-level requirements and configuration settings. Resultant design can then be further used by analysis and design modules. The aircraft can be analyzed in terms of aerodynamics, weight etc. in the former module while a specific part of the aircraft such as the cabin or control surfaces can be designed in the latter module. Workflow modules assists the Initiator by means of implementing design workflows.

The design process in the Initiator begins with definition of top-level requirements related to the mission, range, passengers/cargo and airports. Moreover, configuration and performance parameters are set at the start. Considering the requirements a Class 1 weight estimation is performed, in which the wing loading and thrust-to-weight ratio are determined. This is followed by Class 2 weight estimation whose results are

aerodynamically analyzed by AVL VLM. Class 2.5 method is performed for the wing and fuselage weight. The resultant calculated weight is compared to the previous estimation and the process continues by feeding back the weight and performance data until the weight converges. Having the aircraft weight converged, the performance of the aircraft is estimated. When the calculated range among the performance parameters is converged to the required degree, the final optimum geometry is obtained. [10] [11]

2.3.2. FLIGHT MECHANICS TOOLBOX

Flight Mechanic Toolbox (FMT), is a Matlab/Simulink modeling environment that has been developed in TU Delft to be applied as a part of an in house design optimization framework. A single full non-linear aircraft model is generated in the toolbox by integrating the sub models of aerodynamics, structures, flight control and propulsion disciplines. The aircraft data required for the sub models as well as the model fidelity are supplied by the user as input. Using the model input an automatic model is constructed in Matlab which is followed by the aircraft model generation in Simulink.

The input required to analyze trimmed condition, time domain simulations and handling qualities are

- Aircraft mass and inertia matrix
- Forces and moments derivatives
- Control surface information and their delta values
- Reference values as length,area,etc. [12]

Outputs of the analysis of the created aircraft model include [13]

- Basic aircraft performance
- Handling qualities
- Aircraft response to atmospheric turbulence

.

3

METHODOLOGY

The method that is developed for inertia estimation is explained. Calculation of control and stability derivatives is briefly mentioned.

3.1. INERTIA ESTIMATION

The traditional way of weight breakdown of the aircraft into groups is followed in this method. As in proposed [14] and [15] the aircraft is divided into three main groups namely Airframe Structure, Propulsion and Equipment with each having several sub weight groups. Here, the airframe structure group is composed of load-carrying components of the aircraft, which are wing, fuselage, empennage, landing gear, and nacelle section. The propulsion group consists of the engine(s), items related to engine installation and fuel system. The latter group contains APU, flight controls, electrical systems, hydraulic, avionics, and other instruments. These subgroups are gathered in groups with respect to their shapes. As mentioned, the fuselage and nacelle are considered as bodies of revolution while wing, vertical stabilizer and horizontal stabilizer are gathered in a group considering them to be similar in the sense of surface shape. Remaining elements of the aircraft including the landing gear, propulsion group and equipments are considered to be point masses and their inertia is calculated according to that assumption. The coordinate axis is shown in Figure 3.1.

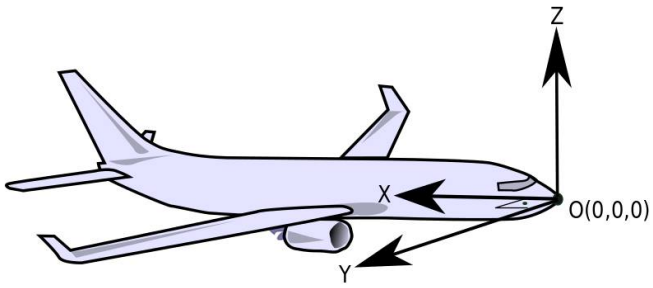

Figure 3.1: Coordinate axis

3.1.1. BODIES OF REVOLUTION

The inertia estimation model for bodies of revolution is based on the series of cross sections along the longitudinal body axis. The weight is distributed linearly into cross sections based on their areas which is calculated as follows.

$$W_i = W_f \frac{A_{\text{fus}_i}}{\sum A_{\text{fus}_i}} \tag{3.1}$$

Having obtained the weight at each cross section, it is further divided into eight lumped masses around the perimeter of those sections. The angular and radial locations of each lumped mass can be seen in Figure 3.2.

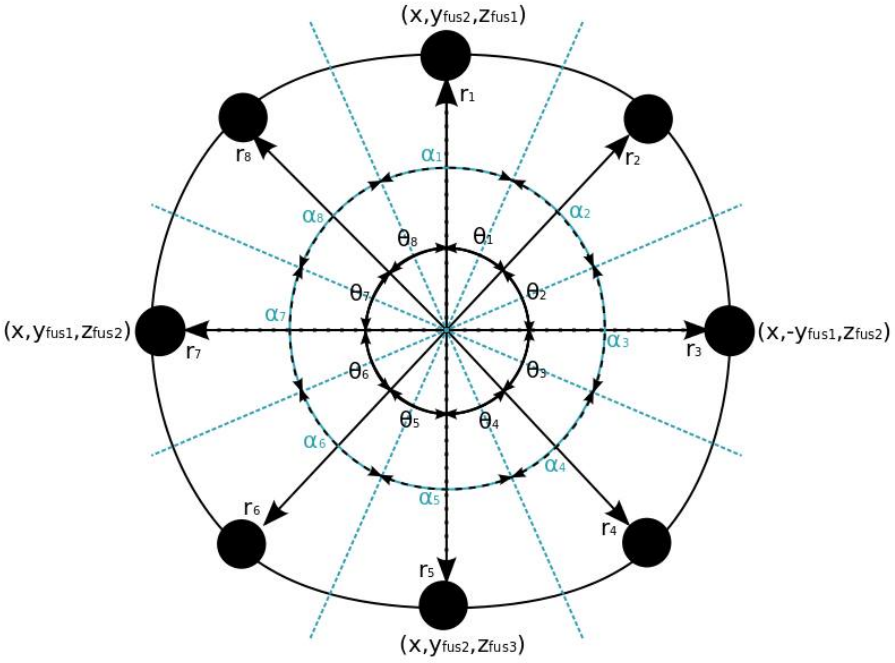

Figure 3.2: Angular and radial locations of lumped masses

The radial locations of the point masses which are shown in Figure 3.2 are calculated as follows.

$$r_1 = z_{\text{fus}_1} - z_{\text{fus}_2} \tag{3.2}$$

$$r_2 = \rho_{12}\sqrt{\left(z_{\text{fus}_1} - z_{\text{fus}_2}\right)^2 + \left(y_{\text{fus}_2} - y_{\text{fus}_1}\right)^2} \tag{3.3}$$

$$r_3 = y_{\text{fus}_2} - y_{\text{fus}_1} \tag{3.4}$$

$$r_4 = \rho_{23}\sqrt{\left(z_{\text{fus}_2} - z_{\text{fus}_3}\right)^2 + \left(y_{\text{fus}_2} - y_{\text{fus}_1}\right)^2} \tag{3.5}$$

$$r_5 = z_{\text{fus}_2} - z_{\text{fus}_3} \tag{3.6}$$

$$r_6 = r_4 \tag{3.7}$$

$$r_7 = r_3 \tag{3.8}$$

$$r_8 = r_2 \tag{3.9}$$

The angular locations are calculated as follows.

$$
\begin{aligned}
\theta_1 &= \tan^{-1}\left(\frac{y_{\text{fus}_2}-y_{\text{fus}_1}}{z_{\text{fus}_1}-z_{\text{fus}_2}}\right) & \alpha_1 &= \theta_1 \\
\theta_2 &= 90^\circ - \theta_1 & \alpha_2 &= \frac{\theta_1+\theta_2}{2} \\
\theta_3 &= \tan^{-1}\left(\frac{z_{\text{fus}_2}-z_{\text{fus}_3}}{y_{\text{fus}_2}-y_{\text{fus}_1}}\right) & \alpha_3 &= \frac{\theta_1+\theta_2}{2} \\
\theta_4 &= 90^\circ - \theta_3 & \alpha_4 &= \frac{\theta_3+\theta_4}{2} \\
\theta_5 &= \theta_4 & \alpha_5 &= \theta_4 \\
\theta_6 &= \theta_3 & \alpha_6 &= \alpha_4 \\
\theta_7 &= \theta_2 & \alpha_7 &= \alpha_3 \\
\theta_8 &= \theta_1 & \alpha_8 &= \alpha_2
\end{aligned}
$$

Having defined the angular and radial locations of each mass point, the centers of gravity can be calculated for each of them. The c.g. of masses in x direction is taken as the value of x location of the cross section they are assigned to. Point locations in y and z direction are calculated as follows.

$$
\begin{aligned}
y_{\text{cg}_1} &= y_{\text{fus}_1} & z_{\text{cg}_1} &= z_{\text{fus}_1} \\
y_{\text{cg}_2} &= r_2\cos\theta_2 & z_{\text{cg}_2} &= z_{\text{fus}_2} + r_2\sin\theta_2 \\
y_{\text{cg}_3} &= y_{\text{fus}_2} - y_{\text{fus}_1} & z_{\text{cg}_3} &= z_{\text{fus}_2} \\
y_{\text{cg}_4} &= r_4\sin\theta_4 & z_{\text{cg}_4} &= z_{\text{fus}_2} - r_4\cos\theta_4 \\
y_{\text{cg}_5} &= y_{\text{cg}_1} & z_{\text{cg}_5} &= z_{\text{fus}_3} \\
y_{\text{cg}_6} &= -y_{\text{cg}_4} & z_{\text{cg}_6} &= z_{\text{cg}_4} \\
y_{\text{cg}_7} &= -y_{\text{cg}_3} & z_{\text{cg}_7} &= z_{\text{cg}_3} \\
y_{\text{cg}_8} &= -y_{\text{cg}_2} & z_{\text{cg}_8} &= z_{\text{cg}_2}
\end{aligned}
$$

Obtained lumped mass cg locations along the body is shown in Figure 3.3.

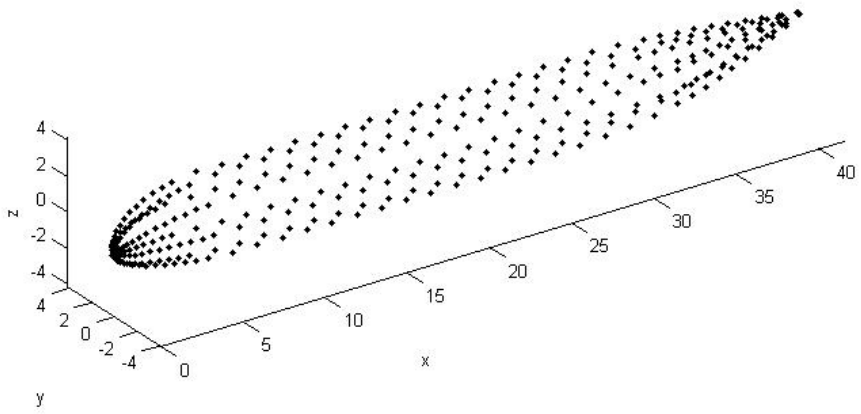

Figure 3.3: Lumped masses along the cross section of body

The arc length over each point mass along the cross section is calculated as follows

$$s_{\text{pm}} = r_{\text{pm}}\alpha_{\text{pm}} \tag{3.10}$$

where pm represents the lumped point mass number. In the calculation of fuselage inertia, for the mass point number 5, which represents the bottom point, the equation is multiplied with a factor, taking the floor into account. The factor is given as 1.0 for nose and tail sections while it is 2.0 for the center cross sections of the fuselage. Following this, the weight is distributed to each point mass based on the arc length as follows.

$$m_{\text{pm}} = m_i\frac{s_{\text{pm}}}{\sum s} \tag{3.11}$$

Having obtained the weight and c.g. of each point mass, the moment of inertia can be calculated as follows.

$$I_{xx_{\text{pm}}} = m_{\text{pm}}\left[\left(y_{\text{cg}_{\text{pm}}} - Y_{\text{cg}}\right)^2 + \left(z_{cg_{\text{pm}}} - Z_{\text{cg}}\right)^2\right] \tag{3.12}$$

$$I_{yy_{\text{pm}}} = m_{\text{pm}} \left[\left(z_{\text{cg}_{\text{pm}}} - Z_{\text{cg}} \right)^2 + \left(x_{\text{cg}_{\text{pm}}} - X_{\text{cg}} \right)^2 \right] \tag{3.13}$$

$$I_{zz_{\text{pm}}} = m_{\text{pm}} \left[\left(x_{\text{cg}_{\text{pm}}} - X_{\text{cg}} \right)^2 + \left(y_{\text{cg}_{\text{pm}}} - Y_{\text{cg}} \right)^2 \right] \tag{3.14}$$

$$I_{xz_{\text{pm}}} = m_{\text{pm}} \left[\left(x_{\text{cg}_{\text{pm}}} - X_{\text{cg}} \right) + \left(z_{\text{cg}_{\text{pm}}} - Z_{\text{cg}} \right) \right] \tag{3.15}$$

The moments of inertia for the eight points are summed at their cross sections. The total moment of inertia of the body of revolution is finally calculated by summing up each cross section inertia.

$$I_{xx} = \sum_{i=1}^{N_{\text{st}}} \sum_{pm=1}^{8} I_{xx_{\text{pm}}} \tag{3.16}$$

$$I_{yy} = \sum_{i=1}^{N_{\text{st}}} \sum_{pm=1}^{8} I_{yy_{\text{pm}}} \tag{3.17}$$

$$I_{zz} = \sum_{i=1}^{N_{\text{st}}} \sum_{pm=1}^{8} I_{zz_{\text{pm}}} \tag{3.18}$$

$$I_{xz} = \sum_{i=1}^{N_{\text{st}}} \sum_{pm=1}^{8} I_{xz_{\text{pm}}} \tag{3.19}$$

3.1.2. LIFTING SURFACES

The inertia estimation model for lifting surfaces, which would be applicable for wing, horizontal tail, vertical tail and canard surface, is based on the series of planar lumped masses in chord-wise direction. Assuming a linear weight variation along the span, the lifting surface is divided into a number of span-wise stations. Each station is then divided into cross sections in accordance with the spar positions. The required spar positions are obtained from Geometry module. The weight dispersion of a cross section, which is represented by five lumped masses, can be seen in Figure3.4.

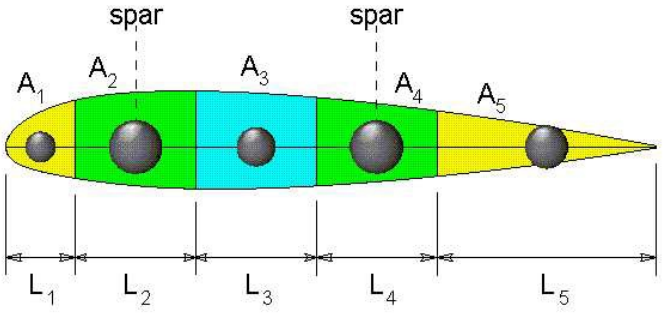

Figure 3.4: Lumped masses along the cross section of lifting surface, [6]

Each cross section is assumed to have skin and ribs weight based on their division lengths and division areas respectively. The weight of cross sections which include spar positions are contributed by spar weight as well.

The semi-thickness distribution of an airfoil shape is given as follows.

$$\pm y_t = \frac{(t/c)}{0.20} \left(0.29690\sqrt{x} - 0.12600x - 0.35160x^2 + 0.28430x^3 - 0.10150x^4 \right) \tag{3.20}$$

The area of the airfoil is then calculated by integrating the equation with respect to x direction and multiplying by 2 to take the area above and below the mean line into account.

$$A_{\text{airfoil}} = 10C_n^2\,(t/c)\left(0.197933x^{3/2} - 0.063x^2 - 0.1172x^3 + 0.071075x^4 - 0.0203x^5\right) \tag{3.21}$$

where $C_n = c_r\left[1-\eta_i(1-\lambda_i)\right]$
The start and end points of each airfoil segment cross section, which is shown in Figure 3.4, are defined for the integration in Table 3.1.

Table 3.1: Start and end points of airfoil segments

Airfoil Segment	Start Point	End Point
1	0	$0.5xfs$
2	$0.5x_{\text{fs}}$	$0.5(x_{\text{fs}} + x_{\text{ms}})$
3	$0.5(x_{\text{fs}} + x_{\text{ms}})$	$0.5(x_{\text{ms}} + x_{\text{rs}})$
4	$0.5(x_{\text{ms}} + x_{\text{rs}})$	$0.5(1 + x_{\text{rs}})$
5	$0.5(1 + x_{\text{rs}})$	1.0

Having defined the airfoil segments' start and end point as well as their areas, the c.g. of each segment can be calculated. The center of gravity on y axis on one station is taken as the value of the y location of that station as it does not vary chord-wise. It is defined as follows.

$$Y_{\text{cg}_i} = \frac{i}{N_{\text{st}}}\frac{b}{2} - \frac{1}{2}\frac{\frac{b}{2}}{N_{\text{st}}} \tag{3.22}$$

The center of gravity on z axis depends on the dihedral angle of the lifting surface and it is the same value for each segment on a station as dihedral angle does not vary chord-wise. It is defined as follows, where the dihedral angle is in radians.

$$Z_{\text{cg}_i} = Z_{\text{apex}} + Y_{\text{cg}_i}\tan\gamma \tag{3.23}$$

In order to determine the x location of c.g. of each segment, the local chord as well as the local apex point of the station are required. Local chord of the station is calculated as below.

$$c_i = c_r\left(1 - \frac{(i-0.5)(1-\lambda)}{N_{\text{st}}}\right) \tag{3.24}$$

Local apex point of each station is calculated as follows, where the leading edge sweep angle is in radians.

$$X_{\text{apex}_i} = X_{\text{apex}} + Y_{\text{cg}_i}\tan\Lambda_{\text{LE}} \tag{3.25}$$

After obtaining the required values, the c.g. in x location is calculated for each segment as follows.

$$X_{\text{cg}_{i,1}} = X_{\text{apex}_i} + \frac{L_1}{2}c_i \tag{3.26}$$

$$X_{\text{cg}_{i,2}} = X_{\text{apex}_i} + (x_{\text{fs}}/c)c_i \tag{3.27}$$

$$X_{\text{cg}_{i,3}} = X_{\text{apex}_i} + (x_{\text{ms}}/c)c_i \tag{3.28}$$

$$X_{\text{cg}_{i,4}} = X_{\text{apex}_i} + (x_{\text{rs}}/c)c_i \tag{3.29}$$

$$X_{\text{cg}_{i,5}} = X_{\text{apex}_i} + \frac{L_4+1}{2}c_i \tag{3.30}$$

The lifting surface is finally represented by lumped masses distributed along both the chord and span that can be seen in Figure 3.5.

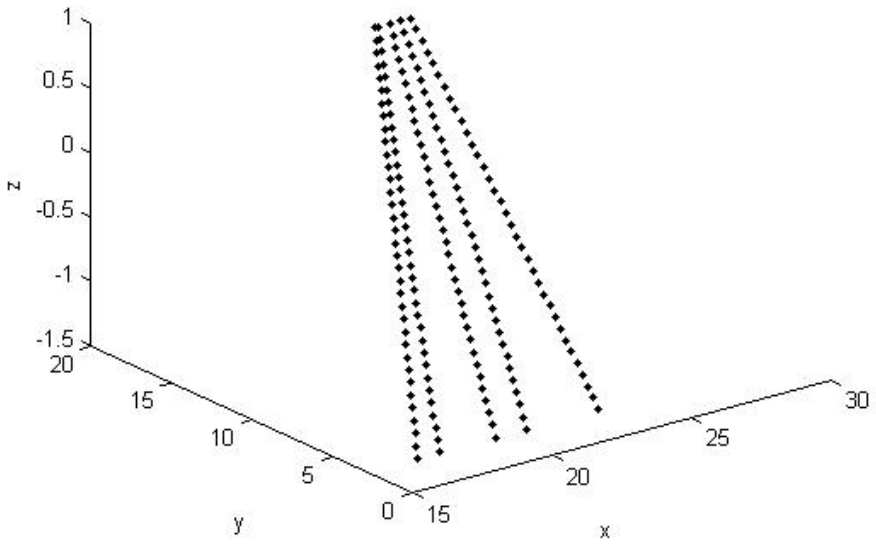

Figure 3.5: Representation of the lifting surface with lumped masses, positioned wrt fuselage nose

In order to find a trade in weight distribution along stations, an intermediate calculation parameters is introduced as

$$\text{par} = B_1 - A_1 \tag{3.31}$$

where A_1 and B_1 represents masses of first and second station respectively. They are found by the use of derivative of the linearly varied mass along the span which is defined as

$$a = -m\left(\frac{\frac{c_r(1-\lambda)}{\sum c_i}}{N_{\text{st}}}\right)^2 \tag{3.32}$$

Using this parameter A_1 and B_1 are calculated as follows.

$$A_1 = \frac{b^2}{4N_{\text{st}}^2}\frac{a}{2} + \frac{b}{2N_{\text{st}}}C_1 \tag{3.33}$$

$$B_1 = \frac{3b^2}{2N_{\text{st}}^2}\frac{a}{4} + \frac{b}{2N_{\text{st}}}C_1 \tag{3.34}$$

where the constant C_1 is

$$C_1 = \frac{2}{b}\left(\frac{m}{2} - \frac{b^2}{8}a\right) \tag{3.35}$$

Hence, the intermediate calculation parameter is found by the difference of A_1 and B_1. Having calculated those parameters the chord-wise weight distribution along one station can be calculated. As mentioned, the chord-wise weight distribution is dependent on the area and length of each segment which are already calculated. Besides those geometrical parameters, the fraction of skin, ribs and spar weights to the whole wing weight are required. However, the EMWET module in Initiator does not provide those required weight

components separately. Because of this lack, the skin and spar weight contributions are calculated by the use of thickness outputs of EMWET as well as already known wing geometry parameters such as chord and span lengths. Both skin and spar geometries are assumed to be rectangular frustum which can be seen in Figure3.6.

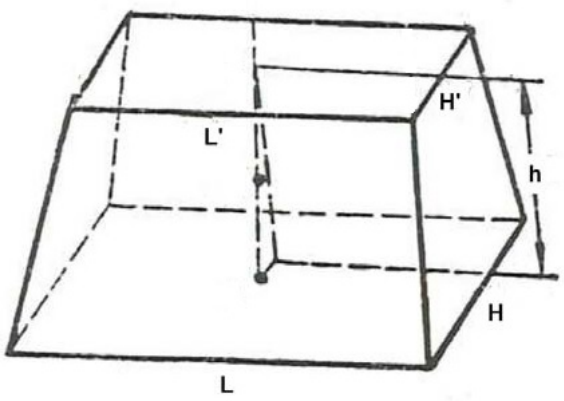

Figure 3.6: Rectangular frustum

The volume of a truncated rectangular frustum is given as

$$V = \frac{h}{6}\left[LH + (L+L')(H+H') + L'H'\right] \tag{3.36}$$

where h, L, and H represent height, length and height respectively and all of which are shown in the Figure 3.6. In the equation, the characters with prime represent the same but for the ending surface of the geometry. In other words, for a wing while L and H represent the length height of the root surface, L' and H' represent the length and height of the tip surface. In the presence of a kink on the wing, the volume has to be calculated from root to kink and kink to tip and summed up.

Airfoil non-dimensional coordinates (U,V) from trailing edge to leading edge and from there to trailing edge are imported from $Airfoil$ object in Initiator for each section (root,kink,tip). Upper and lower V points are obtained for each U point, whose example can be seen in Figure 3.7. Obtained coordinates are scaled to the local chord length in order to get the real airfoil thickness at that section. This airfoil data is used in further calculations of weight contributions.

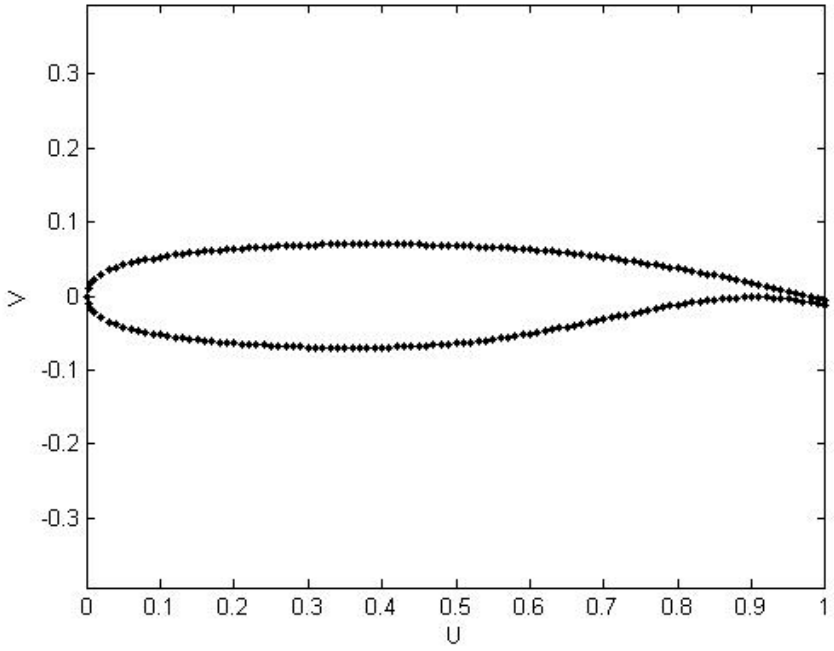

Figure 3.7: Example of an airfoil coordinates

The calculation of spar weight fraction starts by defining parameters. The thickness of the spar at one section is defined as H in Figure 3.6 and the thickness of the spar at the next section as H'. The height of the spar is represented by the L in Figure 3.6 while L' represents the height at the following section. The distance between two sections is defined by h.

To begin with, the U point on the chord which represents the spar position is found which is followed by obtaining the corresponding upper and lower V data. The length of the spar in z direction is calculated by the distance between gathered V data. The procedure is followed for each spar at each section which results in the required L and L' values for all. The thickness of the spars at each section is gathered as an output from EMWET module. Hence, H and H' values are found as well. The remaining required value, h is calculated for each segment, i.e from root to kink and from kink to tip, by multiplying the span length with span-wise section position differences. After obtaining the geometrical parameters, the volume of the spar is calculated and multiplied by the density of the spar material.

The calculation of the skin weight fraction starts assuming the skin consists of panels in order to find the arc length in an easier approach. On the contrary to geometry definitions of spar calculations, L in Figure 3.6 is taken as the thickness and H as the skin length. The assumed panel lengths are calculated by the use of airfoil points U and V. Hence, the H and H' values of the upper and lower skin are found by the total panel length. L and L' values, which represent the thicknesses at successive sections, are obtained from EMWET. The distance from one section to the other, which is represented by h in the Figure 3.6, is calculated by the use of same logic that is used for the h in spar calculations. Hence, tThe volume of the upper and lower skin are calculated by the use of calculated geometrical parameters. The result is multiplied with the density of the skin material so that the weight contribution of the skin is achieved.

Ribs weight contribution to the wing is calculated by [16] as follows.

$$m_{\text{rib}} = k_r \rho_{\text{material}} S_w \left(t_{ref} + \frac{t_{r_w} + t_{t_w}}{2} \right) \tag{3.37}$$

where $k_r = 0.5 \times 10^{-3}$, $t_{\text{ref}} = 1.0m$, and t_{r_w} and t_{t_w} represents the thicknesses of rib at root and tip sections.

Having obtained all required parameters, chord-wise weight distribution is calculated as below.

$$W_{i,1} = \left[L_1 F_{\text{skin}} + \left(\frac{A_{\text{airfoilsegment1}_i}}{A_{\text{airfoil}_i}} \right) F_{\text{ribs}} \right] \left[A_1 + par(i-1) \right] \tag{3.38}$$

$$W_{i,2} = \left[(L_2 - L_1) F_{\text{skin}} + \left(\frac{A_{\text{airfoilsegment2}_i}}{A_{\text{airfoil}_i}} \right) F_{\text{ribs}} + F_{\text{fs}} \right] \left[A_1 + \text{par}(i-1) \right] \tag{3.39}$$

$$W_{i,3} = \left[(L_3 - L_2) F_{\text{skin}} + \left(\frac{A_{\text{airfoilsegment3}_i}}{A_{\text{airfoil}_i}} \right) F_{\text{ribs}} + F_{\text{ms}} \right] \left[A_1 + \text{par}(i-1) \right] \tag{3.40}$$

$$W_{i,4} = \left[(L_4 - L_3) F_{\text{skin}} + \left(\frac{A_{\text{airfoilsegment4}_i}}{A_{\text{airfoil}_i}} \right) F_{\text{ribs}} + F_{\text{rs}} \right] \left[A_1 + \text{par}(i-1) \right] \tag{3.41}$$

$$W_{i,5} = \left[(1 - L_4) F_{\text{skin}} + \left(\frac{A_{\text{airfoilsegment5}_i}}{A_{\text{airfoil}_i}} \right) F_{\text{ribs}} \right] \left[A_1 + \text{par}(i-1) \right] \tag{3.42}$$

After calculating weight and c.g. of each point mass, the moment of inertia at each station can be determined as follows.

$$I_{xx_{i,j}} = m_{i,j} \left[\left(y_{\text{cg}_i} - Y_{\text{cg}} \right)^2 + \left(z_{\text{cg}_i} - Z_{\text{cg}} \right)^2 \right] \tag{3.43}$$

$$I_{yy_{i,j}} = m_{i,j} \left[\left(z_{\text{cg}_i} - Z_{\text{cg}} \right)^2 + \left(x_{\text{cg}_{i,j}} - X_{\text{cg}} \right)^2 \right] \tag{3.44}$$

$$I_{zz_{i,j}} = m_{i,j} \left[\left(x_{\text{cg}_{i,j}} - X_{\text{cg}} \right)^2 + \left(y_{\text{cg}_i} - Y_{\text{cg}} \right)^2 \right] \tag{3.45}$$

$$I_{xz_{i,j}} = m_{i,j} \left[\left(x_{\text{cg}_{i,j}} - X_{\text{cg}} \right) + \left(z_{\text{cg}_i} - Z_{\text{cg}} \right) \right] \tag{3.46}$$

The moments of inertia of five point masses which represent five airfoil segments are summed at their station. The total moment of inertia of the lifting surface is finally calculated by summing up each station's inertia value and multiplying by 2.

$$I_{xx} = 2 \sum_{i=1}^{N_{\text{st}}} \sum_{j=1}^{5} I_{xx_{i,j}} \tag{3.47}$$

$$I_{yy} = 2 \sum_{i=1}^{N_{\text{st}}} \sum_{j=1}^{5} I_{yy_{i,j}} \tag{3.48}$$

$$I_{zz} = 2 \sum_{i=1}^{N_{\text{st}}} \sum_{j=1}^{5} I_{zz_{i,j}} \tag{3.49}$$

$$I_{xz} = 2 \sum_{i=1}^{N_{\text{st}}} \sum_{j=1}^{5} I_{xz_{i,j}} \tag{3.50}$$

HORIZONTAL AND VERTICAL STABILIZER

Initiator does not use EMWET for the weight calculations of horizontal and vertical stabilizers which is why the mentioned methodology of lifting surface inertia calculations cannot be used. The required separate skin, spar and ribs weights can not be calculated due to the lack of thicknesses of those components. Therefore, DATCOM [5] method is implemented in order to find the moment of inertia of lifting surfaces in the absence of EMWET results.

In order to calculate the pitching and yawing moment of inertia of the horizontal and vertical surfaces respectively, DATCOM represents the lifting surface and the mass distribution with respect to this surface shape in Figure 3.8

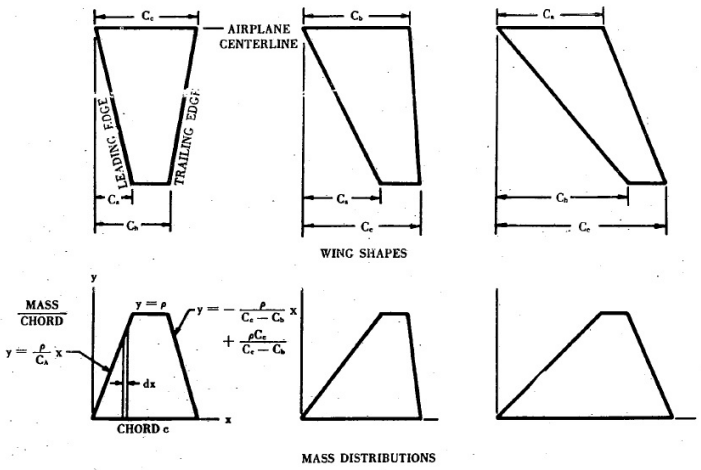

Figure 3.8: Surface shape and its corresponding mass distribution, [5]

Here, C_a, C_b, and C_c represent the smallest, intermediate and the largest value of the following parameters

c_r $\frac{btan\Lambda_{LE}}{2}$ $c_t + \frac{btan\Lambda_{LE}}{2}$

The slopes of mass distribution graph, y_1, y_2, and y_3 from 0 to C_a, C_a to C_b and C_b to C_c respectively, are defined as below.

$$y_1 = \frac{\rho}{C_a} x \tag{3.51}$$

$$y_2 = \rho \tag{3.52}$$

$$y_3 = -\frac{\rho}{C_c - C_b} x + \frac{\rho C_c}{C_c - C_b} \tag{3.53}$$

where ρ is the weight to chord ratio of the surface and is calculated as follows.

$$\rho = \frac{W}{0.5(-C_a + C_b + C_c)} \tag{3.54}$$

The inertia is derived by assumed mass distribution is written as follows.

$$I = \frac{\rho}{12}\left(-C_a^3 + C_b^3 + C_c^2 C_b + C_c C_b^2 + C_c^3\right) \tag{3.55}$$

Hence, moment of inertia on its own centroid is calculated as follows, where the o in subscripts represent the centroidal inertia.

$$I_o = K_o \left[I - \frac{(\sum mx)^2}{\sum m} \right] \tag{3.56}$$

where K_o is an empirical constant and is given as 0.771 for any horizontal and vertical stabilizer [5].

Horizontal Stabilizer Pitching

The centroidal pitching moment of inertia of the horizontal stabilizer is calculated by solving Equation 3.56 with substitution of horizontal stabilizer parameters.

Horizontal Stabilizer Rolling

The centroidal rolling moment of inertia is given by the following equation.

$$I_{o_x} = \frac{W b^2 K_4}{24}\left(\frac{c_{r_{ht}} + 3c_{t_{ht}}}{c_{r_{ht}} + c_{t_{ht}}}\right) \tag{3.57}$$

where the constant K_4 is obtained from the Figure B.1 given in Appendix B.

The centroidal yawing moment of inertia is given as

$$I_{o_z} = I_{o_y} + I_{o_x} \tag{3.58}$$

Vertical Stabilizer Rolling
The centrodial rolling moment of inertia for the vertical stabilizer is given as

$$I_{o_x} = \frac{W_v b_v^2 K_5}{18}\left(1 + \frac{2c_{r_v} c_{t_v}}{(c_{r_v} + c_{t_v})^2}\right) \tag{3.59}$$

where the constant K_5 is obtained from the Figure B.2 given in Appendix B.

Vertical Stabilizer Yawing
It is calculated by solving equation 3.56 with vertical stabilizer parameters.

Vertical Stabilizer Pitching
The centroidal pitching moment of inertia for the vertical stabilizer is the sum of rolling and yawing moments of inertia.

$$I_{o_y} = I_{o_x} + I_{o_z} \tag{3.60}$$

Having calculated the moment of inertia values about the centroidal axis of the bodies, the total moment of inertia can be calculated. Following equations are solved for both horizontal and vertical surfaces by substituting respective parameters.

$$I_{xx} = I_{o_x} + m_{\text{stab}}\left(\left(y_{\text{cg}_{\text{stab}}} - Y_{\text{cg}}\right)^2 + \left(z_{\text{cg}_{\text{stab}}} - Z_{\text{cg}}\right)^2\right) \tag{3.61}$$

$$I_{yy} = I_{o_y} + m_{\text{stab}}\left(\left(x_{\text{cg}_{\text{stab}}} - X_{\text{cg}}\right)^2 + \left(z_{\text{cg}_{\text{stab}}} - Z_{\text{cg}}\right)^2\right) \tag{3.62}$$

$$I_{zz} = I_{o_z} + m_{\text{stab}}\left(\left(x_{\text{cg}_{\text{stab}}} - X_{\text{cg}}\right)^2 + \left(y_{\text{cg}_{\text{stab}}} - Y_{\text{cg}}\right)^2\right) \tag{3.63}$$

$$I_{xz} = m_{\text{stab}}\left(x_{\text{cg}_{\text{stab}}} - X_{\text{cg}}\right)\left(z_{\text{cg}_{\text{stab}}} - Z_{\text{cg}}\right) \tag{3.64}$$

3.1.3. POINT MASSES

Remaining aircraft components are assumed to be point masses for simplicity. The inertia estimation of the point masses are calculated by following equations.

$$I_{xx} = m_{\text{comp}}\left(\left(y_{\text{cg}_{\text{comp}}} - Y_{\text{cg}}\right)^2 + \left(z_{\text{cg}_{\text{comp}}} - Z_{\text{cg}}\right)^2\right) \tag{3.65}$$

$$I_{yy} = m_{\text{comp}}\left(\left(x_{\text{cg}_{\text{comp}}} - X_{\text{cg}}\right)^2 + \left(z_{\text{cg}_{\text{comp}}} - Z_{\text{cg}}\right)^2\right) \tag{3.66}$$

$$I_{zz} = m_{\text{comp}}\left(\left(x_{\text{cg}_{\text{comp}}} - X_{\text{cg}}\right)^2 + \left(y_{\text{cg}_{\text{comp}}} - Y_{\text{cg}}\right)^2\right) \tag{3.67}$$

$$I_{xz} = m_{\text{comp}}\left(x_{\text{cg}_{\text{comp}}} - X_{\text{cg}}\right)\left(z_{\text{cg}_{\text{comp}}} - Z_{\text{cg}}\right) \tag{3.68}$$

3.2. CONTROL AND STABILITY DERIVATIVES ESTIMATION

Handling qualities are significantly dependent on the stability and control properties of the aircraft [17]. Those characteristics are essential to be determined to be able to analyze the aircraft dynamic behavior. Stability and control characteristics of the aircraft are fundamentally contributed by the aerodynamics of the aircraft and its controls. The calculation method is directly based on [15].

3.2.1. STABILITY DERIVATIVES

The fundamental stability derivatives that are calculated for the purpose of the project

- Angle-of-attack stability derivatives
  $C_{L_\alpha}, C_{D_\alpha}, C_{m_\alpha}$
- Angle-of-sideslip stability derivaties
  $C_{y_\beta}, C_{l_\beta}, C_{n_\beta}$
- Roll rate stability derivatives
  $C_{y_p}, C_{l_p}, C_{n_p}$
- Pitch rate stability derivatives
  $C_{L_q}, C_{D_q}, C_{m_q}$
- Yaw rate stability derivatives
  $C_{y_r}, C_{l_r}, C_{n_r}$

ANGLE-OF-ATTACK STABILITY DERIVATIVES

Lift-due-to-angle-of-attack derivative, C_{L_α}

Lift-due-to-angle-of-attack derivative is contributed by wing-fuselage and horizontal stabilizers. Wing-fuselage contribution, which is the wing-fuselage lift curve slope, is found by the multiplication of wing lift curve slope and wing-fuselage interference factor which is dependent on equivalent fuselage diameter and wing span. The contribution of a horizontal stabilizer is calculated by the use of its lift curve slope, dynamic pressure ratio to the one of the main wing, wetted area ratio, and downwash gradient or upwash gradient depending on if it is the horizontal tail or the canard respectively.

Drag-due-to-angle-of-attack derivative, C_{D_α}

Drag-due-to-angle-of-attack derivative calculation is dependent on the calculated lift-due-to-angle-of-attack derivative, the aspect ratio of the main wing, Oswald factor and the lift coefficient at steady state level flight.

Pitching moment-due-to-angle-of-attack derivative, C_{m_α}

Pitching moment-due-to-angle-of-attack derivative is calculated by lift-due-to-angle-of-attack derivative and airplane pitching moment variation with lift coefficient. The latter parameter is estimated by the difference between the location of the moment reference center, which is chosen to be the center of gravity of the main wing in this project, in fractions of m.g.c. and the location of the aircraft aerodynamic center in fractions of the m.g.c.. The location of the aircraft aerodynamic center in fractions of the m.g.c. is computed by the use of wing-fuselage, horizontal tail, and canard aerodynamic center locations.

ANGLE-OF-SIDESLIP STABILITY DERIVATIVES

Sideforce-due-to-sideslip derivative, C_{y_β}

The sideforce-due-to-sideslip derivative is composed of three contributors which are the main wing, fuselage and vertical tail. The wing contribution is related to the dihedral angle. The fuselage contribution is dependent on the wing-fuselage interference factor and fuselage cross section area at the point where the flow ceases to be potential. Those parameters are calculated with respect to wing positioning in z-axis and equivalent fuselage diameter. Vertical tail contribution is computed by using vertical tail lift curve slope, effective vertical tail and other vertical tail parameters such as the aspect ratio and sweep angle.

Rolling-moment-due-to-sideslip derivative, C_{l_β}

Rolling-moment-due-to-sideslip derivative is contributed by wing-fuselage combination, horizontal tail and vertical tail. Wing-fuselage contribution is a function of wing geometry parameters such as quarter-chord

sweep angle, semi-chord sweep angle, dihedral angle, and compressibility correction factors of those parameters. The horizontal tail contribution is computed from the horizontal tail dihedral effect, and the ratio of horizontal tail area and span to the ones of main wing. The vertical tail contribution is found by using the sideforce-due-to-sideslip, and location of vertical tail with respect to the aircraft c.g. in x and z directions.

Yawing-moment-due-to-sideslip derivative, C_{n_β}
Yawing-moment-due-to-sideslip derivative is contributed by the wing, fuselage and vertical tail. However, the wing contribution is important only at high angles of attack which is why it is neglected in this project. The fuselage contribution is dependent on the ratio of fuselage side area and its maximum width to the ones of the wing.The ratio is multiplied with two empirical factors which are related to Reynold's number and wing-fuselage interference separately. The vertical tail contribution is a function of the sideforce-due-to-sideslip derivative. Other required parameters in order to compute the contribution are related to the vertical tail positioning with respect to aircraft aerodynamic center and the main wing span.

ROLL RATE DERIVATIVES

Side-force-due-to-roll-rate derivative, C_{y_p}
The side-force-due-to-roll-rate derivative is primarily influenced by the vertical tail. It is the function of vertical tail contribution to sideforce-due-to-sideslip derivative, vertical tail positioning with respect to aircraft aerodynamic center, and main wing span.

Rolling-moment-due-to-roll-rate derivative, C_{l_p}
The rolling-moment-due-to-roll-rate derivative is contributed by the wing, horizontal tail and vertical tail. The horizontal tail contribution is computed by using the roll-damping derivative of the horizontal tail, and area and span ratios of the horizontal tail to the wing. The vertical tail contribution is a function of vertical contribution to side-force-due-to-sideslip, and the ratio of vertical tail position with respect to the aircraft aerodynamic center divided by the main wing span.

Yawing-moment-due-to-roll-rate derivative, C_{n_p}
The yawing-moment-due-to-roll-rate derivative has two contributors which are the main wing and the vertical tail. The former contribution is calculated by considering the wing twist angle, flap deflection, and lift curve slope. Vertical tail contribution depends on the vertical tail's contribution to side-force-due-to-sideslip-angle derivative, main wing span, and the vertical tail positioning.

PITCH RATE DERIVATIVES

Lift-due-to-pitch-rate derivative, C_{L_q}
The lift-due-to-pitch-rate derivative is contributed by the wing, horizontal tail and the canard. The horizontal tail contribution is estimated by the lift curve slope of the canard, its dynamic pressure ratio the wing, and the volume coefficient. Canard's contribution, which is a negative contribution, is calculated with the same procedure with appropriate substitution of canard parameters for horizontal tail parameters.

Drag-due-to-pitch-rate derivative, C_{D_q}
The drag-due-to-pitch-rate derivative is assumed to be negligible.

Pitching-moment-due-to-pitch-rate derivative, C_{m_q}
The pitching-moment-due-to-pitch-rate derivative is contributed by the wing, horizontal tail and the canard. The horizontal tail and canard contributions are functions of their lift curve slope, volume coefficient, dynamic pressure ratio to the wing, their aerodynamic center positioning with respect to the aircraft center of gravity.

YAW RATE DERIVATIVES

Side-force-due-to-yaw-rate derivative, C_{y_r}
The side-force-due-to-yaw-rate derivative is primarily affected by the vertical tail. It is a function of vertical tail contribution to the side-force-due-to-sideslip-angle, vertical tail positioning and main wing span.

Rolling-moment-due-to-roll-rate derivative, C_{l_r}
The rolling-moment-due-to-roll-rate derivative is influenced by the wing and vertical tail. The wing contribution is calculated by the use of wing lift coefficient, the slope of the rolling moment due to roll rate, the slope of the low-speed rolling moment due to yaw rate, wing twist and dihedral angles, flap deflection and its effect on the rolling moment due to roll rate. The vertical tail contribution is determined by the vertical tail contribution to side-force-due-to-sideslip-angle derivative, vertical tail positioning, and the main wing span.

Yawing-moment-due-to-yaw-rate derivative, C_{n_r}
The yawing-moment-due-to-yaw-rate derivative is contributed by the main wing and the vertical tail. The wing contribution is determined by wing lift coefficient, wing zero-lift drag coefficient, lift effect of the wing yaw damping derivative, and drag effect of the wing yaw damping derivative, where last two parameters are functions of wing taper ratio, quarter-chord sweep angle, and aspect ratio. The vertical tail contribution is affected by the vertical tail contribution to side-force-due-to-sideslip-angle derivative, vertical tail positioning, and main wing span.

3.2.2. CONTROL DERIVATIVES

Calculated control derivatives are listed as follows.

- Aileron control derivatives
  $C_{y_{\delta_a}}, C_{l_{\delta_a}}, C_{n_{\delta_a}}$
- Elevator control derivatives
  $C_{L_{\delta_e}}, C_{D_{\delta_e}}, C_{m_{\delta_e}}$
- Rudder control derivatives
  $C_{y_{\delta_r}}, C_{l_{\delta_r}}, C_{n_{\delta_r}}$
- Canardvator control derivatives
  $C_{L_{\delta_c}}, C_{D_{\delta_c}}, C_{m_{\delta_c}}$

AILERON CONTROL DERIVATIVES

Side-force-due-to-aileron derivative, $C_{y_{\delta_a}}$
The side-force-due-to-aileron derivative is negligible for most conventional aileron arrangements which is why it is taken to be 0.

Rolling-moment-due-to-aileron derivative, $C_{r_{\delta_a}}$
The rolling-moment-due-to-aileron derivative is dependent on inboard and outboard aileron locations, aileron rolling moment parameter, rolling effectiveness which is a function of aileron chord ratio to the wing, and the wing aspect ratio.

Yawing-moment-due-to-aileron derivative, $C_{n_{\delta_a}}$
The yawing-moment-due-to-aileron derivative is found by using the wing lift coefficient, rolling-moment-due-to-aileron derivative. Correction is applied for yawing moment due to aileron deflection, which is influenced by the wing taper ratio, aspect ratio and the lateral positioning of the aileron on the sing span.

RUDDER CONTROL DERIVATIVES

Side-force-due-to-rudder derivative, $C_{y_{\delta_r}}$
The side-force-due-to-rudder derivative is found from the vertical tail airfoil lift curve slope, effective vertical tail area, rudder-span factor, lift effect of the yaw damping derivative, and drag effect of the yaw damping derivative.

Rolling-moment-due-to-rudder derivative, $C_{r_{\delta_r}}$
The rolling-moment-due-to-rudder derivative is a function of the side-force-due-to-rudder derivative, main wing span, and vertical tail positioning with respect to the aircraft center of gravity.

Yawing-moment-due-to-rudder derivative, $C_{n_{\delta_r}}$
The yawing-moment-due-to-rudder derivative is influenced by the same parameters with the rolling-moment-due-to-rudder derivative.

ELEVATOR CONTROL DERIVATIVES

Lift-due-to-elevator derivative, $C_{L_{\delta_e}}$
The lift-due-to-elevator derivative is a function of the lift-due-to-stabilizer-incidence. The estimation is also affected by the elevator span factor, chord ratio of the elevator to the horizontal tail, and the airfoil lift curve slope of the horizontal tail.

Drag-due-to-elevator derivative, $C_{D_{\delta_e}}$
The drag-due-to-elevator derivative is computed in the same way as the lift, with the replacement of drag-due-to-stabilizer-incidence to the lift-due-to-stabilizer-incidence. Drag-due-to-stabilizer-incidence derivative is influenced by the horizontal tail lift coefficient, aspect ratio, airfoil lift curve slope and dynamic pressure ratio to the wing.

Pitching-moment-due-to-elevator derivative, $C_{m_{\delta_e}}$
The pitching-moment-due-to-elevator derivative is also calculated by the same principle with the substitution of pitching-moment-due-to-stabilizer-incidence to lift-due-to-stabilizer-incidence. The pitching-moment-due-to-stabilizer-incidence is affected by the horizontal tail airfoil lift curve slope, volume coefficient, dynamic pressure ratio to the main wing.

CANARDVATOR CONTROL DERIVATIVES

Lift-due-to-canardvator derivative, $C_{L_{\delta_c}}$
The lift-due-to-canardvator derivative is a function of the lift-due-to-canard-incidence derivative, which is influenced by the canard airfoil lift curve slope, and ratios of area and dynamic pressure ratio to the wing. The estimation is also affected by the canardvator span factor, chord ratio of the canardvator to the canard, and the airfoil lift curve slope of the canard.

Drag-due-to-elevator derivative, $C_{D_{\delta_c}}$
The drag-due-to-elevator derivative is computed in the same way as the lift, with the replacement of drag-due-to-canard-incidence to the lift-due-to-canard-incidence. The drag-due-to-canard-incidence is a function of the canard lift coefficient, airfoil lift curve slope, aspect ratio and dynamic pressure ratio to the wing.

Pitching-moment-due-to-canardvator derivative, $C_{m_{\delta_c}}$
The pitching-moment-due-to-canardvator derivative is also calculated by the same principle with the substitution of pitching-moment-due-to-canard-incidence to lift-due-to-canard-incidence. The pitching-moment-due-to-canard-incidence is determined by the canard airfoil lift curve slope, volume coefficient, and the dynamic pressure ratio to the wing.

3.3. MATHEMATICAL MODEL FOR AIRCRAFT BEHAVIOR ESTIMATION

Determination of the handling qualities of an aircraft requires aerodynamic forces and moments of the aircraft. They are calculated by using stability and control derivatives as follows.

$$X = (qS)\left((C_L - C_{D_\alpha})\alpha - C_{D_q}\frac{q\bar{c}}{2V} - C_{D_{\delta_e}}\delta_e\right) \tag{3.69}$$

$$Y = (qS)\left(C_{y_\beta}\beta + C_{y_p}\frac{pb}{2V} + C_{y_r}\frac{rb}{2V} + C_{y_{\delta_a}}\delta_a + C_{y_{\delta_r}}\delta_r\right) \tag{3.70}$$

$$Z = (qS)\left(-(C_{L_\alpha} + C_D)\alpha - C_{L_q}\frac{q\bar{c}}{2V} - C_{L_{\delta_e}}\delta_e\right) \tag{3.71}$$

$$L = (qSb)\left(C_{l_\beta}\beta + C_{l_p}\frac{pb}{2V} + C_{l_r}\frac{rb}{2V} + C_{l_{\delta_a}}\delta_a + C_{l_{\delta_r}}\delta_r\right) \tag{3.72}$$

$$M = (qS)\left(-(C_{m_a}\alpha + C_{m_q}\frac{q\bar{c}}{2V} + C_{m_{\delta_e}}\delta_e\right) \tag{3.73}$$

$$N = (qSb)\left(C_{n_\beta}\beta + C_{n_p}\frac{pb}{2V} + C_{n_r}\frac{rb}{2V} + C_{n_{\delta_a}}\delta_a + C_{n_{\delta_r}}\delta_r\right) \tag{3.74}$$

4

VALIDATION

In order to ensure the credibility of implemented methods, a validation study is performed.

4.1. VALIDATION OF INERTIA ESTIMATION METHOD

4.1.1. ACCURACY OF THE IMPLEMENTED METHOD

In order to be able to rely on the proposed inertia estimation method, validation of the programming is of importance. A validation on the accuracy of implemented method is performed with an example aircraft. The reference aircraft is chosen to be Fokker 100 due to its available real data. Fokker 100 can be seen in Figure 4.1.

Figure 4.1: Reference aircraft Fokker 100

The comparison of the obtained values and real data are shown in Table 4.1.

Table 4.1: Comparison of moment of inertia values for Fokker100

Inertia (kgm^2)	Real Data	Obtained Value	Error Percentage
I_{xx}	252960	248000	1.96
I_{yy}	1668670	1792600	7.43
I_{zz}	1846990	1958000	6.01
I_{xz}	87200	74300	14.79

The comparison of calculated values to real data shows that the error is less than 8 percent for the moments of inertia. The highest error percentage occurs in I_{xz} product of inertia with 15 percent. Sensitivity analysis is conducted in order to see if those error percentages are acceptable in the estimation of handling qualities. Both longitudinal and lateral/directional handling qualities are examined using the real value and estimated value of the inertia.

The comparison of phugoid damping ratio is shown in Table 4.2.

Table 4.2: Comparison of phugoid damping ratio values

Fokker 100 Data	ζ_p	Corresponding Level
Real data	0.0202	Level 2
Estimated I_{xx}	0.0202	Level 2
Estimated I_{yy}	0.0178	Level 2
Estimated I_{zz}	0.0202	Level 2
Estimated I_{xz}	0.0202	Level 2

It is clearly seen that the phugoid damping ratio is only affected by the pitching moment of inertia I_{yy}, which is an expected result as it is the only moment of inertia that influences longitudinal behavior of the aircraft. The difference of phugoid damping ratio is found to be 11 percent which in fact does not lead to any change in the level of handling quality.

Following the phugoid mode, the longitudinal behavior is examined by comparison of short period undamped natural frequency values of each case whose result is shown in Figure 4.2.

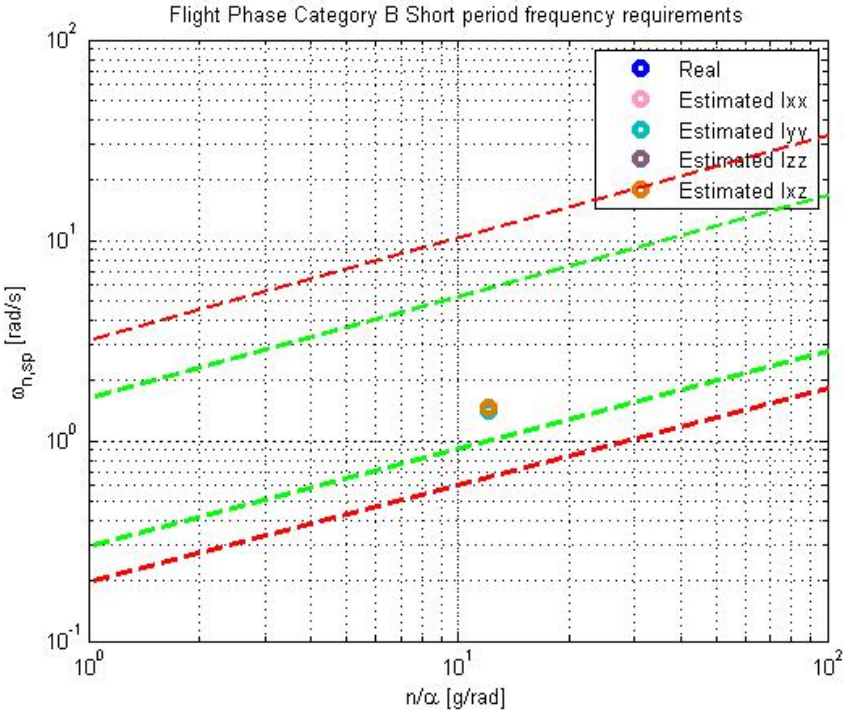

Figure 4.2: Comparison of short period undamped natural frequency values

In Figure 4.2, it is seen that results of short period frequency requirement are matching for real data, real data using estimated I_{xx}, real data using estimated I_{zz}, and real data using estimated I_{xz}, while the result of real data using estimated I_{yy} has a slight difference. This difference can be seen more clearly in Figure 4.3, and

can evidently be said that it is negligible.

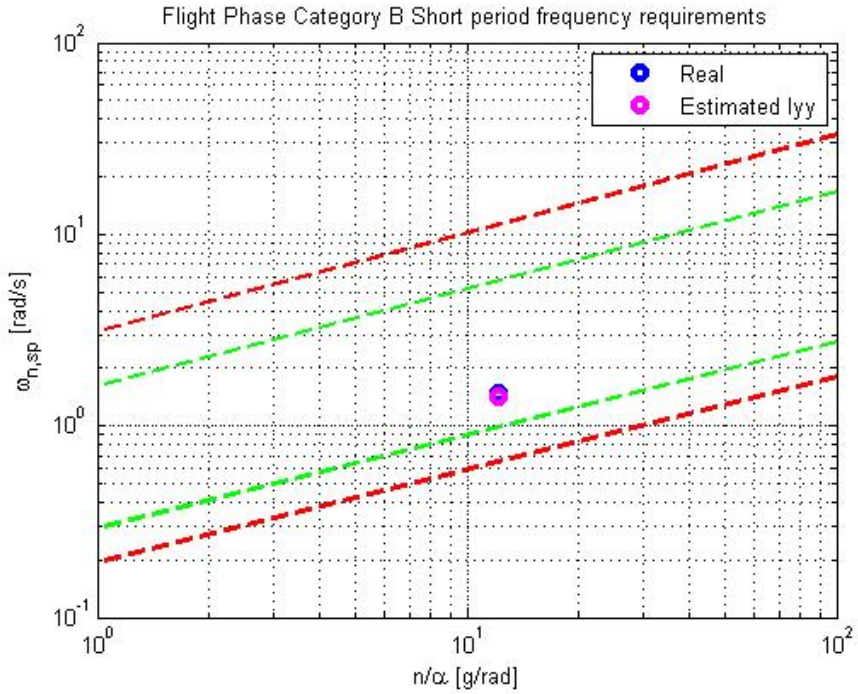

Figure 4.3: Comparison of short period undamped natural frequency values with different pitching moment of inertia

Obtained short period damping ratios for each study case and corresponding quality level are shown in Table 4.3.

Table 4.3: Short period damping ratio results

Fokker 100 Data	ζ_{sp}	Corresponding Level
Real data	0.6516	Level 1
Estimated I_{xx}	0.6516	Level 1
Estimated I_{yy}	0.6594	Level 1
Estimated I_{zz}	0.6516	Level 1
Estimated I_{xz}	0.6516	Level 1

Similar to phugoid damping ratio results, only difference in short period damping ratios appears in the data with estimated I_{yy}.

CAP and short period damping ratio values each case are shown in Figure4.4.

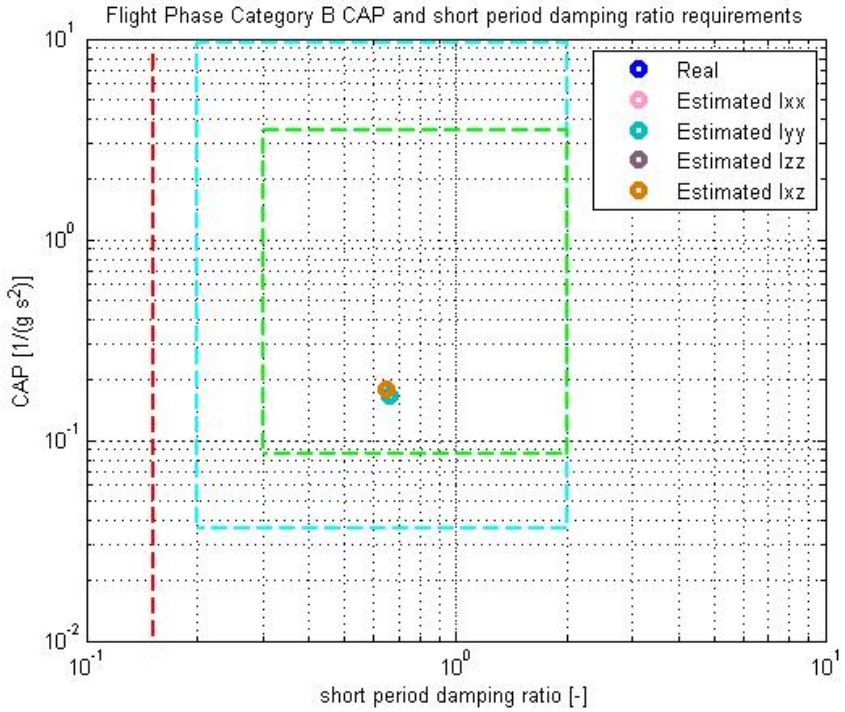

Figure 4.4: Comparison of CAP and short period damping ratio values

CAP and short period damping ratio requirements are precisely matching for each case except the real data using estimated I_{yy}. The slight distinction can be seen in Figure 4.5.

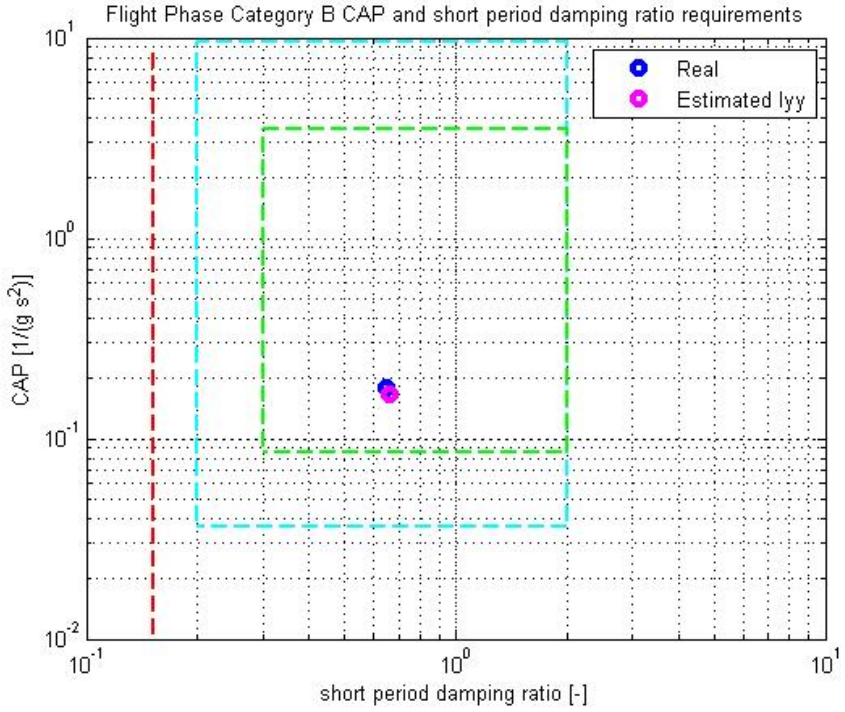

Figure 4.5: Comparison of CAP and short period damping ratio values

The error percents in longitudinal handling quality requirements are found to be less than 12% which conse-

quently does not influence the level. Hence, it can be concluded that the 7.43% error in pitching moment of inertia I_{yy} is an acceptable value regarding the changes in longitudinal behavior of the aircraft.

Secondly, the lateral/directional handling quality requirements are examined in terms of their sensitivity to changes in moment of inertia results.

Dutch roll undamped natural frequency and damping ratio results are shown in Table 4.4 .

Table 4.4: Comparison of Dutch roll undamped natural frequency and damping ratio

Fokker 100 Data	ζ_d	ω_{n_d}	$\zeta_d\omega_{n_d}$
Real data	0.8009	0.3622	0.2901
Estimated I_{xx}	0.8013	0.3621	0.2902
Estimated I_{yy}	0.8009	0.3622	0.2901
Estimated I_{zz}	0.7957	0.3547	0.2822
Estimated I_{xz}	0.8010	0.3622	0.2901

Due to the fact that lateral/directional modes are only influenced by lateral/directional moments of inertia, the Dutch roll natural frequency and damping ratio results with estimated I_{yy} are precisely same with the ones that are calculated using the real data. The Dutch roll natural frequency is inversely proportional to square root of yawing moment of inertia I_{zz}. Therefore, the error percentage in the estimated value of I_{zz} is directly observed in the result of ω_{n_d}. Likewise, Dutch roll damping ratio is primarily influenced by I_{zz}, where only 0.65% error occurs due to a 6.01% error in the estimation of moment of inertia. Furthermore, the product of inertia I_{xz}, which has the highest error percentage compared to its real value, has almost negligible effect on Dutch roll.

The calculated spiral mode time constant values and their corresponding quality levels are presented in Table4.5.

Table 4.5: Comparison of minimum time to double the amplitude in spiral mode

Fokker 100 Data	Min T_{2s} (sec)
Real data	-3.4768
Estimated I_{xx}	-3.4755
Estimated I_{yy}	-3.4768
Estimated I_{zz}	-3.5351
Estimated I_{xz}	-3.4765

In Table reftable:F100spiralsensitivity it seen that the spiral time constant results are found to be negative even for the real data. Therefore the calculation process is checked in FMT in order to ensure the reliability. Same result is acquired by using the empirical spiral mode time constant equation given in Ref [**?**]. Hence it can be concluded that calculation process is reliable. However this shows that Fokker 100 is not satisfactory to meet the spiral mode criteria.

Comparison of roll mode time constants are shown in Table 4.6.

Table 4.6: Comparison of roll mode time constant

Fokker 100 Data	T_r (sec)	Corresponding Level
Real data	0.2688	Level 1
Estimated I_{xx}	0.2636	Level 1
Estimated I_{yy}	0.2688	Level 1
Estimated I_{zz}	0.2687	Level 1
Estimated I_{xz}	0.2688	Level 1

The roll mode time constant is influenced directly by the rolling moment of inertia I_{xx} and slightly by the yawing moment of inertia I_{zz}. An insignificant distinction on roll mode time constant is seen between the real data and the real data using estimated I_{zz}, which does not require a high concern. However, the influence of the 1.9% lower estimation of I_{xx} is directly observed in Table 4.6, which shows that roll mode time constant is highly sensitive to the changes in I_{xx}. Owing to a good approximation of rolling moment of inertia, the difference on results is acceptable.

4.1.2. COMPUTATION TIME

As it is stated in the goal of the project, the estimation is required to be rapid. The computational time of moment of inertia estimation is found to be approximately 12 seconds, which is a satisfactory value.

4.2. VALIDATION OF CONTROL AND STABILITY DERIVATIVES ESTIMATION METHOD

4.2.1. ACCURACY OF THE IMPLEMENTED METHOD

In order to be able to rely on the implementation of control and stability derivatives estimation method, validation of the programming is of importance. A validation on the accuracy of implemented method is performed with an example aircraft, which is chosen to be Boeing 747 due to its available data in Ref [18]. Boeing 747-100 can be seen in Figure 4.6.

Figure 4.6: Reference aircraft Boeing 747-100

The comparison of longitudinal stability derivatives is shown in Table 4.7 with error percentages.

Table 4.7: Comparison of longitudinal stability derivatives of Boeing 747-100

Derivative (1/rad)	Real Data	Obtained Value	Error Percentage
C_{L_α}	5.70	4.07	28.5
C_{D_α}	0.66	0.57	13.66
C_{m_α}	-1.26	-1.17	6.82
C_{L_q}	5.4	4.69	13.15
C_{D_q}	NA	0	NA
C_{m_q}	-20.80	-15.09	27.45

Among the obtained results C_{L_α} and C_{m_q} have the highest error percentages. The former derivative is one of the paramount parameters in longitudinal behavior, which means an error like this may result in big dif-

ferences. Unexpected behaviors in study cases may be explained due to a possible error in C_{L_α} calculations. Due to the lack data, a sensitivity analysis cannot be performed on this.
The comparison of lateral stability derivatives is shown in Table 4.8 with error percentages.

Table 4.8: Comparison of lateral/directional stability derivatives of Boeing 747-100

Derivative (1/rad)	Real Data	Obtained Value	Error Percentage
C_{y_β}	-0.96	-0.68	29.16
C_{l_β}	-0.22	-0.256	15.7
C_{n_β}	0.15	0.139	7.53
C_{y_p}	NA	-0.1136	NA
C_{l_p}	-0.45	-0.335	25.55
C_{n_p}	-0.121	-0.186	53.72
C_{y_r}	NA	0.593	NA
C_{l_r}	0.101	0.099	1.98
C_{n_r}	-0.30	-0.32	6.67

Considering lateral/directional stability derivatives the highest error percentages are seen in derivatives due to roll rate. Therefore, this should be taken into account in case of abnormal lateral/directional handling quality results. Moreover, the side-force-due-to-sideslip-angle C_{y_β} has a high error compared to real value. However this can be acceptable since C_{y_β} has often negligible effect on the aircraft dynamics [19].

4.2.2. COMPUTATION TIME

Similar to inertia estimation module, the module for control and stability estimations is required to be rapid. The computational time of this estimation module is found to be approximately 3 seconds, which is a highly satisfactory result.

5

CASE STUDIES

In this chapter results of implemented methods are presented as well as their influence on handling quality assessment.

5.1. CHOSEN CONFIGURATIONS

As it is stated, three different configurations are examined. Conventional configuration is the most common design of currently operating aircrafts. Choosing this configuration might be advantageous due to the fact that it has proved itself safe. The geometry of the created aircraft can be seen in Figure 5.1.

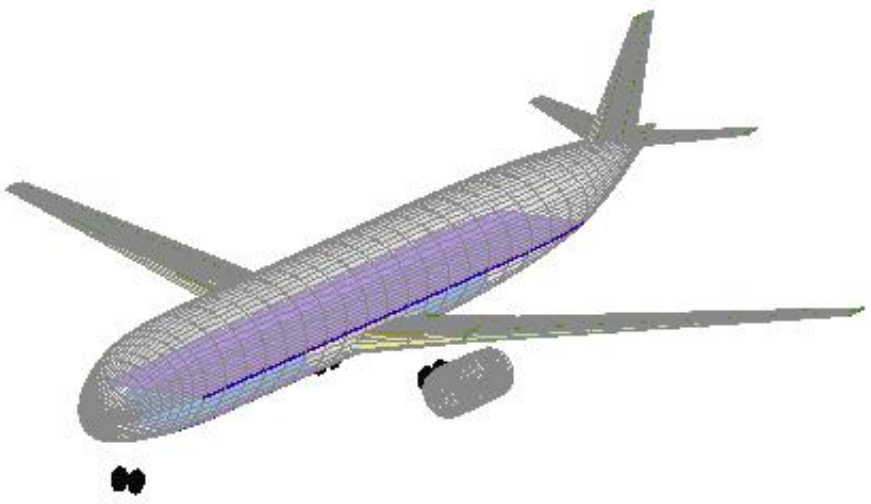

Figure 5.1: Conventional configuration based on A320-200

Second configuration is chosen to be canard. This aircraft configuration consists of a horizontal stabilizer

which is located in front of the main wing unlike the conventional configuration. The interest on the canard configuration aircraft dates back to the first days of aviation, which was Wright Brothers' first flight attempt with a heavier-than-air vehicle. [20] Following this, use of the canard has been experimented occasionally throughout the history. Among the advantages and drawbacks of a canard configuration, the main difference between such a configuration and the conventional tail airplane is the destabilizing pitching moment generation [20]. The aircraft model with a canard as a horizontal stabilizer is created based on a A320-200 conventional aircraft, which can be seen in Figure5.2.

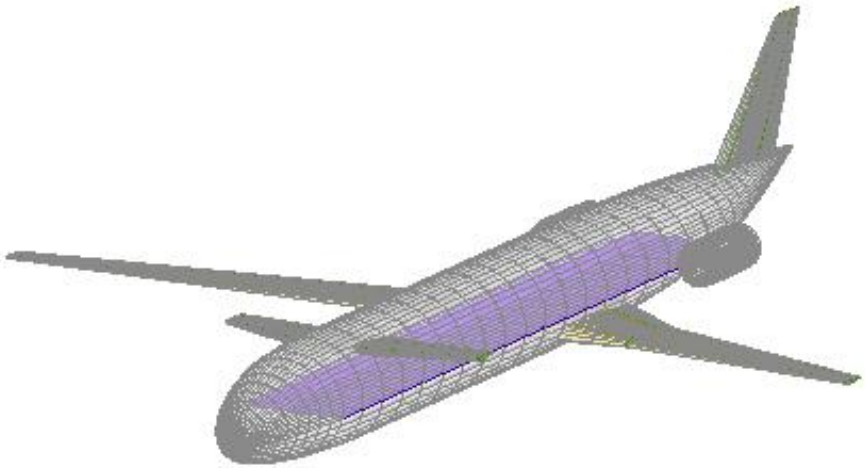

Figure 5.2: Canard configuration based on A320-200 conventional aircraft

Third study case is chosen to be three surface aircraft. A three surface configuration consists of main wing, canard and horizontal wing. The main purpose of this design is to locate the c.g. such that all surfaces can contribute to the total lift. This leads to a reduction in induced drag but an increase in interference drag [20]. There are few flying examples of this configuration, one of which is Piaggio P-180 Avanti. The aircraft model having both a horizontal tail and a canard is created based on a A320-200 conventional aircraft, which can be seen in Figure5.3.

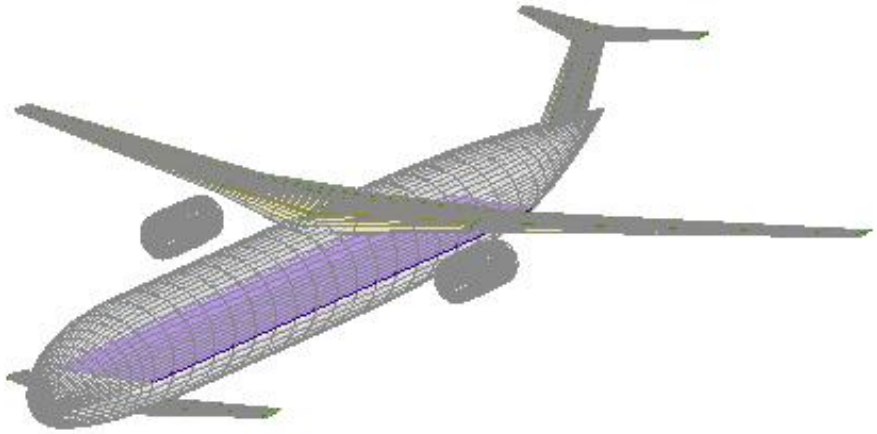

Figure 5.3: TSA configuration based on A320-200 conventional aircraft

Geometric parameters of components having high contributions to mass are presented in Appendix A for each configuration.

5.2. INERTIA ESTIMATION RESULTS

Estimated moment of inertia values for each configuration is presented in Table 5.1. The aircrafts have 37021 kg, 32025 kg, and 36152 kg empty operating masses. Tsa has the highest values of inertia which means, the configuration would have a higher resistance to angular acceleration about any axis of rotation. The opposite holds true for the canard configuration except about the pitching axis, where conventional configuration would have a lower resistance.

Table 5.1: Estimated inertia of the conventional configuration

Inertia (kgm^2)	Conventional	Canard	TSA
I_{xx}	1062400	703300	1136100
I_{yy}	3092400	3163400	3301300
I_{zz}	4015300	3778000	4257800
I_{xz}	104470	36512	179390

Rolling moment of inertia I_{xx} is influenced by the mass distribution along y and z axes. Average fuselage height and width of configurations are similar which leads to insignificant contribution to the differences of I_{xx} values. Therefore, the influence of mass distribution along z axis is dominated primarily by the tail. Even though the position of vertical tail at each configuration is almost the same, geometrical parameters and masses are different which results in higher contribution in conventional configuration and followed by tsa and canard successively. Horizontal tail positioning has an important influence with respect to the significant

difference in positioning between conventional and tsa. T-tail of tsa leads to significantly higher contribution than the conventional tail configuration. When the mass distribution along the y axis is considered, distinctions occur primarily due to horizontal lifting surfaces and positioning of engines on them. Canard configuration has its' engines positioned relatively closer to the fuselage center section which lowers the moment arm and hence the moment of inertia. Engines of conventional and tsa configurations have their engines positioned almost in same locations while the former has a larger mass than the latter configuration. This results in higher contribution of engines to the rolling moment of inertia of conventional aircraft. Despite the fact that engine contribution is highest in conventional configuration, tsa has the highest I_{xx} owing to one more horizontal lifting surface than other two configurations, which results in significantly higher mass distribution along y axis and to t-tail configuration which results in significantly higher mass distribution along z axis.

The pitching moment of inertia I_{yy} is influenced by the mass distribution along x and z axes. The fuselage has an important contribution to I_{yy} having a large mass distributed along the roll axis. Moreover, I_{yy} is highly affected by tails' positioning and masses, due to comparably long distances in x axis with respect to aircraft center of gravity. Likewise its effect on rolling moment of inertia, vertical positioning of the horizontal tail affects the pitching moment of inertia. Results show that tsa has the highest I_{yy} which is followed by canard and conventional aircraft with 2% and 6% differences successively.

The yawing moment of inertia I_{zz} is a function of the mass distribution along x and y axes. The reason behind I_{zz} being the highest moment of inertia in each configuration, is the imposed effect of large mass distribution along x axis due to highest mass contributor fuselage and comparably large mass distribution along y axis due to second highest mass contributor main wing.

A significant difference between inertia values is seen in I_{xz} parameter. Canard configuration has a noticeably smaller product of inertia compared to other two configurations. As the mathematical definition suggests, this inertial property is affected by the distance between aircraft c.g. and the position of the component on x and z axes. The primary reason of such a distinction is the approximately 20% lower fuselage mass of the canard configuration.

5.3. CONTROL AND STABILITY DERIVATIVES ESTIMATION RESULTS

The longitudinal stability and control derivatives for each configuration is presented in Table 5.2 and Table 5.3.

Table 5.2: Estimated longitudinal stability derivatives of each configuration

Derivative (1/rad)	Conventional	Canard	TSA
C_{L_α}	4.9728	5.6731	6.1071
C_{D_α}	0.2975	0.3271	0.3803
C_{m_α}	-0.7581	-3.1717	-0.9825
C_{L_q}	16.6636	-7.6720	18.3165
C_{D_q}	0	0	0
C_{m_q}	-19.6469	-9.4333	-42.5697

The lift-due-to-aoa derivative C_{L_α} is highest at tsa configuration and is followed by canard and conventional aircrafts respectively. This derivative is influenced by wing-body interaction, horizontal tail downwash effect and canard upwash effect. Conventional aircraft is only influenced by the downwash, while the canard aircraft is influenced by the upwash. Therefore, even though both configurations have almost identical wing-body lift curve slope, the difference occurs due to comparably higher upwash effect on the canard aircraft than the downwash contribution to conventional aircraft. The reason behind tsa having the highest value of C_{L_α} is that it is contributed by all mentioned properties. Hence, even though tsa also has similar wing-body lift curve slope, the total derivative increases owing to two horizontal stabilizers. The drag-due-to-aoa C_{D_α} derivative is proportional to C_{L_α}, which leads to the same ranking of configurations. The pitching-moment-due-to-aoa C_{M_α} of the canard aircraft is significantly higher than other two configurations. C_{M_α} is dependent on both C_{L_α} and the distance between aircraft center of gravity and aircraft aerodynamic center. The latter is defined by wing mean aerodynamic center, and the shift due to fuselage and horizontal stabilizers.

Among longitudinal derivatives, the most noticeable difference is seen in the lift-due-to-pitch-rate derivative, C_{L_q} due to different sign of canard configuration. This derivative is contributed by horizontal lifting surfaces, and it highly depends on those surfaces' aerodynamic center positions with respect to aircraft center of gravity. Wing contribution is computed by using the distance between aircraft c.g. and wing mean aerodynamic center in x-direction. For canard configuration the wing mean aerodynamic center is in front of the aircraft c.g. which yields this distance negative and consequently leads to a negative lift derivative contribution. The pitching-moment-due-to-pitch-rate derivative C_{m_q} is too high for tsa which is due to high contributions of both wing and the horizontal tail. Due to high distances between those surfaces' aerodynamic center and the aircraft center of gravity, the derivative results in such a large value.

Table 5.3: Estimated longitudinal stability and control derivatives of the conventional configuration

Derivative (1/rad)	Conventional	Canard	TSA
$C_{L_{\delta_e}}$	0.2297	-	2.6055
$C_{D_{\delta_e}}$	0.9720	-	0.8381
$C_{m_{\delta_e}}$	-0.7660	-	-0.7625
$C_{L_{\delta_c}}$	-	0.2541	0.2639
$C_{D_{\delta_c}}$	-	1.0914	1.1334
$C_{m_{\delta_c}}$	-	0.4892	0.6435

The pitching control is provided by the elevator or/and canardvator. In Table 5.3, it is clearly seen that horizontal tail and canard affects the pitching moment in opposite ways, where canardvator has a destabilizing effect on pitching moment while the horizontal tail provides stabilizing effect.

The lateral/directional stability and control derivatives for each configuration is presented in Table 5.4 and Table 5.5.

Table 5.4: Estimated lateral/directional stability derivatives of each configuration

Derivative (1/rad)	Conventional	Canard	TSA
C_{y_β}	-0.4808	-0.5517	-0.6044
C_{l_β}	-0.0994	-0.0735	-0.1128
C_{n_β}	-0.0302	-0.0535	-0.0784
C_{y_p}	-0.0409	-0.0382	-0.0239
C_{l_p}	-0.2685	-0.2952	-2.0696
C_{n_p}	-0.0703	-0.0609	-0.1098
C_{y_r}	0.2861	0.3104	0.2693
C_{l_r}	0.0432	0.0253	0.0250
C_{n_r}	-0.1728	-0.1806	-0.1507

Among the stability derivatives due to sideslip angle, the rolling-moment-due-to-sideslip-angle C_{l_β} is related to roll stiffness of the aircraft, which provides the aircraft the tendency to fly with wings level. When the aircraft rolls to an angle, a weight component occurs in the y direction, which induces a sideslip velocity. The product of this sideslip angle and C_{l_β} tends to bring the wings level. This derivative is highly affected by the main wing dihedral angle, aspect ratio, and sweep angle as well as the wing-fuselage lift coefficient. Latter term is significantly higher than for tsa than other two configurations which leads to the highest value of C_{l_β}.

The yawing-moment-due-to-sideslip-angle derivative C_{n_β} represents the yaw stiffness of the aircraft, which means a perturbation in β would produce a restoring yawing moment that tends to keep the velocity vector in the plane of symmetry [19]. Therefore the aircraft should have a positive C_{n_β} in order to have a positive yaw stiffness. The primary contributors to this derivative are the fuselage and vertical tail, where the former one has a negative influence on the contrary to the positive contribution of vertical tail. In Table 5.4 it is seen that none of the configurations have positive yaw stiffness. These results show that yawing moment created by

vertical tail of each configuration fails to overcome the fuselage drag due to large body side areas. This can be overcome by either designing the vertical tail larger or positioning it more rearward and higher with respect to aircraft center of gravity, in other words by making the vertical tail more effective.

The rolling-moment-due-to-roll-rate C_{l_p}, in other words damping-in-roll derivative, expresses the aircraft's resistance to rolling, and should always be negative. Even though each configuration seems to achieve the damping in roll, the tsa configuration has significantly higher value. This derivative is contributed by the wing and vertical tail. The reason of this notable value of tsa is found to be due to dihedral effect parameter of wing which is a function of wing position in z-direction and dihedral angle. Both conventional and canard configurations have low wings while tsa has higher wing which results in such a distinct result.

The yawing-moment-due-to-roll-rate C_{n_p} is one of the cross derivatives, which means it causes coupling between rolling and yawing motions. Both wing and vertical tail contributes to this derivative, where the vertical tail influence is comparably lower than the main wing. The tsa having the highest wing contribution is followed by the conventional and canard successively which is directly observed on the total derivatives.

In Table 5.4, one of the important derivatives is the rolling-moment-due-to-yaw-rate C_{l_r} which expresses a cross derivative. It is contributed by the wing and vertical tail, where the latter one is the primary contributor. This contribution is highly affected by the vertical tail aerodynamic center position with respect to the aircraft center of gravity. The difference between those points in both x and z axes is lowest for tsa configuration which results in the lowest primary contribution.

The yawing-moment-due-to-yaw-rate C_{n_r} is expressed as damping-in-yaw derivative as well. It is always negative, which means a negative yawing moment will be generated due to the increase in profile and induced drag on left wing and the decrease on the right wing which is the result of yaw rate [19]. C_{n_r} results of all configurations satisfy this condition. The derivative is contributed by the main wing and mainly by the vertical tail. The highest yaw damping occurs in canard configuration while the lowest is in tsa. Similar to C_{n_r}, this is due to tsa's comparably smaller distance between its vertical tail aerodynamic center position with respect to the aircraft center of gravity, which is the fundamental property that determines the vertical tail contribution.

Table 5.5: Estimated lateral/directional control derivatives of each configuration

Derivative (1/rad)	Conventional	Canard	TSA
$C_{y_{\delta a}}$	0	0	0
$C_{l_{\delta a}}$	0.1127	0.4173	0.3766
$C_{n_{\delta a}}$	-0.0108	-0.0383	-0.0373
$C_{y_{\delta r}}$	0.8589	1.0937	1.2536
$C_{l_{\delta r}}$	0.1010	0.1120	0.0993
$C_{n_{\delta r}}$	-0.4835	-0.5938	-0.6441

In most flight conditions it is desired to have a zero sideslip angle. This can be maintained with a positive yaw stiffness, which does not hold for any of those configurations. In such situations, in an unsymmetrical thrust or in an unsymmetrical flow field due to turning flight, the sideslip angle is kept zero by using the control moments. This control is primarily by the rudder, and therefore the yawing-moment-due-to-rudder $C_{n_{\delta_r}}$ is an important parameter. Tsa having the highest $C_{n_{\delta_r}}$ has a higher rudder power compared to other configurations.

The rolling control is provided by the ailerons, while they also introduce a yawing moment. Therefore two parameters are important in terms of the aileron effectiveness which are rolling-moment-due-to-aileron derivative $C_{l_{\delta a}}$ and yawing-moment-due-to-aileron derivative $C_{n_{\delta a}}$. $C_{n_{\delta a}}$ expresses the aircraft's tendency for a yawing motion to opposite side due to the higher drag induced on the side with downward aileron. This undesired situation is called adverse yaw and would be high in the canard aircraft, which would introduce difficulties in lateral control.

5.4. HANDLING QUALITIES COMPARISON

Having calculated the inertia matrix and control and stability derivatives, configurations are compared in terms of several handling qualities criterion. Aircrafts are trimmed at same conditions which are presented in Table 5.6.

Table 5.6: Trim conditions

Altitude	1000 m
Airspeed	130 m/s
Flight path angle	0 deg
Heading angle	0 deg
Turn rate	0 deg/s
Sideslip angle	0 deg
Pitch attitude rate	0 deg/s

5.4.1. LONGITUDINAL HANDLING QUALITIES

Handling qualities related to longitudinal dynamics are examined considering two modes which are phugoid and short period.

PHUGOID MODE

As it has been mentioned, phugoid mode is an oscillatory mode which is lightly damped and has a low frequency. The resultant phugoid damping ratio of each configuration and its corresponding handling quality level according to requirements in Table 2.1 is given in Table 5.7.

Table 5.7: Phugoid damping ratio of each configuration

Configuration	ζ_{ph}	Corresponding Level
Conventional	0.0940	Level 1
Canard	0.0317	Level 2
TSA	0.0690	Level 1

As can be seen, only canard configuration cannot satisfy the handling quality in terms of phugoid damping ratio requirement.

SHORT PERIOD MODE

The obtained short period undamped natural frequency values of each study case are shown together in Figure 5.4.

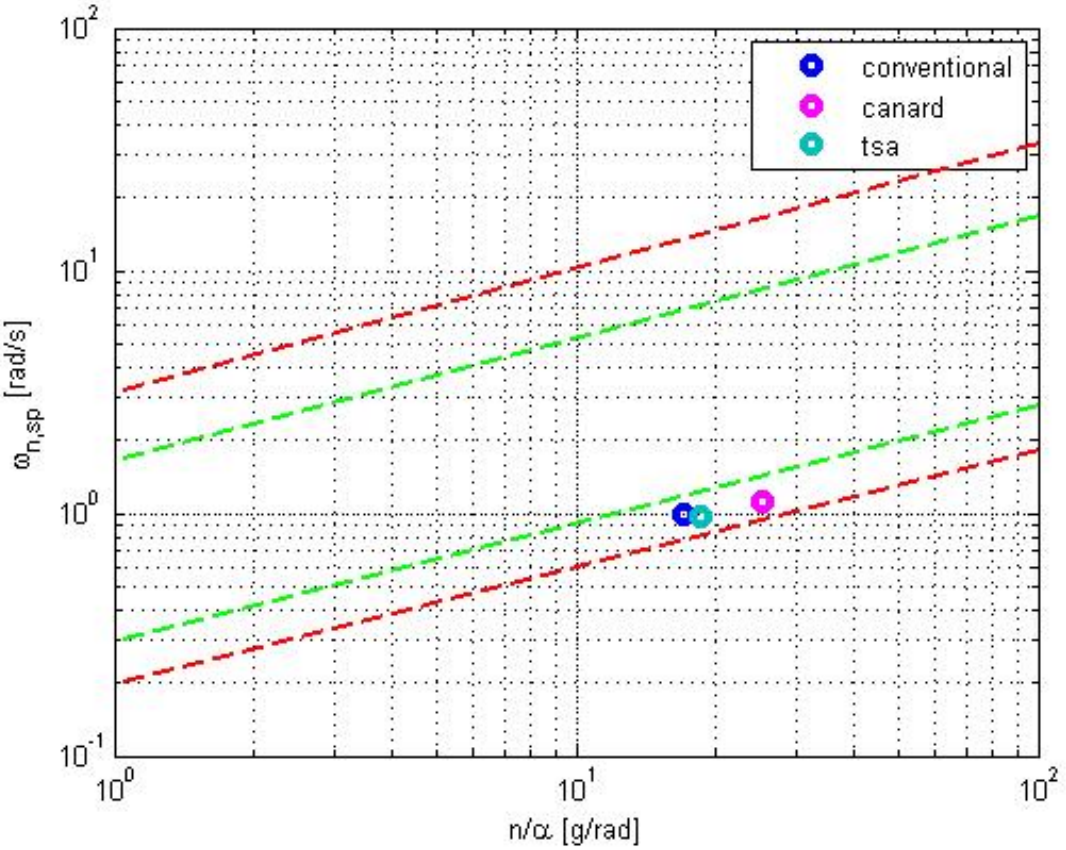

Figure 5.4: Short period undamped natural frequency values for each configuration

In Figure 5.4, each configuration seems to fail achieving level 1 regarding the short period frequency requirement. The short period frequency is dependent on wing planform parameters, drag coefficient, lift-due-to-aoa derivative C_{L_α}, pitching-moment-due-to-aoa derivative C_{m_α}, pitching-moment-due-to-pitch-rate derivative C_{m_q}, and most significantly pitching moment of inertia as the frequency is inversely proportional to the square root of I_{yy}. Compared to conventional configuration, even though tsa has higher values of mentioned derivatives, this is offset by its higher pitching moment of inertia and short period frequency values of those configurations result in similar values.

As mentioned, considering the longitudinal handling qualities, the short period damping ratio has also an important effect. Obtained short period damping ratios for each study case and corresponding quality level are shown in Table 5.8.

Table 5.8: Short period damping ratio results

Configuration	ζ_{sp}	Corresponding Level
Conventional	1	Level 1
Canard	0.6998	Level 1
TSA	1	Level 1

Short period damping ratio is a function of same parameters with the short period frequency. On the contrary to mediocre results in short period undamped frequency results, each configuration achieves level 1 handling quality in short period damping ratio.

CONTROL ANTICIPATION PARAMETER

CAP and short period damping ratio resultant values of each case study are shown in Figure5.5. As mentioned before, in the figure, the region surrounded by the green lines represents Level 1, while the area between that

and blue lines represents Level 2. Level 3 is represented by the red lines.

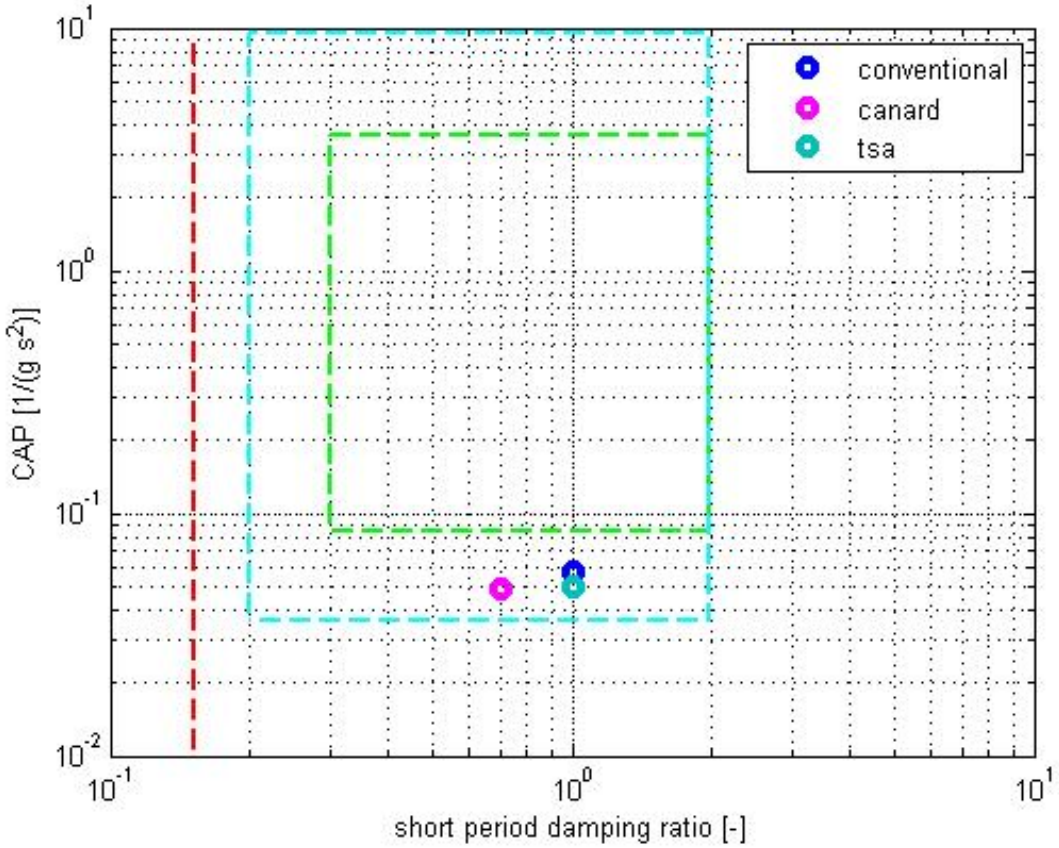

Figure 5.5: CAP and short period damping ratio requirements

According to the Figure5.5 all configurations result in level 2 with respect to CAP and short period damping ratio requirements, where conventional aircraft and tsa have really close results with conventional being slightly closer to Level 1 zone. This is an expected outcome as CAP is proportional to the square of short period frequency, where this parameter is found to be similar as well in Figure 5.4. Configurations need to achieve higher short period frequencies which would consequently lead to significantly higher CAP.

5.4.2. LATERAL/DIRECTIONAL HANDLING QUALITIES

Three modes related to lateral/directional dynamics, namely Dutch roll, spiral and roll modes, are examined for each configuration.

DUTCH ROLL MODE

As mentioned, Dutch roll mode is assessed by its undamped natural frequency and damping ratio. Results of each configuration are shown in Table 5.9.

Table 5.9: Dutch roll undamped natural frequency and damping ratio results for each configuration

Configuration	ζ_d	ω_{n_d}	$\zeta_d \omega_{n_d}$
Conventional	0.1816	0.4576	0.0831
Canard	0.1859	0.3785	0.0704
TSA	0.2993	0.1985	0.0594

According to Table 5.9, conventional aircraft is satisfactory in Dutch roll damping ratio and natural frequency having level 1 handling quality. Canard and tsa meet the requirement of Dutch roll damping ratio however they fail to have satisfactory results in natural frequency. Even the requirement of multiplication ends in level 2 for the conventional aircraft, it can still be regarded as the most satisfactory configuration in terms of Dutch roll.

Dutch roll frequency is influenced directly by the square root of main wing area, span length, yawing-moment-due-to-sideslip-angle derivative C_{n_β} and inversely by the square root of yawing moment of inertia I_{zz}. The reason why conventional configuration satisfies the requirement is that it has noticeably larger main wing area while having mediocre C_{n_β} and I_{zz}. Other two configurations can be improved in terms of Dutch roll undamped natural frequency by obtaining an acceptable yaw stiffness which can be handled by a more effective vertical tail.

SPIRAL MODE

The calculated spiral mode time constant values are presented in Table5.10.

Table 5.10: Results of minimum time to double the amplitude in spiral mode for each configuration

Configuration	Min T_{2s} (sec)
Conventional	2.3169
Canard	2.48
TSA	3.0652

None of the configurations are satisfactory in spiral mode. Spiral mode time constant has dependency on yawing moment of inertia I_{zz}, rolling-moment-due-sideslip-angle derivative C_{l_β}, yawing-moment-due-to-sideslip-angle C_{n_β}, rolling-moment-due-to-roll-rate derivative C_{l_p}, yawing-moment-due-to-roll-rate derivative C_{n_p}, rolling-moment-due-to-yaw-rate derivative C_{l_r}, and yawing-moment-due-to-yaw-rate derivative C_{n_r}. As it has been mentioned C_{l_p} and C_{n_p} results may not be so reliable which may lead to such unusual time constants.

ROLL MODE

Compared values are shown in Table 5.11.

Table 5.11: Roll mode time constant for each configuration

Configuration	T_r (sec)	Corresponding Level
Conventional	0.6264	Level 1
Canard	0.4499	Level 1
TSA	0.1030	Level 1

The roll mode time constant varies inversely by the product of density and velocity. However, the difference of time constant between configurations has no relation with that as they are trimmed at the same altitude and velocity. Besides that relation, roll mode time constant is primarily influenced by rolling moment of inertia I_{xx}, where the higher is the rolling moment of inertia the more rapid is the response to the lateral input. It also has dependence on wing planform parameters, yawing moment of inertia I_{zz}, rolling-moment-due-sideslip-angle derivative C_{l_β}, yawing-moment-due-to-sideslip-angle C_{n_β}, rolling-moment-due-to-roll-rate derivative C_{l_p}, and yawing-moment-due-to-roll-rate derivative C_{n_p}.

5.4.3. OVERVIEW OF LONGITUDINAL AND LATERAL/DIRECTIONAL MODES

Longitudinal handling quality parameters include phugoid, short period mode and CAP requirements. Regarding the phugoid mode, it is observed that only tsa is satisfactory to meet the phugoid damping ratio criteria. It has been seen that configurations have similar results in short period which results in same handling quality levels. These parameters are primarily affected by the pitching moment which is influenced by

horizontal lifting surface sizing and position. Better positioning, i.e. longer distance in x-direction, would lead to better results. Hence, in terms of longitudinal behavior, tsa and conventional configurations have similar handling qualities and better performance than the canard configuration.

In order to have a clear sight on stability of those modes, eigenvalues of each mode of each configuration are presented in Figure 5.6.

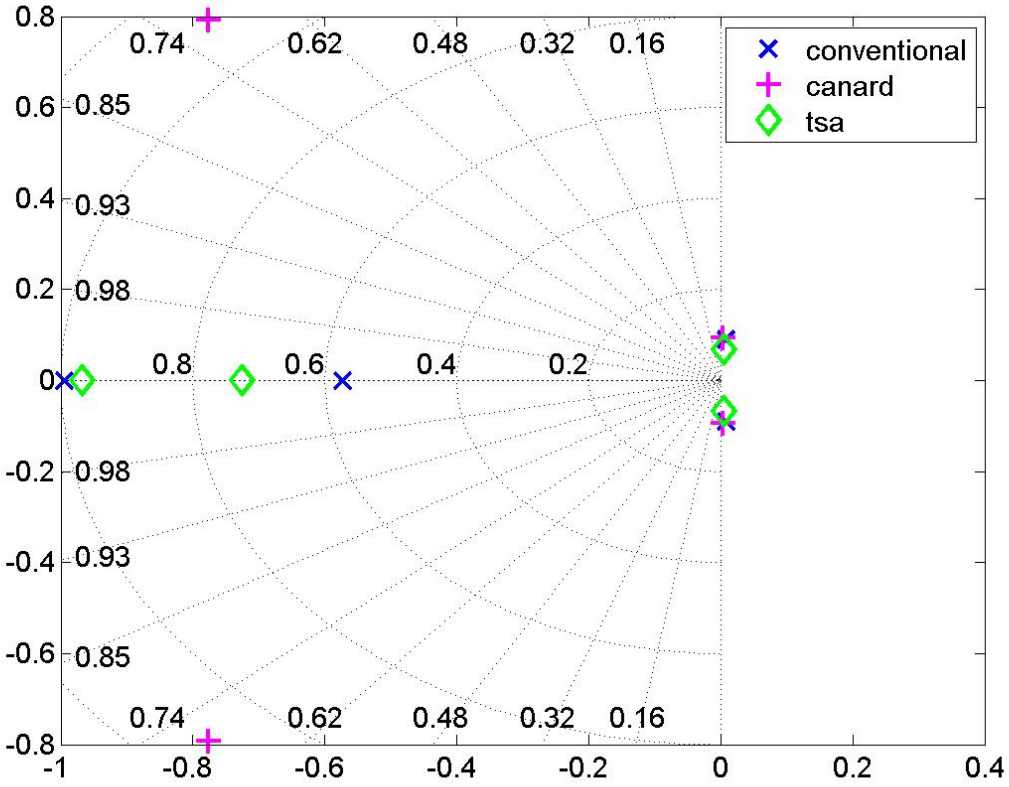

Figure 5.6: Eigenvalues of longitudinal modes

As it has been stated, longitudinal modes include two oscillatory modes which are phugoid and short period. Phugoid modes are recognized due to their light damping (i.e. smaller real part) and low oscillations (i.e. smaller imaginary part). Conversely short period modes are recognized by their high damping (i.e. larger real part) and high high frequency (i.e. larger imaginary part). In Figure 5.6, it is seen that phugoid eigenvalues for each configuration are similar and stable. The conventional and tsa configurationa are found to have two real roots in short period mode, which is due to their damping ratio value of 1.

Lateral/directional handling qualities covers Dutch roll, spiral and roll modes. Dutch roll natural frequency is directly proportional to yawing-moment-due-to-sideslip C_{n_β} and inversely proportional to yawing inertia I_{zz}. The reason why tsa fails to have a satisfactory handling quality with respect to Dutch roll frequency is that it has a comparably higher I_{zz}. As already mentioned, high I_{zz} of tsa is because of the higher number of point masses distributed along the y axis due to its three horizontal surfaces. Dutch roll damping is related to C_{n_β}, C_{y_β}, C_{n_r} derivatives which are highly contributed by the vertical tail geometry and position, and I_{zz}. All configurations satisfy the Dutch roll damping ratio requirement. Roll mode time constant, which is another assessment parameters of lateral/directional handling qualities, meets the requirement for each configuration.

In order to have a clear sight on stability of those modes, eigenvalues of each mode of each configuration are

presented in Figure 5.7.

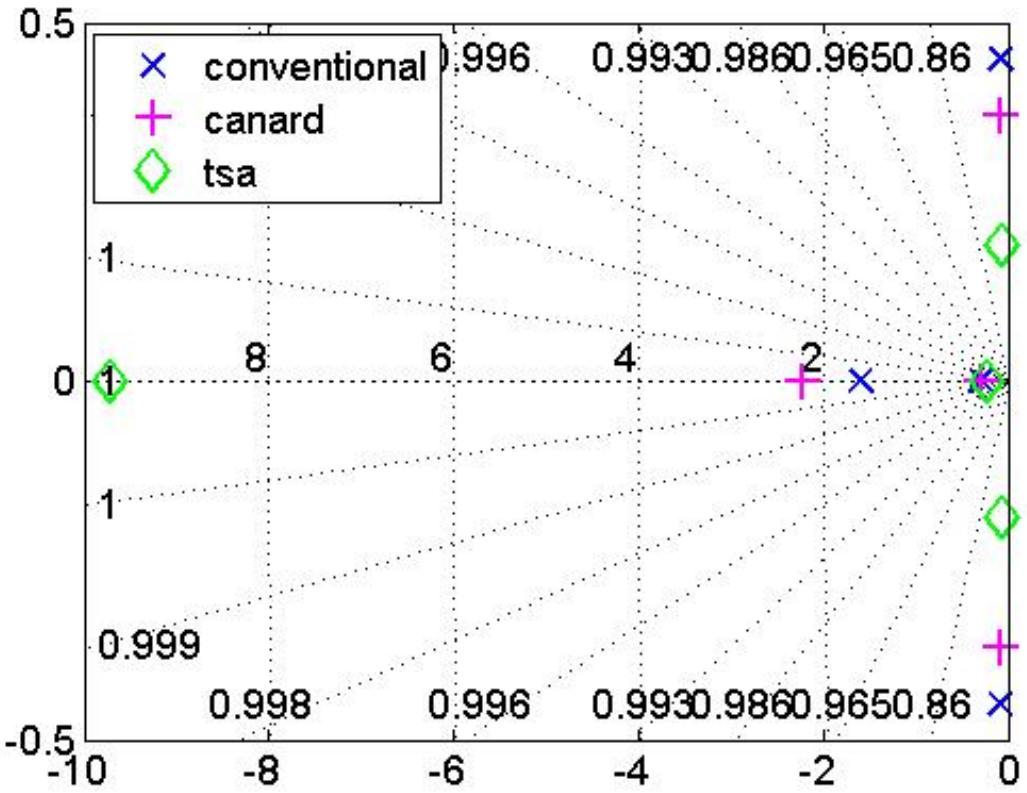

Figure 5.7: Eigenvalues of lateral/directional modes

As it has been mentioned, lateral/directional modes include one oscillatory and two real modes. In Figure 5.7 roll mode eigenvalue of tsa seems to be too high which is not so reliable. Other two configuration has reliable stable values. In order to see the differences of other modes, the figure is zoomed in Figure 5.8. Here, the Dutch roll eigenvalues for each configuration are found to be stable as they are on the negative side. Conventional and canard configurations have higher damping and higher oscillation compared to the tsa. Comparison of spiral eigenvalues show that all configurations have negative real value which actually was not expected as spiral has usually unstable (i.e positive) values.

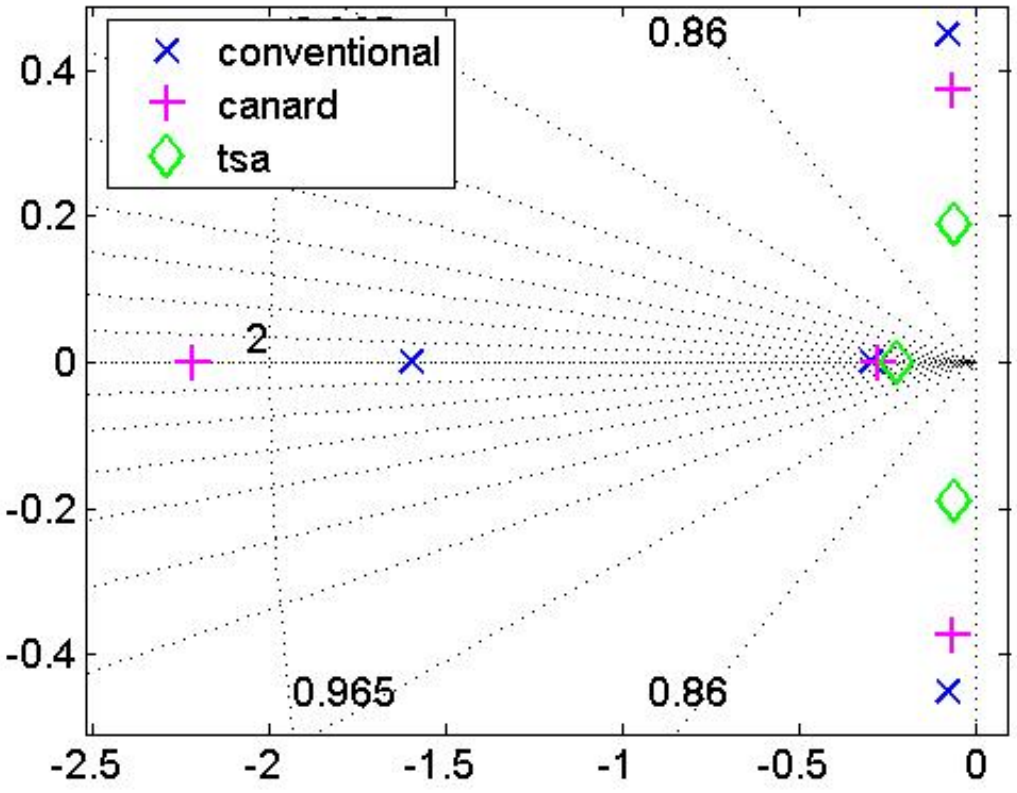

Figure 5.8: Zoomed eigenvalues of lateral/directional modes

6

CONCLUSION

The goal of this project has been defined as

Develop a rapid geometry-based inertia estimation method applicable for different aircraft configurations which would accelerate the estimation of handling qualities in a design environment

In order to reach this goal, the main question of the research has been determined as

How to estimate the inertial properties of conventional and unconventional configurations, as well as control and stability derivatives, to assess handling qualities during the conceptual design phase?

The question was answered considering three parts. The first part focused on inertia estimation, which was determined to be the main goal of the project. After conducting a literature research on existing inertia estimation and weight estimation methods, based on the state-of-art, the aircraft was divided into three categories namely bodies of revolution, lifting surfaces and point masses. Aircraft components were gathered in those categories according to their shapes. Fuselage and nacelle bodies were categorized as bodies of revolution. Lifting surfaces included main wing, horizontal and vertical stabilizers as the name suggests. The rest of the aircraft components were assumed to be point masses. Moments of inertia of components were calculated according to their categorization. This classification has made the calculation process design sensitive and rapid. Second part, which was related to control and stability derivatives estimation, was performed by implementing an available empirical method directly to Initiator. Having calculated the required parameters, attention was given to handling qualities estimation. The outputs of implemented modules in Initiator were used as input for the estimation of handling qualities in FMT.

The implemented method was used in different aircraft configurations. Both inertia and control and stability derivatives of each configuration were calculated in Initiator. They were used as inputs for Flight Mechanics Toolbox to acquire handling qualities. Hence, the influence of configuration on its inertia and consequently on aircraft behavior has been able to examined in a rapid process. The confidence was gained on the accuracy of inertia estimation method by the validation. The error percentages found to be acceptable by conducting a sensitivity analysis on handling quality assessment. A validation study is also performed on the implemented control and stability derivatives estimation method. Calculated control and stability derivatives found to have comparably higher error percentages. Therefore, the comparison of handling qualities with respect to different configurations can not be fully trusted due to low reliability of stability and control derivatives results.

In terms of configuration comparison with respect to longitudinal handling quality assessment conventional configuration and tsa configurations seem to have similar performances. According to lateral/directional handling qualities best performance was observed in conventional configuration. Hence, it can be concluded that conventional aircraft would be the most satisfactory configurations regarding the handling quality assessment while the canard configuration would not be a preferable design.

7

RECOMMENDATIONS

Based on the research performed and obtained results, several recommendations can be given for future research and further improvements.

7.1. RECOMMENDATIONS RELATED TO INERTIA ESTIMATION METHOD

Inertia estimation method is created based on several calculation methods available in the literature. It is given high importance to have the method primarily geometry based. This aim was accomplished for the airframe structures fuselage, nacelle, and main wing. Even though the method implemented to estimate the main wing inertia would be suitable to use for other lifting surfaces, namely horizontal and vertical stabilizers, this was not possible due to the lack of required structural input. As aforementioned in Section 3.1.2, in order to use the lifting surfaces inertia estimation method, weight fractions of spar, skin and ribs to total component weight are required. Since Inertia uses EMWET for the main wing weight calculations, those required parameters were calculated by the use of wing planform parameters and EMWET thickness outputs. However the weight calculations of horizontal and vertical stabilizers are performed by Class 2.5 weight estimation methods. Therefore it is not possible to gather detailed structural information of those surfaces which would be subsequently used to calculate the weight fractions. It would be better to change from that method of calculation into EMWET so that required structural parameters can be determined and the presented lifting surface inertia estimation method can be benefited. This way the empirical relations that are proposed by DATCOM can be omitted and a more physics based calculation of inertia can be performed. This would lead to a significant improvement on the total aircraft inertia estimation considering the sizes of those components.

Another future improvement related to estimation of inertia could be related to the systems and operational items. Weight and center of gravity information of those components are obtained from Class 2.5 weight estimation module. According to the output, those components are considered to be point masses which are located at fuselage c.g. and their inertias are calculated in regard to that. Even though some changes were done in positioning several items, such as repositioning APU more rearward or crew more forward, a layout of the placement of each system along the whole aircraft can be created. This would be much more realistic as aircrafts do not have those items exactly at its fuselage c.g. but has them distributed along the body. Moreover, even though items such as APU or instruments would make sense to be assumed as point masses, this assumption is not as valid for hydraulics or residual fuel as former ones. Therefore, a layout can be assumed based on existing aircraft knowledge which would be comparably more reliable. Hence, the more realistic the replacement of systems and operational items are made, the more accurate the inertia estimation would be.

The validation of the method provided confidence in estimation of moment of inertia. However the error percentages can be decreased by considering mentioned recommendations for future work.

7.2. RECOMMENDATIONS RELATED TO CONTROL AND STABILITY DERIVATIVES ESTIMATION METHOD

As calculation of control and stability derivatives was not the main focus of this thesis, it has been performed by directly implementing the method proposed by [15]. Even though a validation study is performed a sensitivity analysis on handling quality assessment was not performed due to lack of further real data. Therefore the influence of errors occurred in control and stability derivatives estimation on the handling qualities could not be checked. Finding real data of each required input would provide a handling quality comparison with respect to changes in derivatives. Hence, the method can be improved according to outcome.

As it has been mentioned, the position and sizing of lifting surfaces are directly obtained from Geometry module, and do not depend on new design modules in Initiator due to the timing of this thesis. This yields misleading results in especially stability derivatives as they are highly influenced by stabilizer parameters. Vertical tail position with respect to aircraft c.g. and its size is of importance in calculation of stability derivatives due to sideslip angle, roll and yaw rates which consequently affects lateral/directional handling qualities of the aircraft. An increase in vertical tail size or in distance with respect to aircraft c.g. that are obtained from the design modules could yield incomparably improved lateral stability. Likewise, a change in horizontal stabilizers' either position or sizing would have a significant effect on longitudinal stability parameters since it is primarily influenced by that. Pitching moment, which is highly dependent on horizontal stabilizer parameters, would have an improved result which would lead to improved longitudinal handling qualities.

Geometry of control surfaces has to be known in order to calculate the control derivatives. However Initiator does not have such a module that handles the stabilizer surface sizing. Therefore, a simple sizing of ailerons, rudder, elevator and canard control surface was performed with respect to the available aircraft knowledge. Since geometries of all case studies were created based on a A320-200, the sizing of the control surfaces was also done with respect to real sizing of that aircraft. Even though it would give proper results for similar aircrafts it can not be reliable for every configuration. Therefore control surface sizing should be done in a more generic way. Since moment of inertia and handling qualities of the aircraft would eventually have an effect on the sizing of these surfaces, the module to be created should have an iterative process concerning these parameters and should be based on the feedback of those.

Estimation module of control and stability derivatives take angle of attack, angle of sideslip, pitch, roll and yaw rates derivatives leaving the derivatives due to velocity, angle of attack rate, and angle of sideslip rate. This has been done due to lack of time and due to their comparably negligible contributions on total aerodynamic coefficients. In future studies, those derivatives can be added to estimation as well.

II

Implementation

8

IMPLEMENTATION IN INITIATOR

For the purpose of this thesis, an in-house conceptual design tool Initiator is used for inertia and control and stability derivatives estimation. As it has been briefly covered in the tool description, the Initiator activity diagram is presented in Figure 8.1.

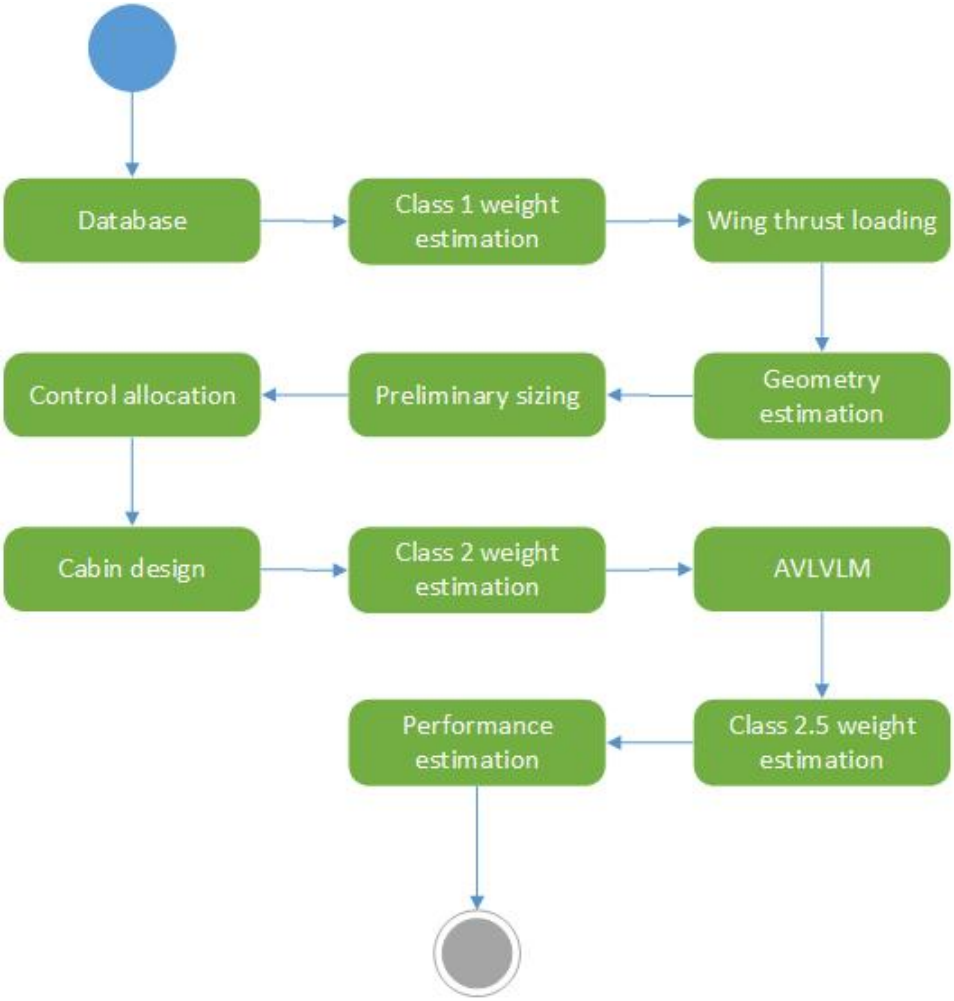

Figure 8.1: Activity diagram of Initiator

The implementation of inertia estimation and control and stability derivative calculation methods in Initia-

tor are explained by the help of activity diagrams in this chapter.

8.1. INERTIA ESTIMATION MODULE

Created inertia estimation module is dependent on the Aircraft Geometry and several results from Class 2.5 Weight Estimation and EMWET modules. Based on the methodology that is presented in Chapter 3, the components' inertias are calculated with different functions according to their shapes.

For the bodies of revolution, which contains fuselage and nacelle shaped components, the geometry data in X,Y,Z directions are gathered. The activity diagram of this function is shown in Figure 8.2.

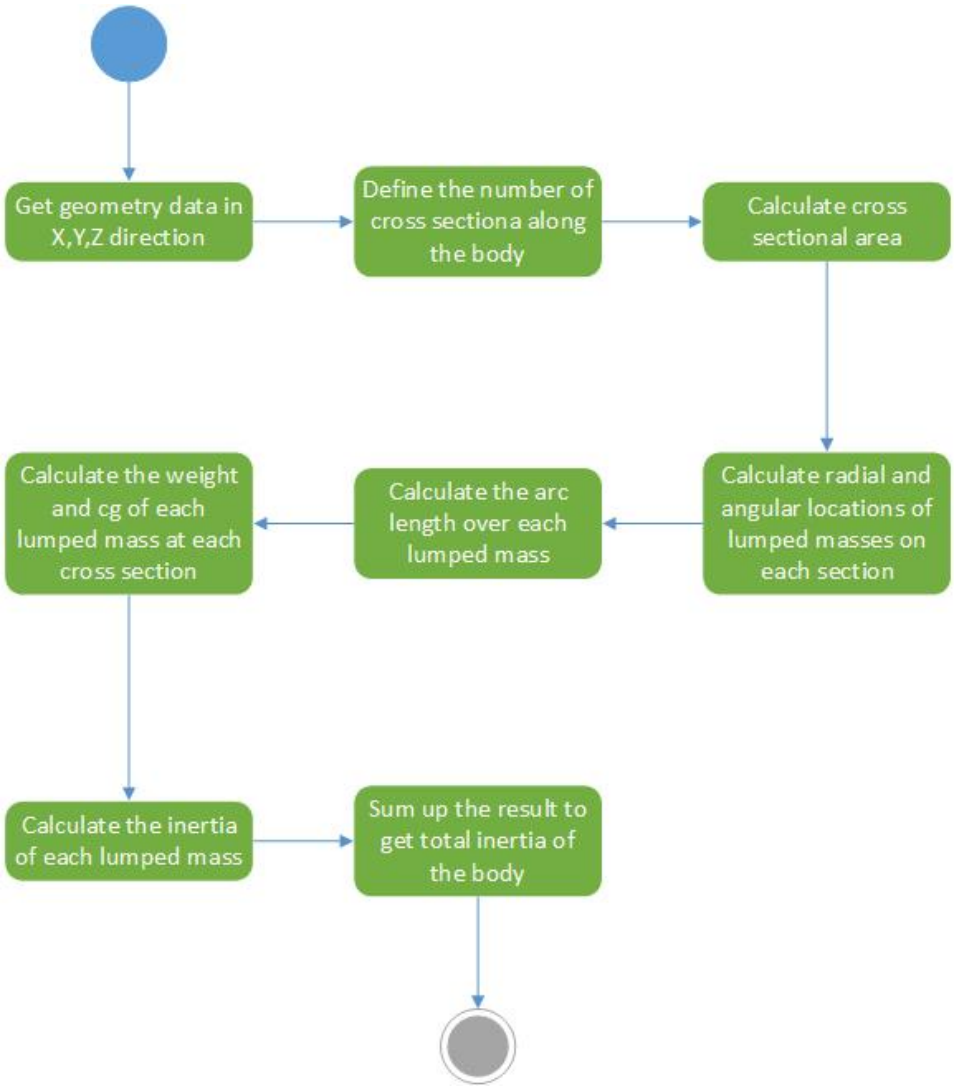

Figure 8.2: Activity diagram of inertia estimation function of bodies of revolution

For the lifting surfaces the activity diagram is shown in Figure 8.3 where the process of subfunction for calculation of the weight fractions are presented in Figure 8.4.

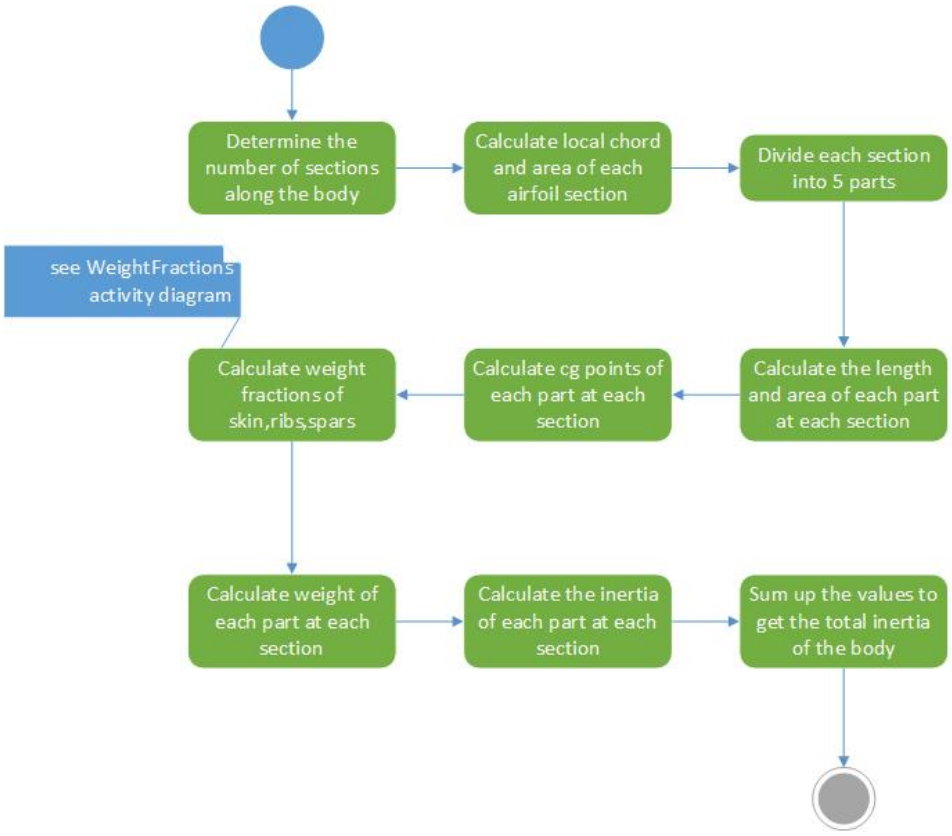

Figure 8.3: Activity diagram of inertia estimation function of lifting surfaces

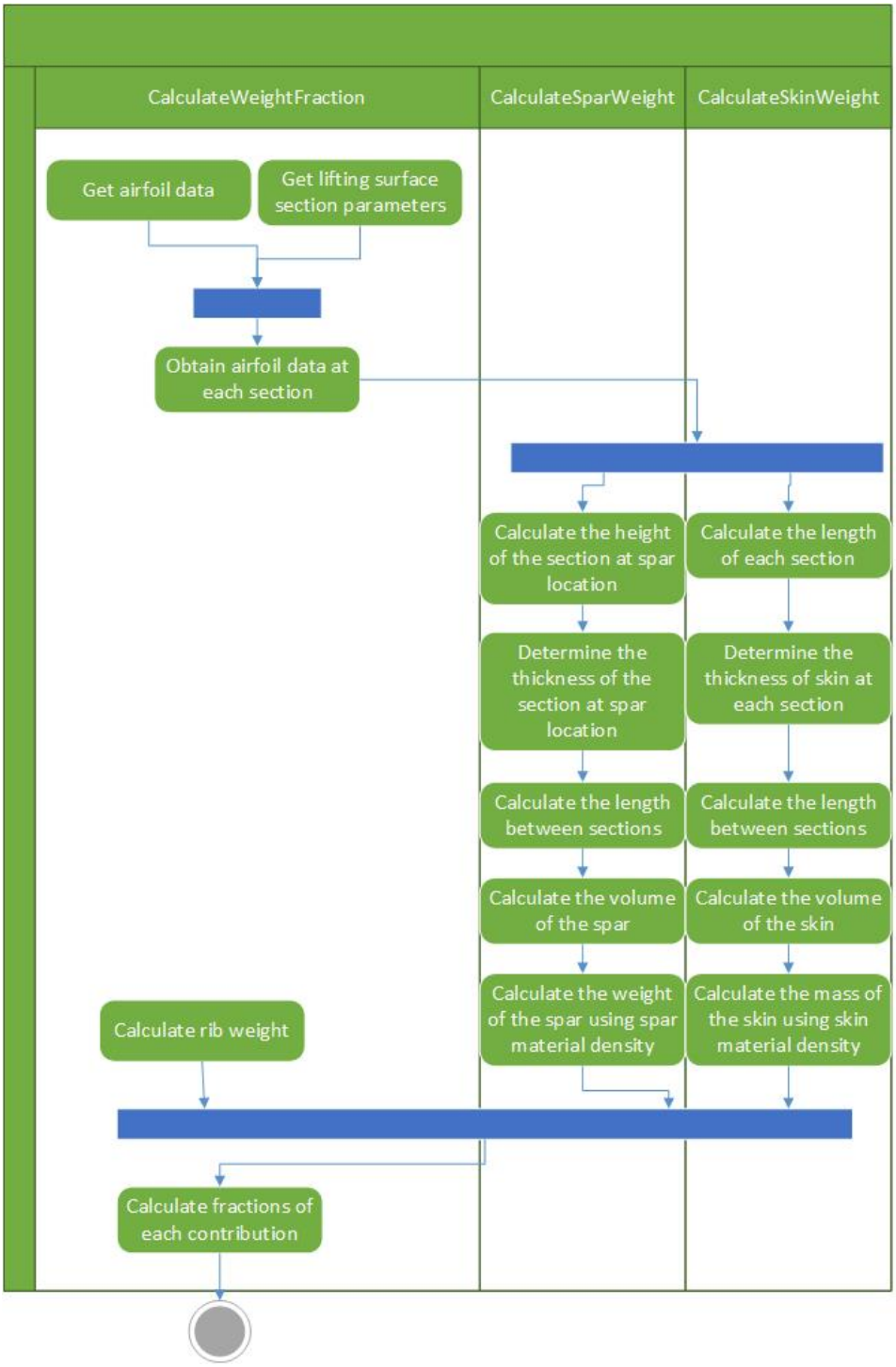

Figure 8.4: Activity diagram of weight fractions calculation

For the rest of the aircraft components such as landing gear, systems and controls PointMassInertiaEstimation function is called. The activity diagram is shown in Figure 8.5.

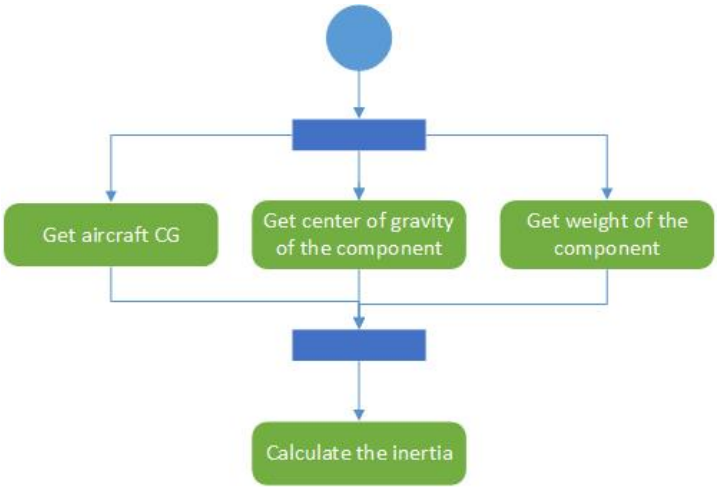

Figure 8.5: Activity diagram of inertia estimation function of point masses

8.2. CONTROL AND STABILITY DERIVATIVES ESTIMATION MODULE

The control and stability derivatives estimation module has dependency on Class2.5 Weight Estimation and EMWET modules. The activity diagram is simply shown in Figure 8.6.

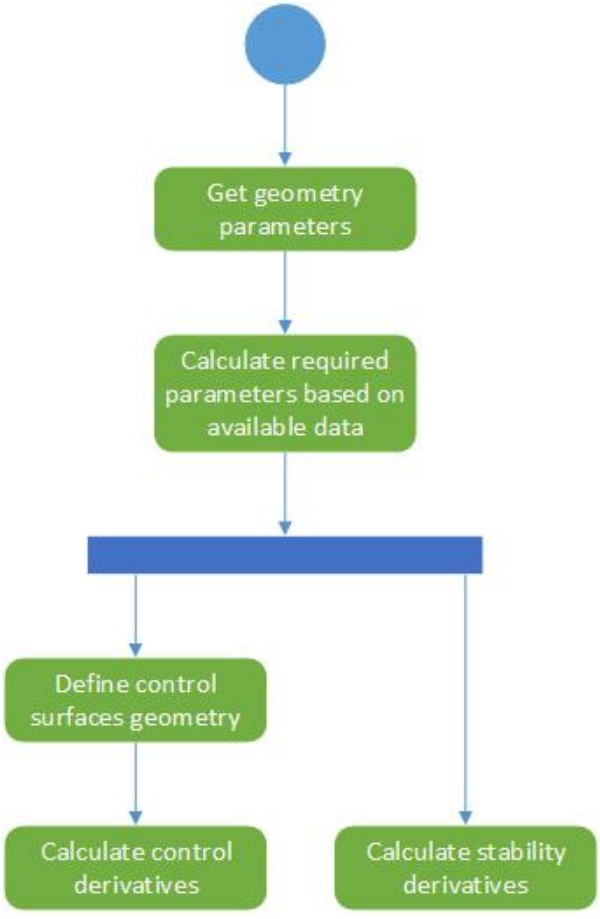

Figure 8.6: Activity diagram of control and stability derivatives estimation module

Activity diagrams for stability derivatives estimation are represented separately as follows.

Stability derivatives due to angle of attack are shown in Figure8.7, Figure 8.8, and Figure8.9.

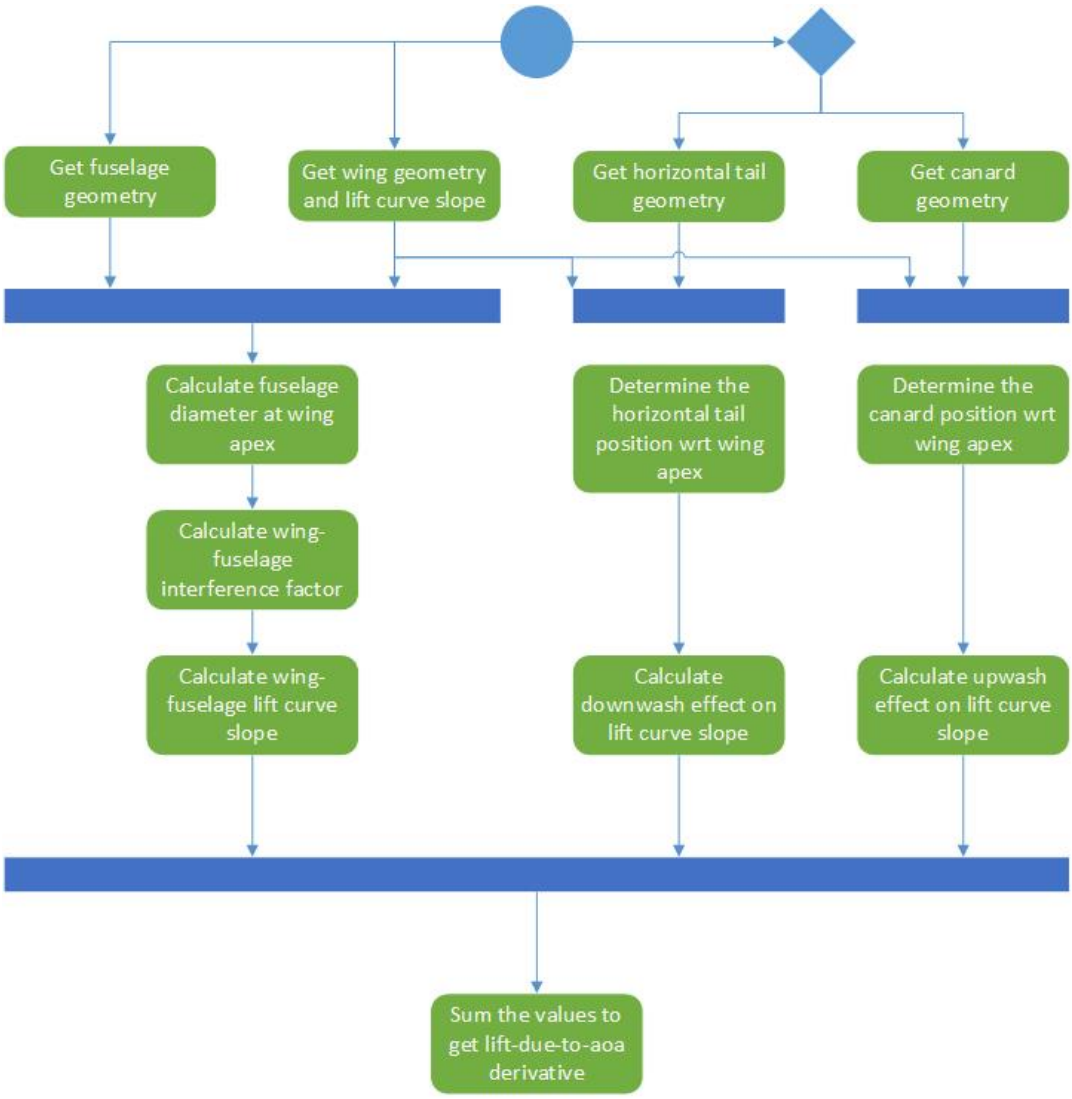

Figure 8.7: Activity diagram of lift-due-to-aoa derivative estimation

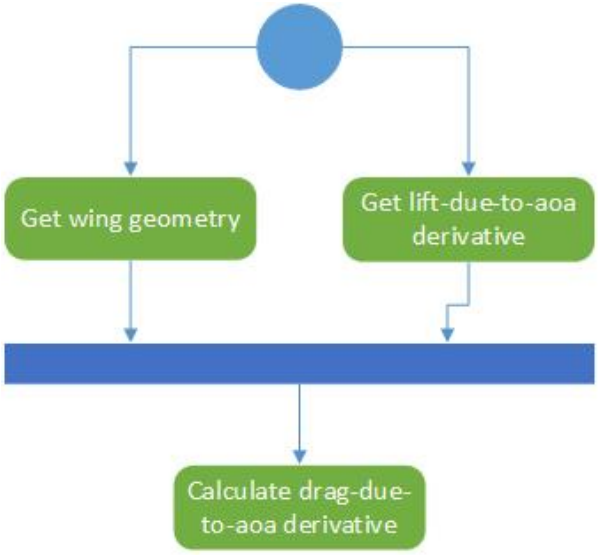

Figure 8.8: Activity diagram of drag-due-to-aoa derivative estimation

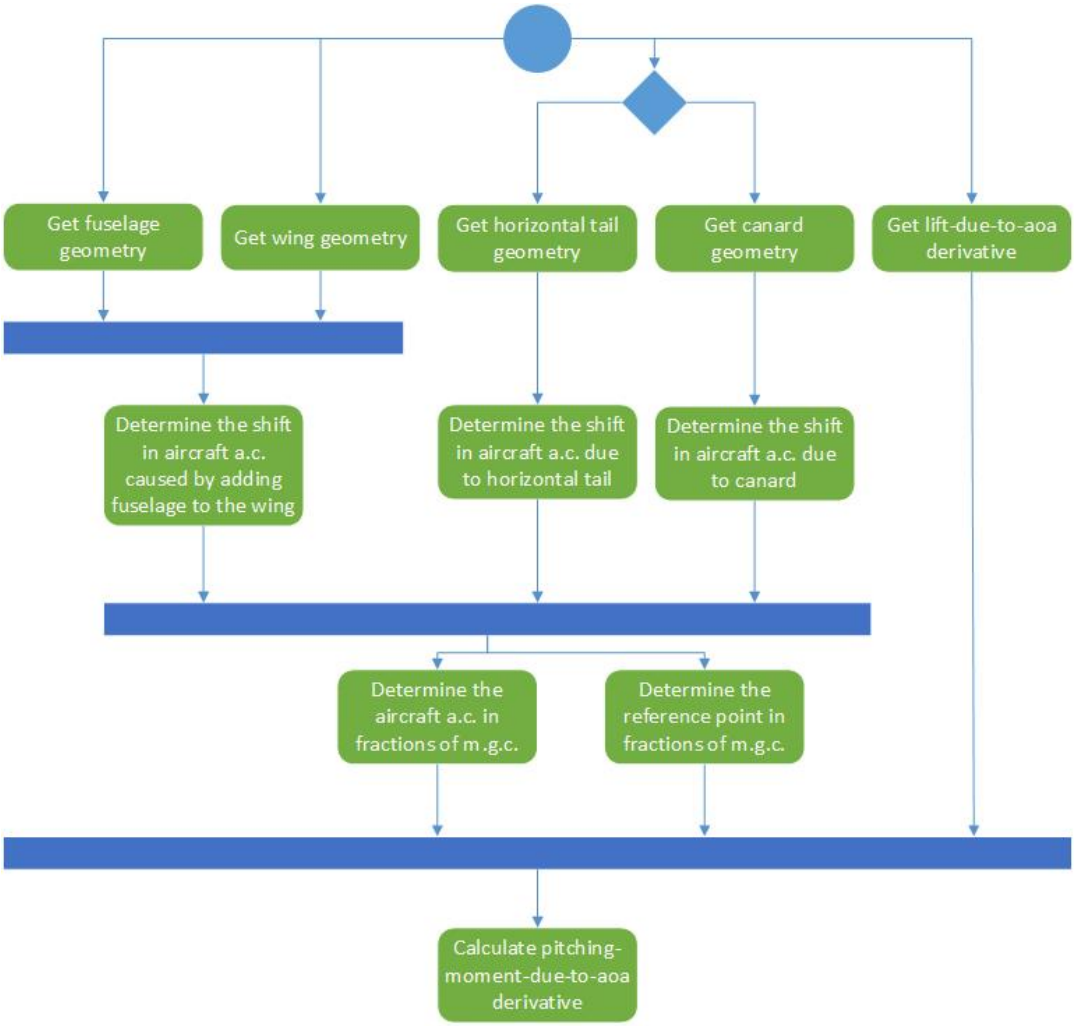

Figure 8.9: Activity diagram of pitching-moment-due-to-aoa derivative estimation

Stability derivatives due to angle of sideslip are shown in Figure8.10, Figure8.11, and Figure8.12.

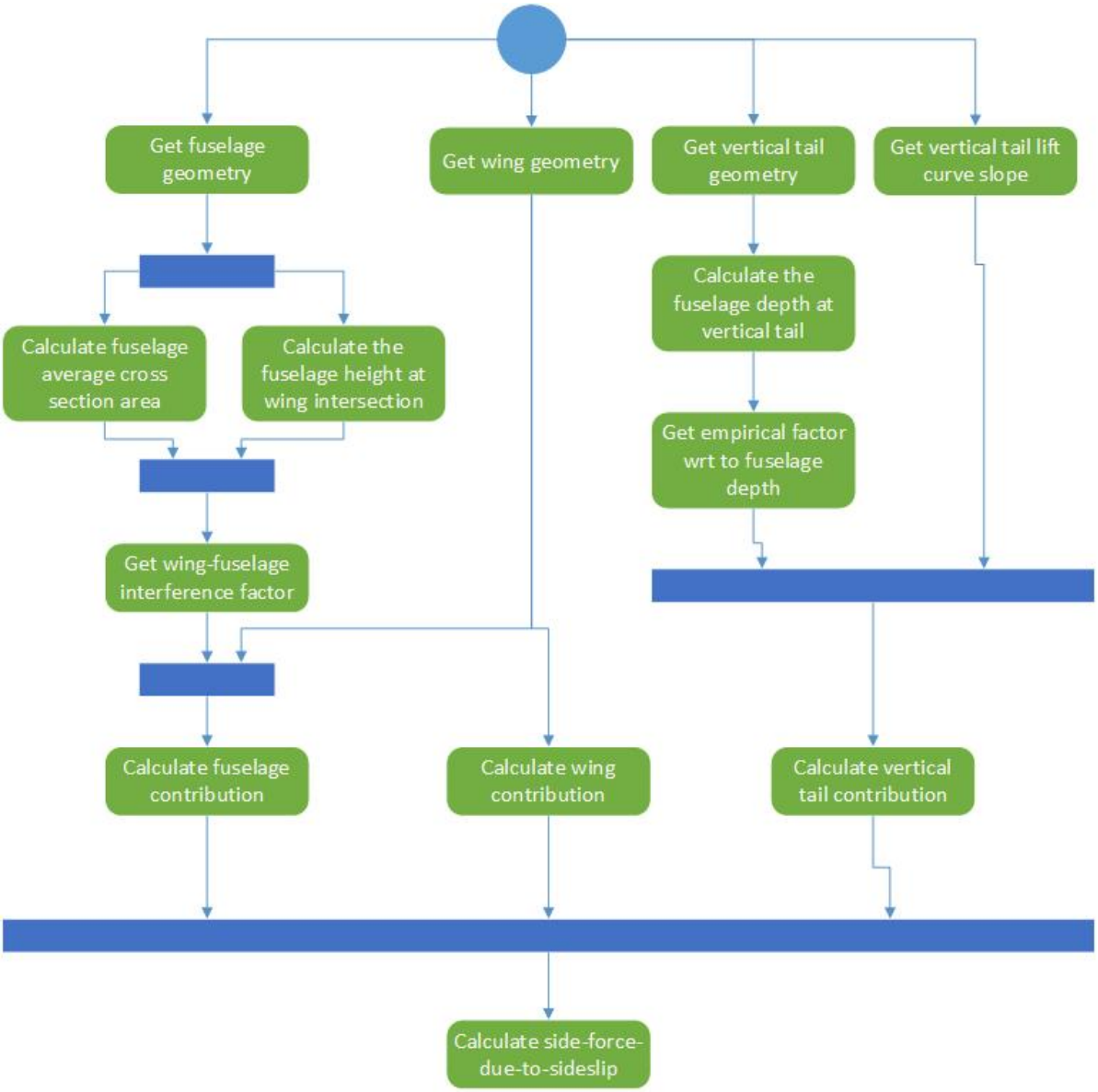

Figure 8.10: Activity diagram of side-force-due-to-sideslip derivative estimation

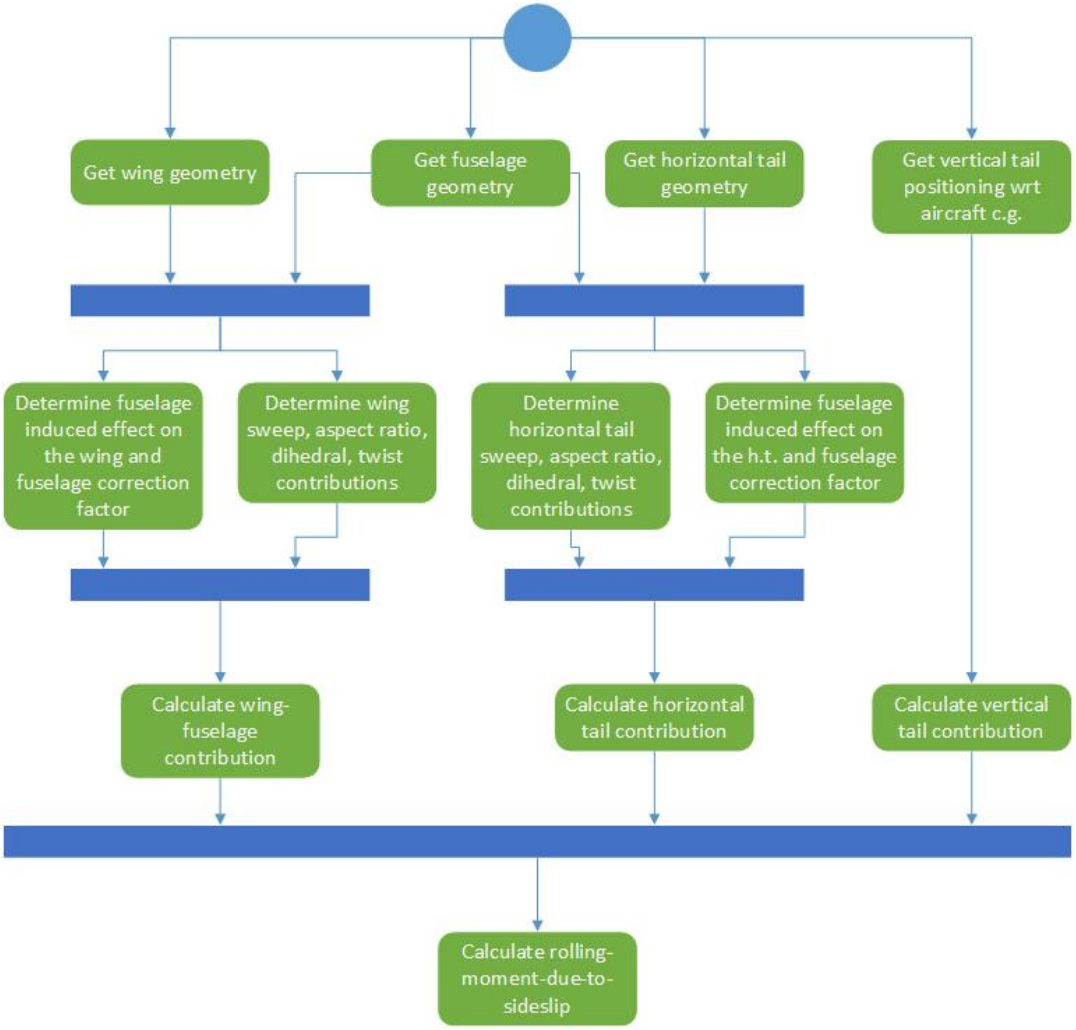

Figure 8.11: Activity diagram of rolling-moment-due-to-sideslip derivative estimation

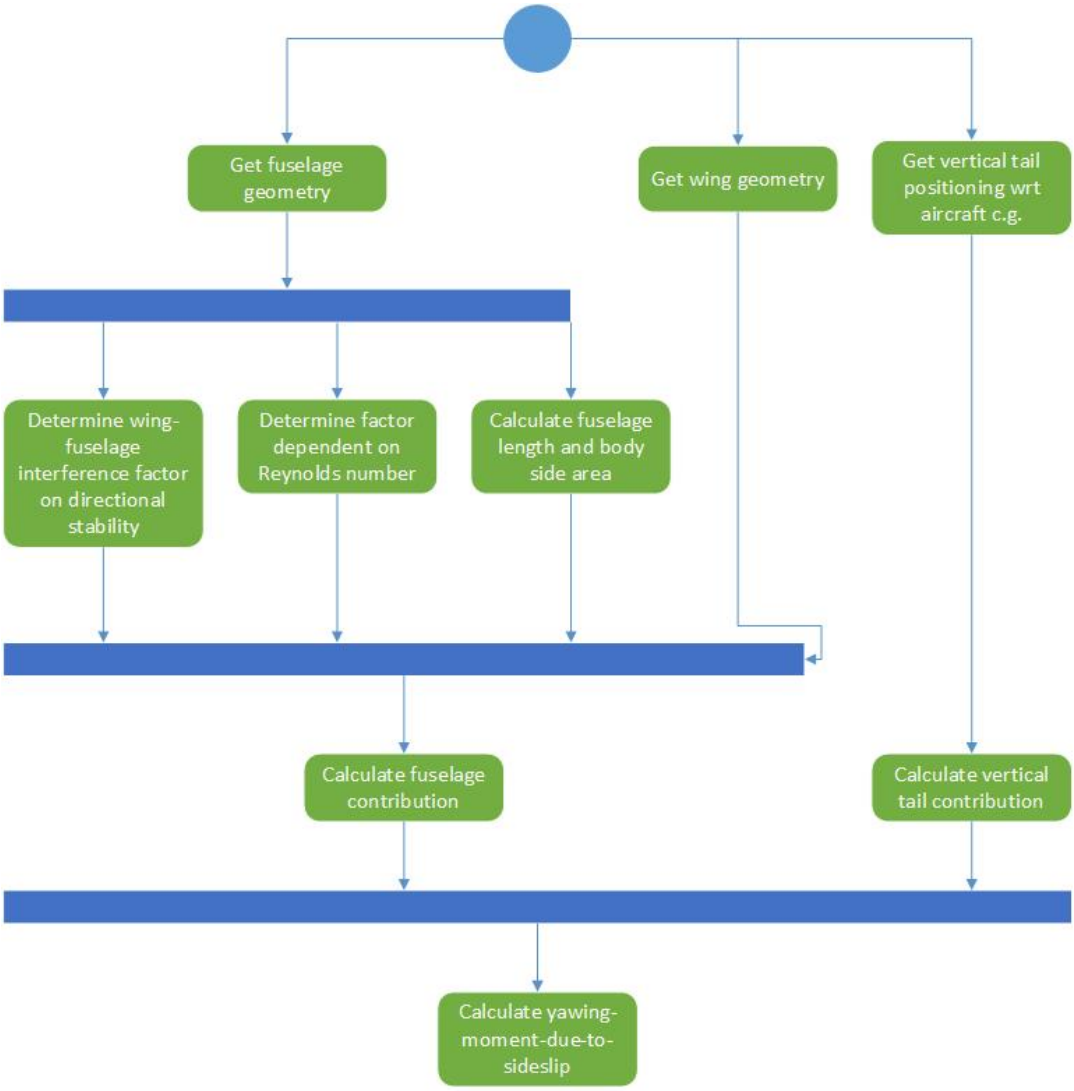

Figure 8.12: Activity diagram of yawing-moment-due-to-sideslip derivative estimation

Stability derivatives due to roll rate are shown in Figure8.13, Figure8.14, and Figure8.15.

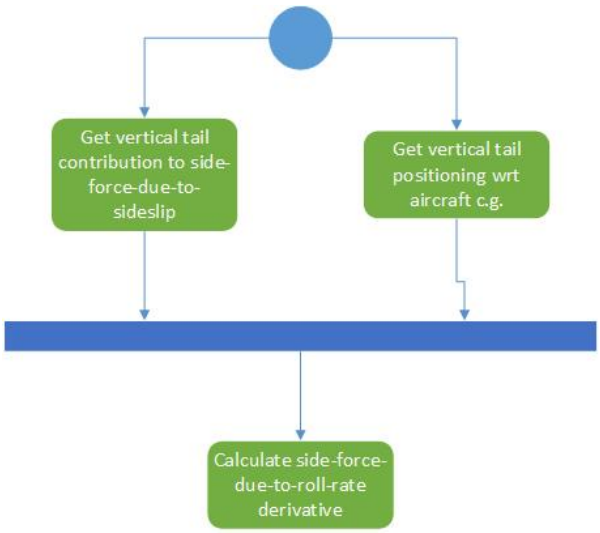

Figure 8.13: Activity diagram of side-force-due-to-roll-rate derivative estimation

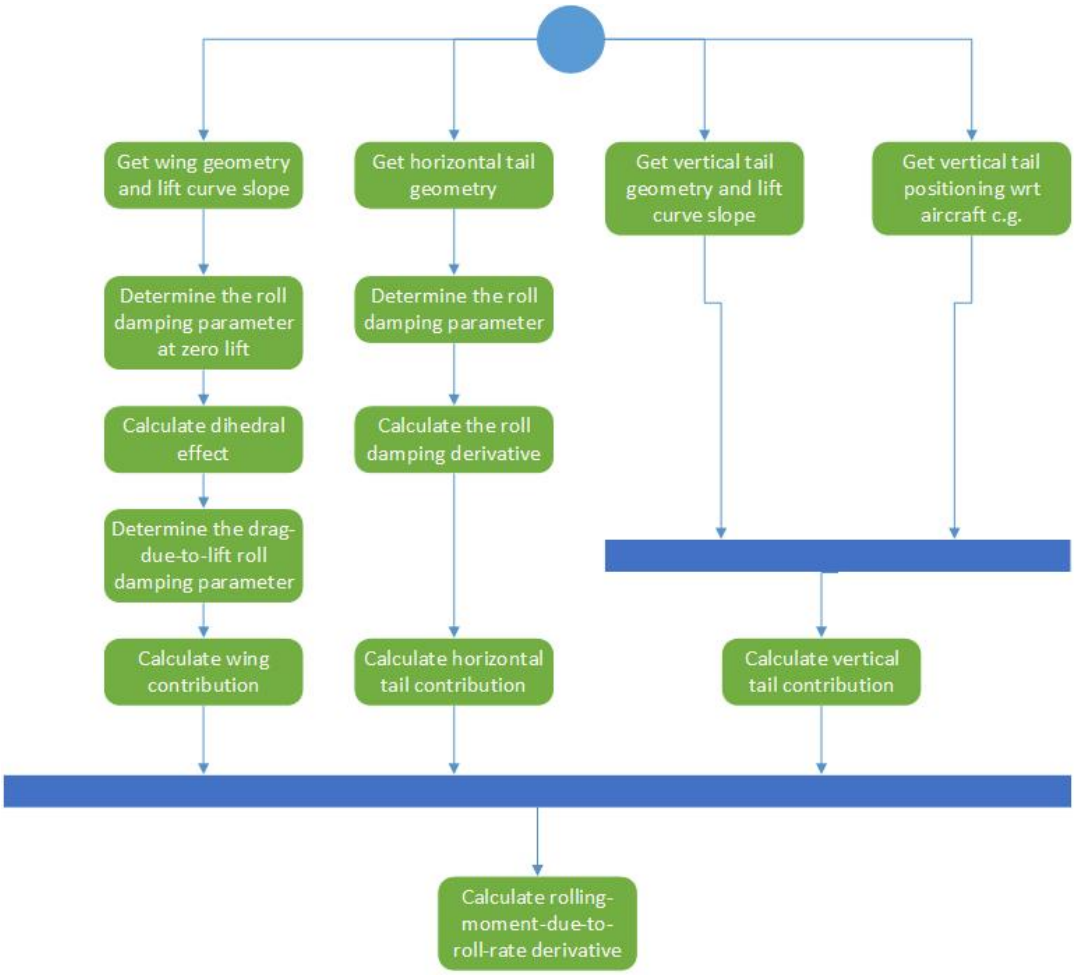

Figure 8.14: Activity diagram of rolling-moment-due-to-roll-rate derivative estimation

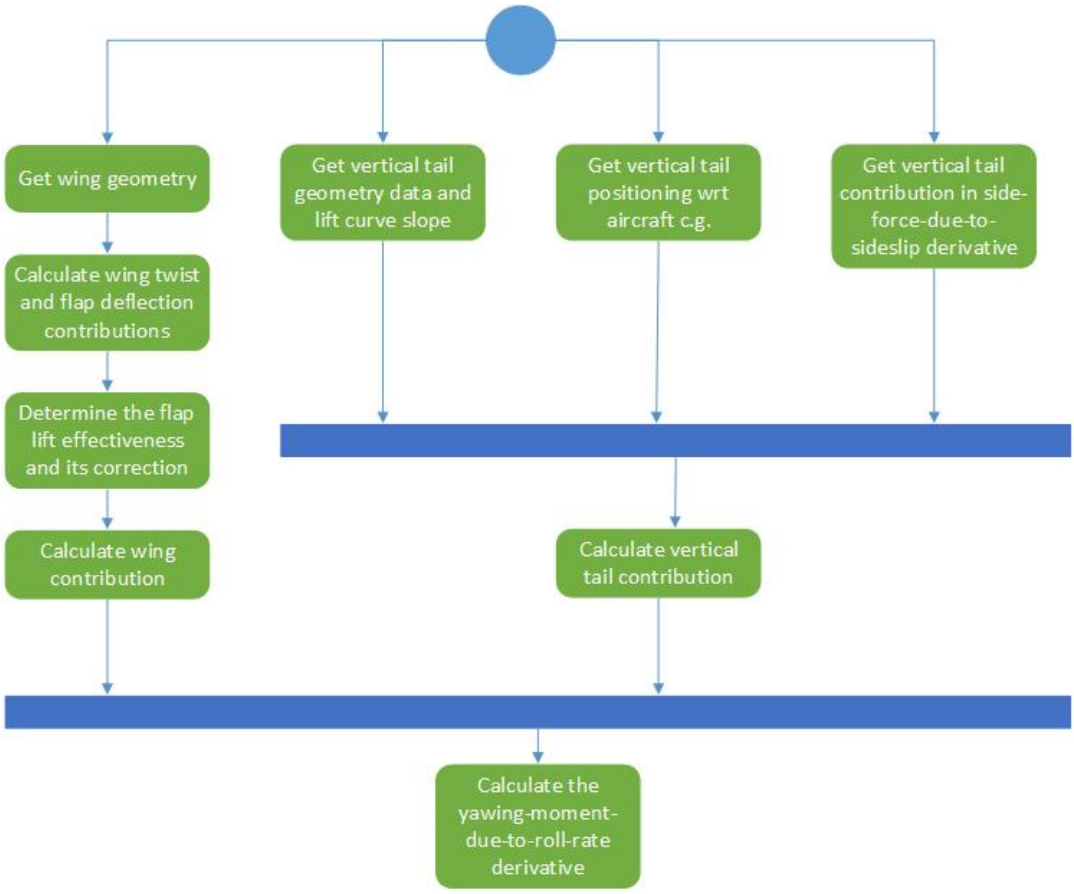

Figure 8.15: Activity diagram of yawing-moment-due-to-roll-rate derivative estimation

Stability derivatives due to pitch rate are shown in Figure 8.16, Figure8.17, and Figure8.18.

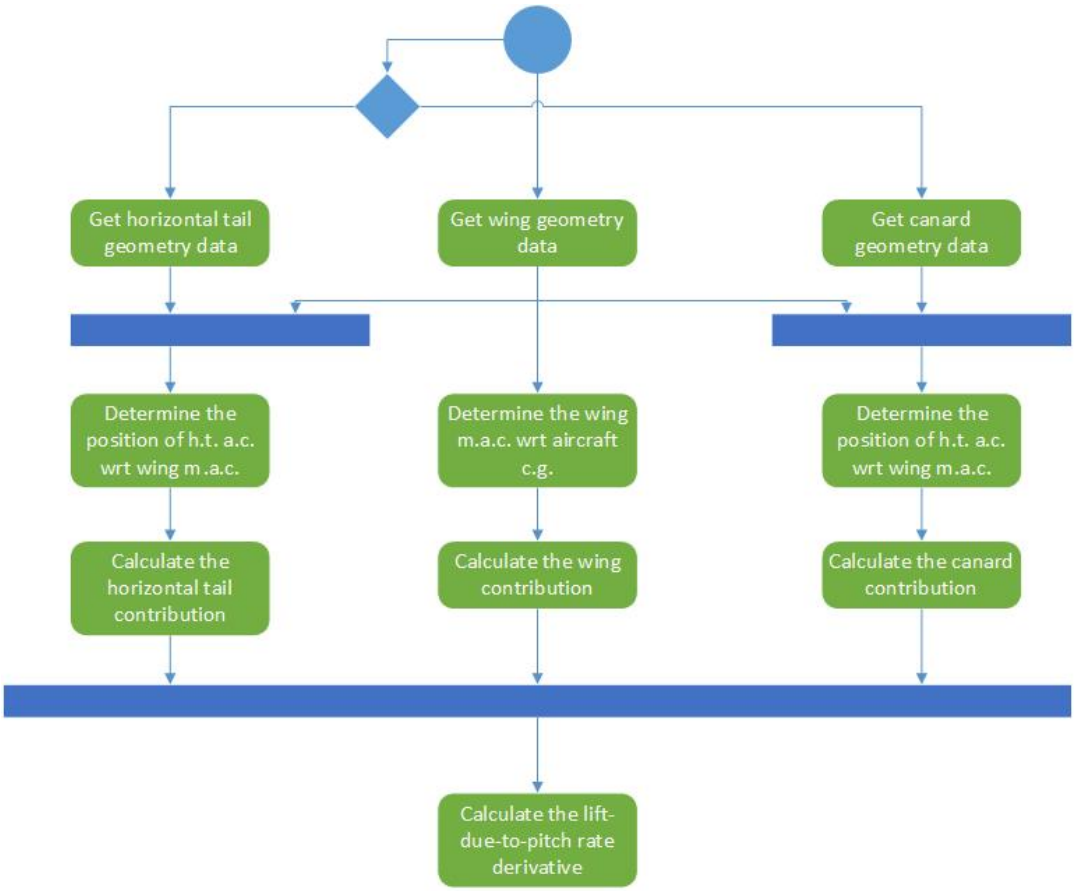

Figure 8.16: Activity diagram of lift-due-to-pitch-rate derivative estimation

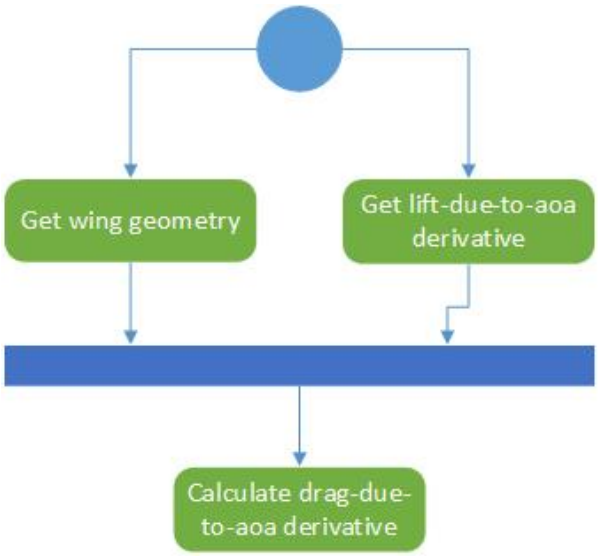

Figure 8.17: Activity diagram of drag-due-to-pitch-rate derivative estimation

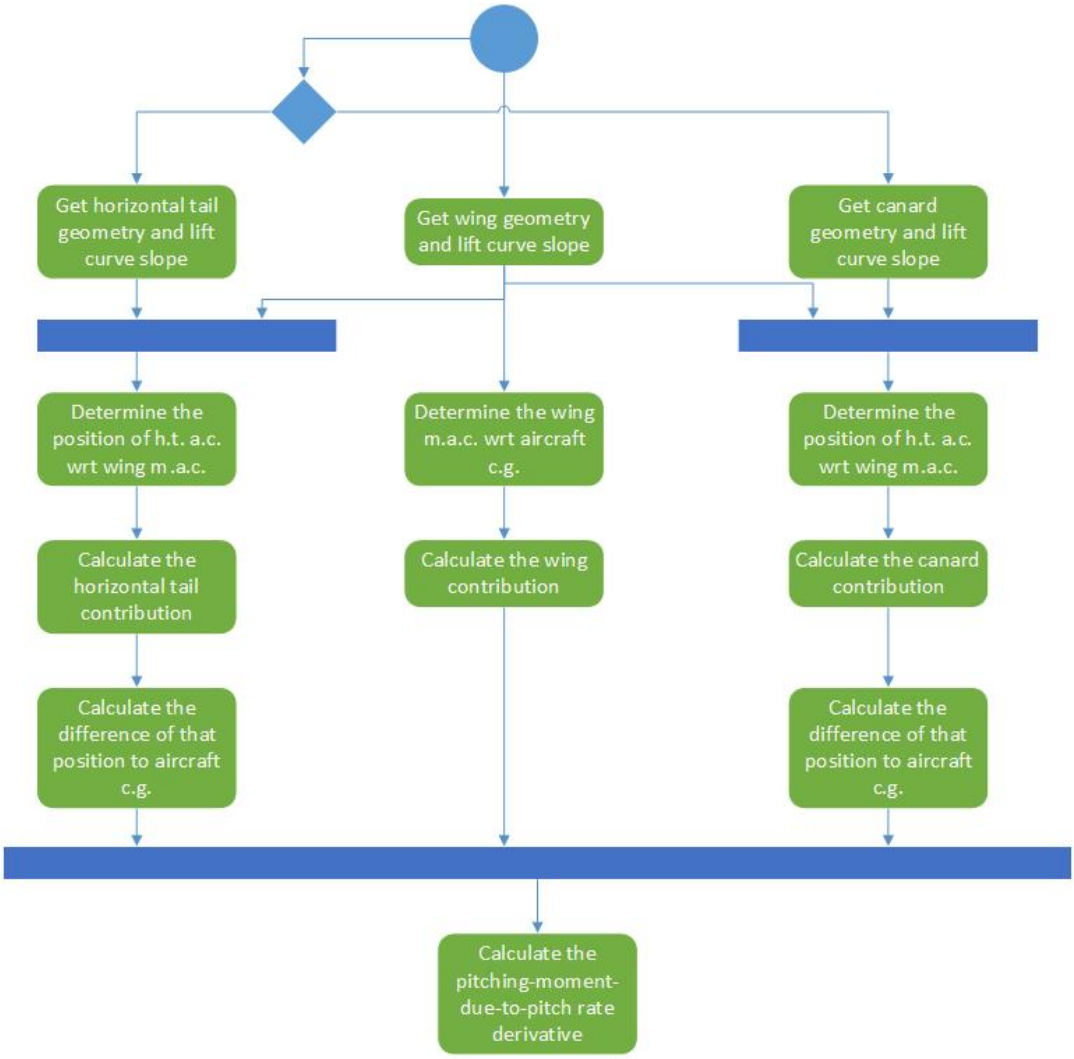

Figure 8.18: Activity diagram of pitching-moment-due-to-pitch-rate derivative estimation

Stability derivatives due to yaw rate are shown in Figure 8.19, Figure 8.20, and Figure 8.21.

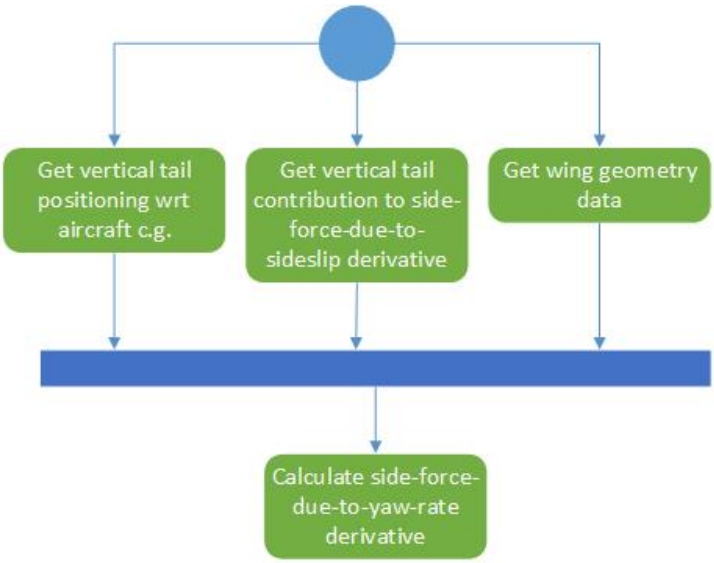

Figure 8.19: Activity diagram of side-force-due-to-yaw-rate derivative estimation

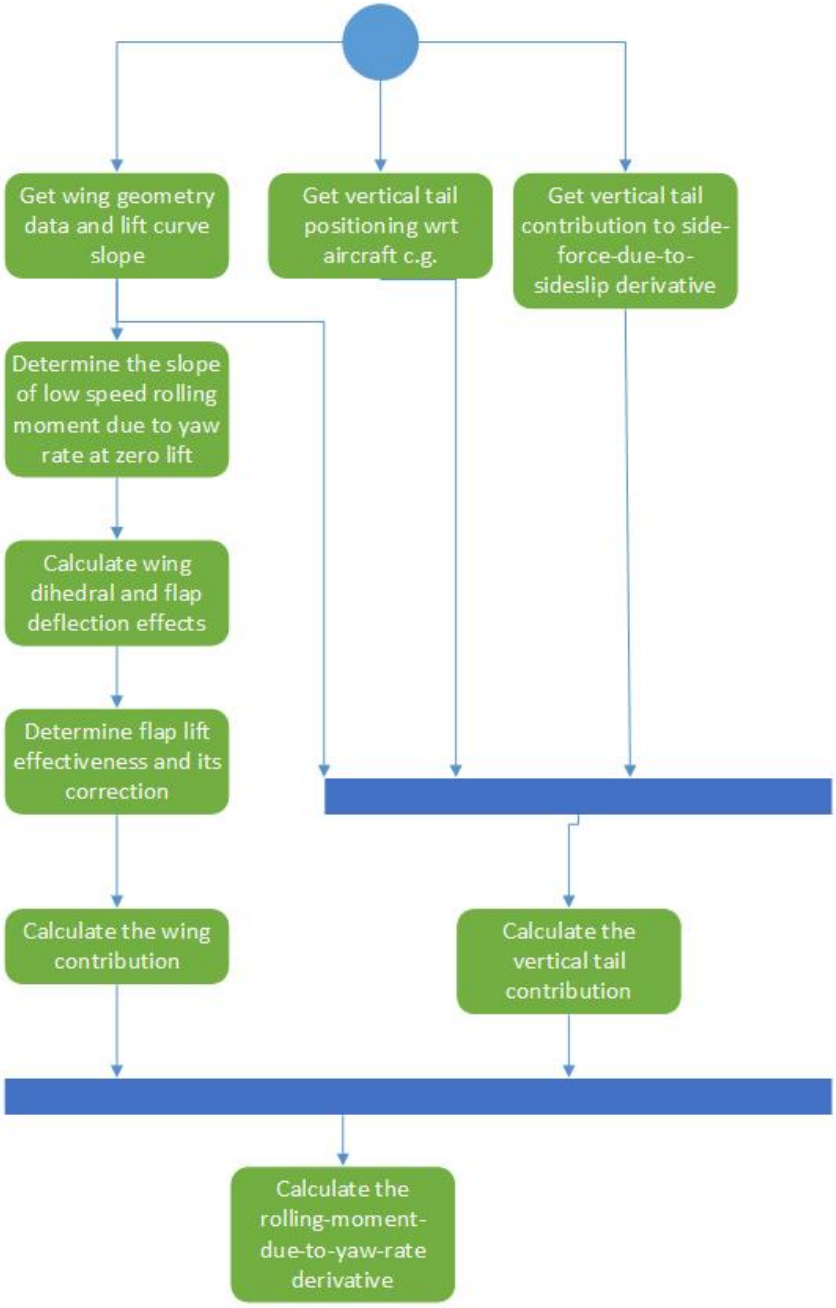

Figure 8.20: Activity diagram of rolling-moment-due-to-yaw-rate derivative estimation

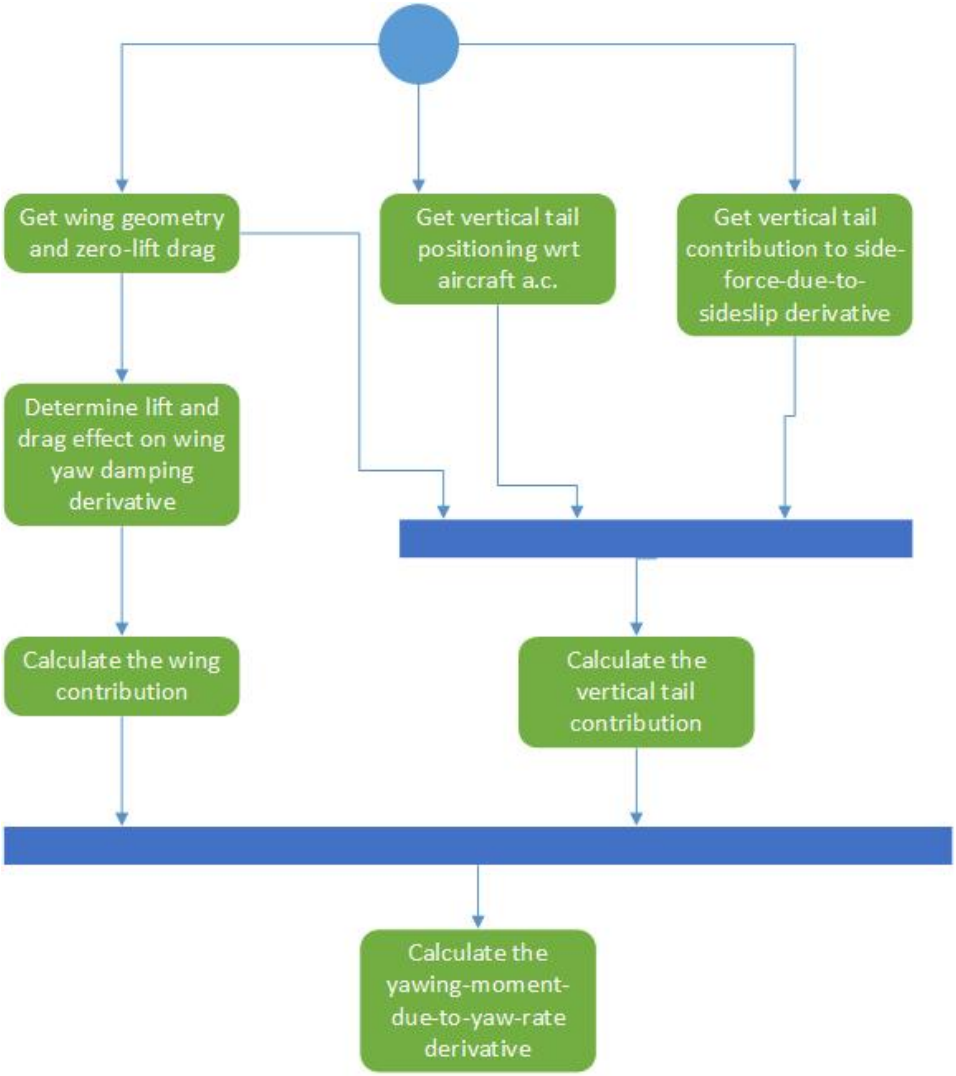

Figure 8.21: Activity diagram of yawing-moment-due-to-yaw-rate derivative estimation

Activity diagrams for control derivatives estimation method are shown in Figure8.22, Figure8.23, Figure8.24, and Figure8.25 for aileron, rudder, elevator and canardvator respectively.

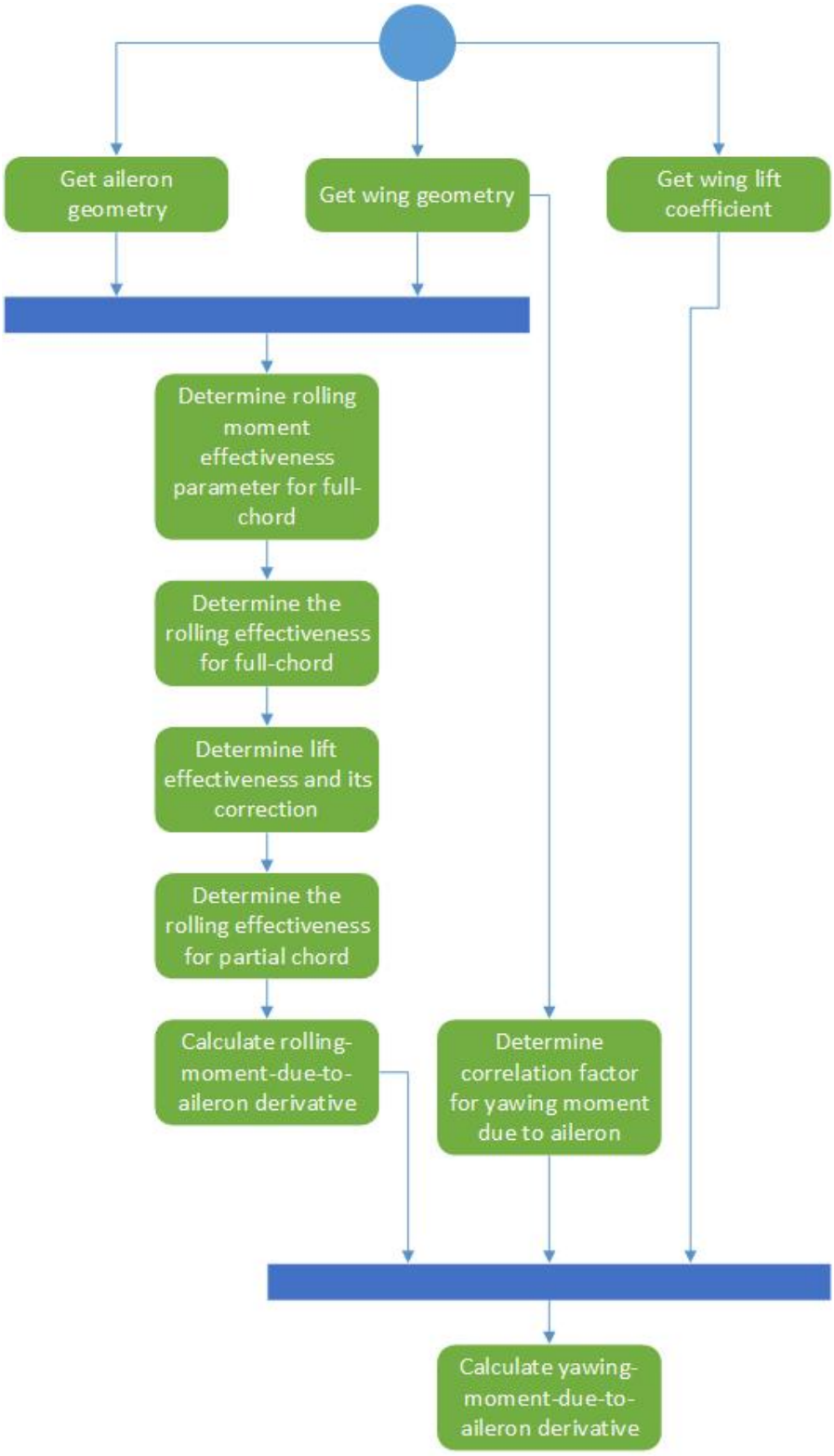

Figure 8.22: Activity diagram of control derivatives due to aileron deflection estimation

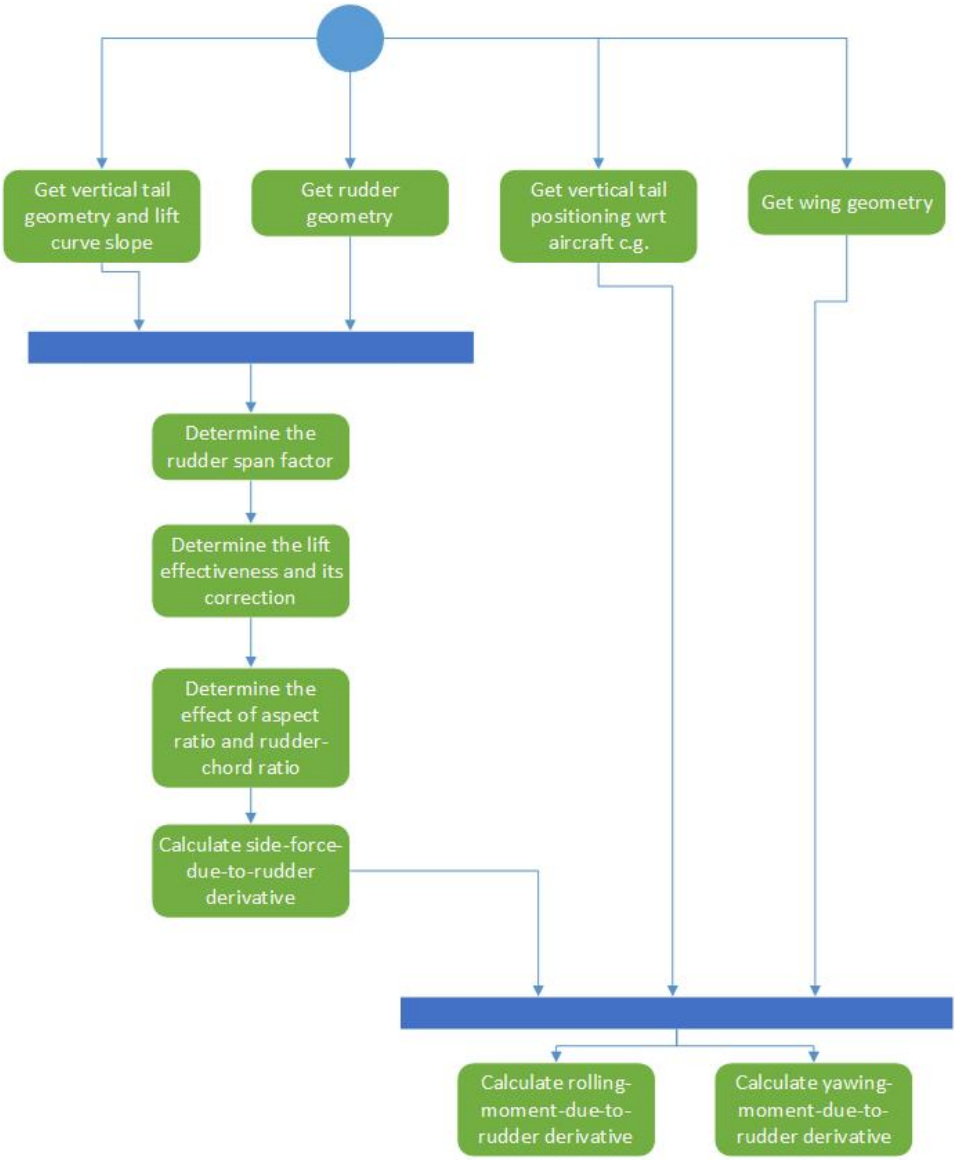

Figure 8.23: Activity diagram of control derivatives due to rudder deflection estimation

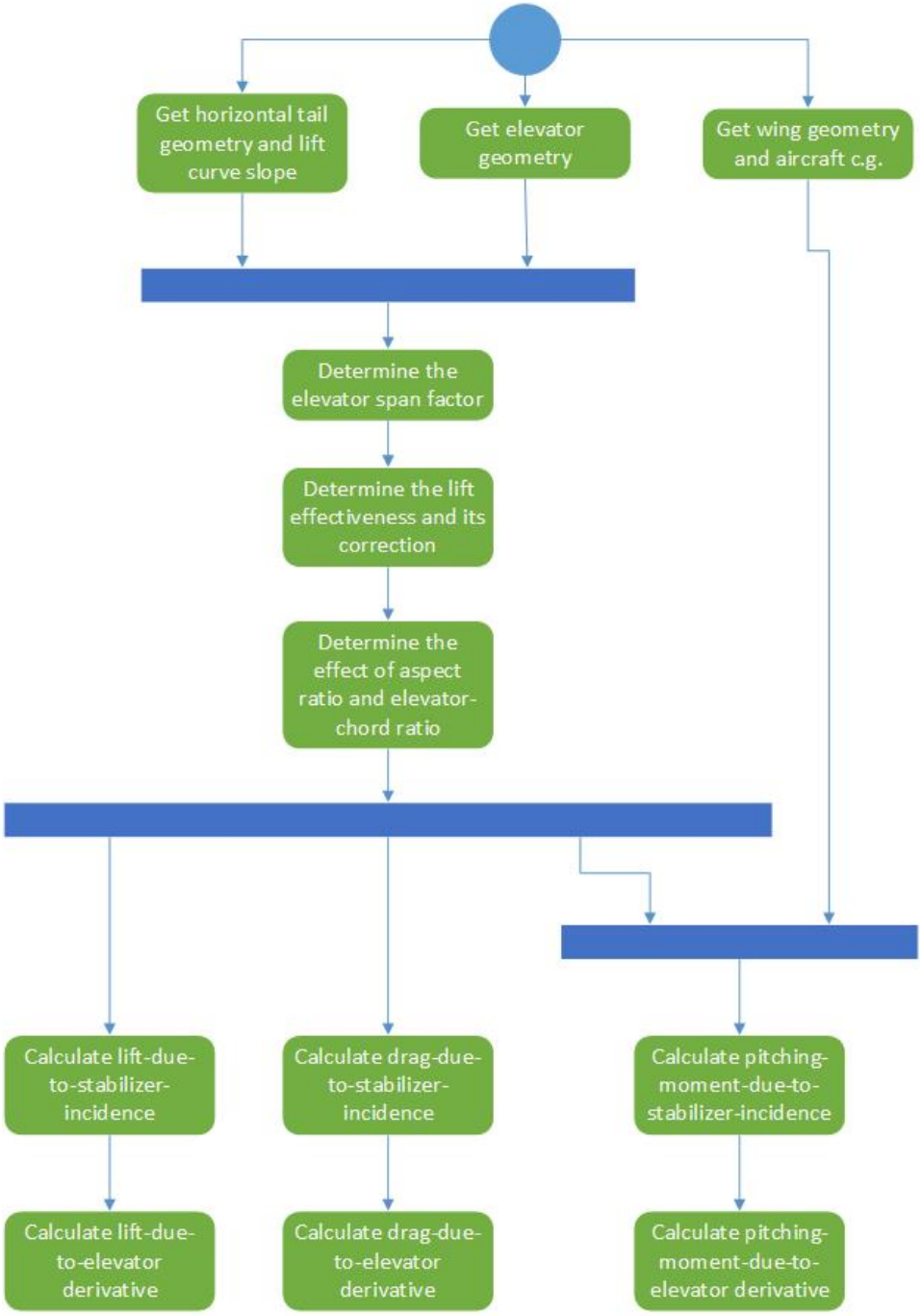

Figure 8.24: Activity diagram of control derivatives due to elevator deflection estimation

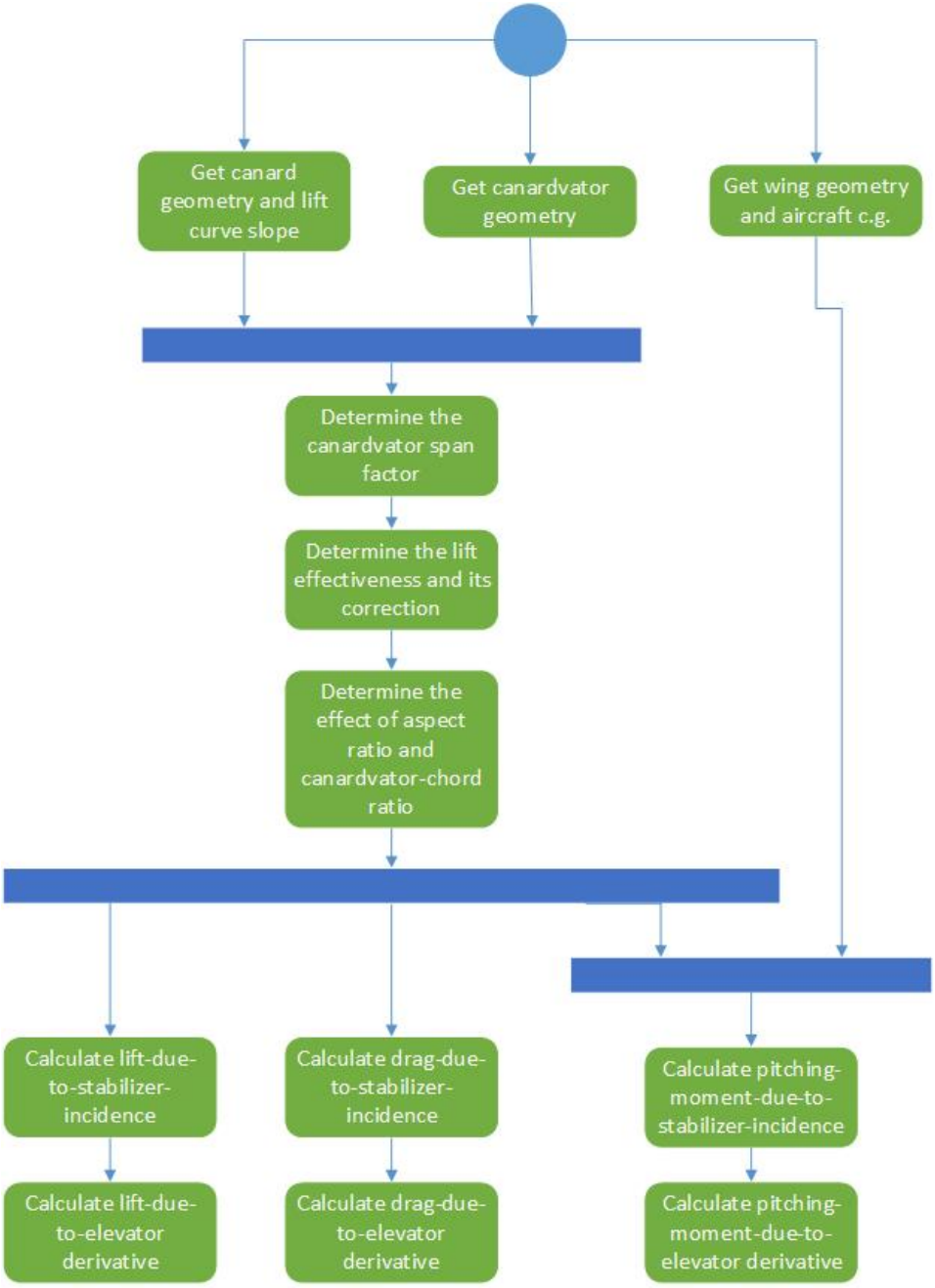

Figure 8.25: Activity diagram of control derivatives due to canardvator deflection estimation

9

Implementation in Flight Mechanics Toolbox

In the scope of this thesis outputs of implemented methods in Initiator are used as inputs in another in-house tool Flight Mechanics Toolbox to obtain handling qualities. Hence in this chapter, the principle of FMT is covered. The adjustments that are made for the examined study cases are briefly explained.

9.1. Flight Mechanics Toolbox Overview

In order to observe the flight dynamics of an aircraft in the FMT, several steps have to be followed. To begin with, a definition file has to be created for the aircraft that is to be examined. This file contains the assigned Simulink models which consider aerodynamics, control surfaces, propulsion system and AFCS with respect to the aircraft. Secondly, a data folder of the aircraft created by using the obtained results from Initiator. Creating the aircraft data file and the required inputs are explained briefly in Section 8.2. Last step before simulating the aircraft is to adjust the Module Library of the FMT which consists of several modules in relation with different disciplines. An adjustment according to the examined aircraft has to be made which is explained in Section 8.3.

Having created the aircraft definition file, obtained the required inputs from already and newly implemented modules in Initiator, and adapted the FMT modules considering the configuration of the aircraft, the flight dynamics analysis can be performed. The aircraft is trimmed with regard to desired conditions which is followed by gathering handling qualities results.

The procedure that is followed is shown in an activity diagram in Figure9.1.

9.2. Creating Aircraft Data File

In order to observe the flight dynamics of an aircraft in the Flight Mechanics Toolbox, a data folder has to be created which consists of aerodynamic, structure, engine and flight control surface data of the aircraft. Required aerodynamic data input are stability and control derivatives, which are calculated within the ControlStabilityDerivatives module in Initiator. The span, mean chord and the surface of the main wing are also inputs of aerodynamic data file and are gathered from Initiator. Structure data of aircraft includes the empty weight and the moment of inertia both of which are obtained from Initiator. Required empty weight is obtained from the Class2.5WeightEstimation module whilst the latter input is the result of the implemented InertiaEstimation module. Engine data file requires the location of the engine(s) from the c.g., maximum and minimum thrust level and the thrust vector angle, which are obtained from Initiator as well. Last data file relates to the flight control of the aircraft and hence control surfaces are defined here. Moreover, actuators data and saturation limits of the control surfaces are assigned in this file.

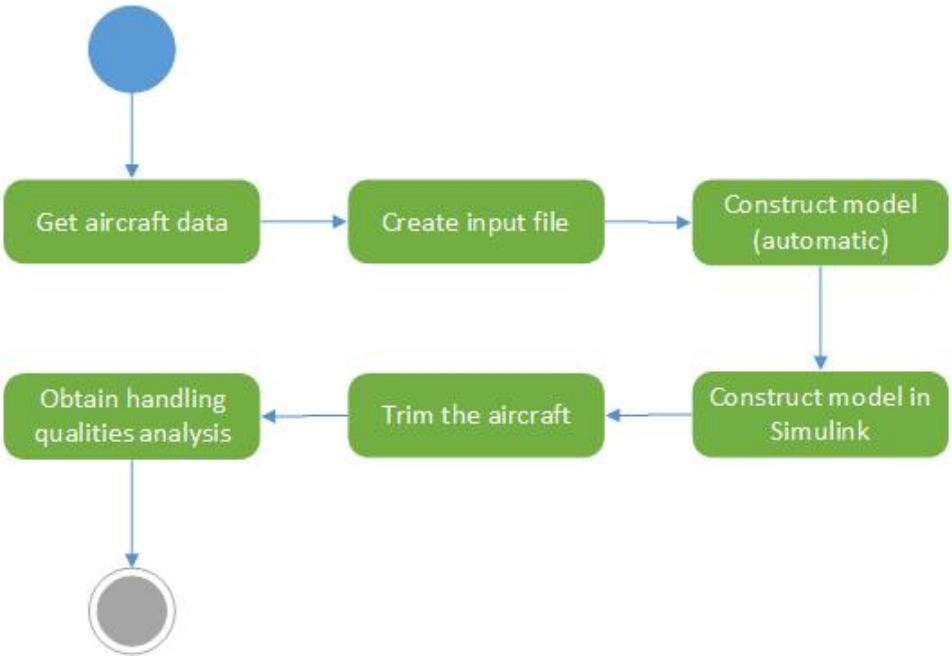

Figure 9.1: Activity diagram of FMT

9.3. ADJUSTING THE MODULE LIBRARY

Both in the **aeromodule** and **controlsurfacemodule** aerodynamic forces and moments are calculated by the use of stability and control derivatives respectively. The structure in Simulink is created according to the forces and moment equations in [15]. It should be noted that **controlsurfacemodule** has to be adapted according to the number of assigned control surfaces of the aircraft.

BIBLIOGRAPHY

[1] B. Chudoba, *Stability and control of conventional and unconventional aircraft configurations: a generic approach* (BoD–Books on Demand, 2001).

[2] G. E. Cooper and R. P. Harper Jr, *The use of pilot rating in the evaluation of aircraft handling qualities*, Tech. Rep. (DTIC Document, 1969).

[3] J. Roskam, *Airplane flight dynamics and automatic flight controls* (DARcorporation, 1995).

[4] C. Lanham, *Inertia Calculation Procedure for Preliminary Design*, Tech. Rep. (DTIC Document, 1979).

[5] *DATCOM 8.1 Aircraft Mass and Inertia*, Tech. Rep. (USAF).

[6] J. P. Pegram and W. A. Anemaat, *Preliminary estimation of airplane moments of inertia using CAD solid modeling*, Tech. Rep. (SAE Technical Paper, 2000).

[7] B. Stevens and F. Lewis, *Aircraft Control and Simulation* (Wiley, 2003).

[8] W. F. Phillips, *Mechanics of flight* (John Wiley & Sons, 2004).

[9] D. A. Caughey, *Introduction to aircraft stability and control course notes for m&ae 5070,* Sibley School of Mechanical & Aerospace Engineering, Cornell University, Ithaca, New York , 14853 (2011).

[10] R. Elmendorp, *Synthesis of novel aircraft concepts for future air travel*, Ph.D. thesis, TU Delft, Delft University of Technology (2014).

[11] R. Schmidt, *A semi-analytical weight estimation method for oval fuselages in novel aircraft configurations*, Ph.D. thesis, TU Delft, Delft University of Technology (2013).

[12] T. Pfeiffer, B. Nagel, D. Bohnke, A. Rizzi, and M. Voskuijl, *Implementation of a heterogeneous, variable-fidelity framework for flight mechanics analysis in preliminary aircraft design,* in *Proceedings of the 60 Deutscher Luft-und Raumfahrtkongress, 27-29 September 2011, Bremen, Duitsland* (DGLR, 2011).

[13] M. Voskuijl, J. de Klerk, and D. van Ginneken, *Flight mechanics modeling of the prandtlplane for conceptual and preliminary design,* in *Variational Analysis and Aerospace Engineering: Mathematical Challenges for Aerospace Design* (Springer, 2012) pp. 435–462.

[14] E. Torenbeek, *Synthesis of subsonic airplane design: an introduction to the preliminary design of subsonic general aviation and transport aircraft, with emphasis on layout, aerodynamic design, propulsion and performance* (Springer Science & Business Media, 2013).

[15] J. Roskam, *Airplane Design: Preliminary Calculation of Aerodynamic, Thrust and Power Characteristics. Determination of Stability, Control and Performance Characteristics: Far and Military Requirements. Airplane Cost Estimation, Design, Development, Manufacturing and Operating* (Roskam aviation and engineering corporation, 1990).

[16] W. Liu and W. A. Anemaat, *A refined method for wing weight estimation and a new method for wing center of gravity estimation,* in *AIAA Aviation Technology Integration and Operation Conference, AIAA*, Vol. 4371 (2013).

[17] M. Cook, *Flight Dynamics Principles: A Linear Systems Approach to Aircraft Stability and Control* (Elsevier Science, 2012).

[18] R. Heffley and W. Jewell, *Aircraft Handling Qualities Data*, Tech. Rep. (NASA contractor report, 1972).

[19] B. Etkin, *Dynamics of flight: stability and control* (John Wiley & Sons Australia, Limited, 1982).

[20] S. Gudmundsson, *General aviation aircraft design: applied methods and procedures* (Butterworth-Heinemann, 2013).

A

APPENDIX A

Geometry and masses of components are presented for each configuration as follows.

Table A.1: Fuselage geometry parameters of each configuration

Fuselage	Conventional	Canard	TSA
Length (m)	41.60	41.53	41.53
Mean width (m)	3.15	3.15	3.15
Mean height (m)	2.9	2.9	2.9
Mass (kg)	9862.4	7718.2	9569.3

Table A.2: Main wing geometry parameters of each configuration

Main Wing	Conventional	Canard	TSA
Span (m)	36.05	35.95	35.95
Root chord (m)	7.70	7.00	6.97
Taper ratio	[0.5739 0.3060]	[0.4952 0.3322]	[0.4931 0.3336]
Sweep angle (deg)	[24.48 24.48]	[-26.16 -26.19]	[26.16 26.16]
Dihedral angle (deg)	[6 6]	[6 6]	[0.33 0.33]
Position (m)	[14.95,0,-1.29]	[21.80,0,-1.29]	[18.9174 0 1.9385]
Mass (kg)	6800.3	5253.7	7358

Table A.4: Vertical stabilizer geometry parameters of each configuration

Vertical tail	Conventional	Canard	TSA
Span (m)	4.35	3.66	3.12
Root chord (m)	4.03	3.39	3.68
Taper ratio	0.35	0.35	0.7
Sweep angle (deg)	36.71	39.25	39.25
Dihedral angle (deg)	0	0	0
Position (m)	[36.32 0 1.29]	[36.89 0 1.29]	[36.61 0 1.29]
Mass (kg)	410.36	336.71	349.94

Table A.3: Horizontal lifting surface geometry

Horizontal Tail	Conventional	Canard	TSA
Span (m)	9.17	-	7.69
Root chord (m)	2.72	-	2.28
Taper ratio	0.35	-	0.35
Sweep angle (deg)	27.41	-	29.30
Dihedral angle (deg)	6	-	0.33
Position (m)	[37.64 0 1.29]	-	[39.43 0 4.42]
Mass	427.58	-	353.21
Canard			
Span (m)	-	10.73	10.90
Root chord (m)	-	2.96	3.01
Taper ratio	-	0.45	0.45
Sweep angle (deg)	-	23.55	23.55
Dihedral angle (deg)	-	0	-0.17
Position (m)	-	[6.2291 0 1.6154]	[4.1527 0 -1.6154]
Mass (kg)	-	534.52	524.71

Table A.5: Engine geometry parameters of each configuration

Engine	Conventional	Canard	TSA
Length (m)	3.52	3.30	3.30
Diameter (m)	1.93	1.70	1.75
Position	[15.1952 6.3093 -2.1097]	[29.0691 3.1746 0]	[19.6303 6.2918 0.6117]
	[15.1952 -6.3093 -2.1097]	[29.0691 -3.1746 0]	[19.6303 -6.2918 0.6117]
Mass (kg)	2656.4	2274.1	2274.1

B

APPENDIX B

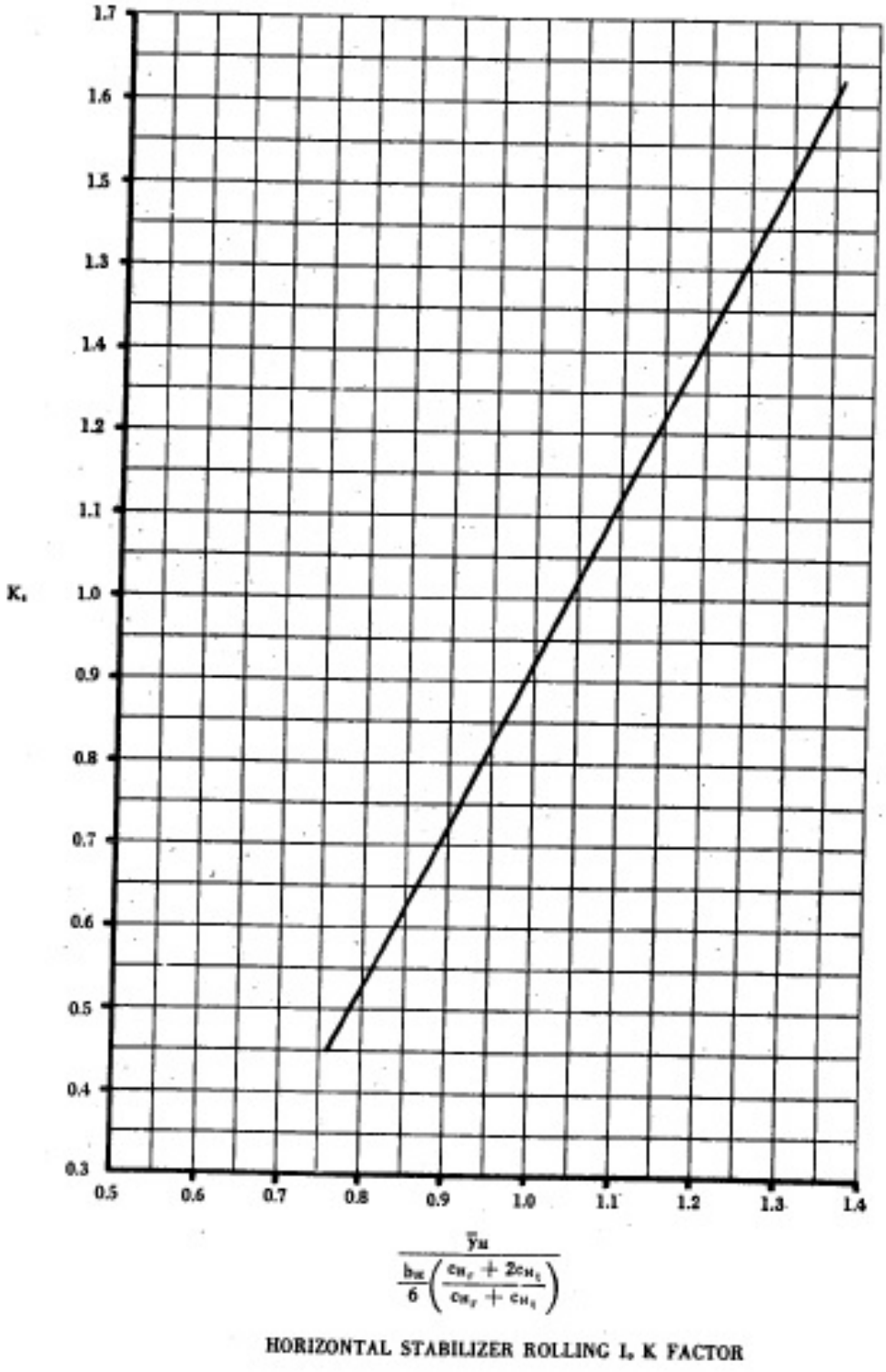

Figure B.1: Horizontal stabilizer rolling inertia K factor, [5]

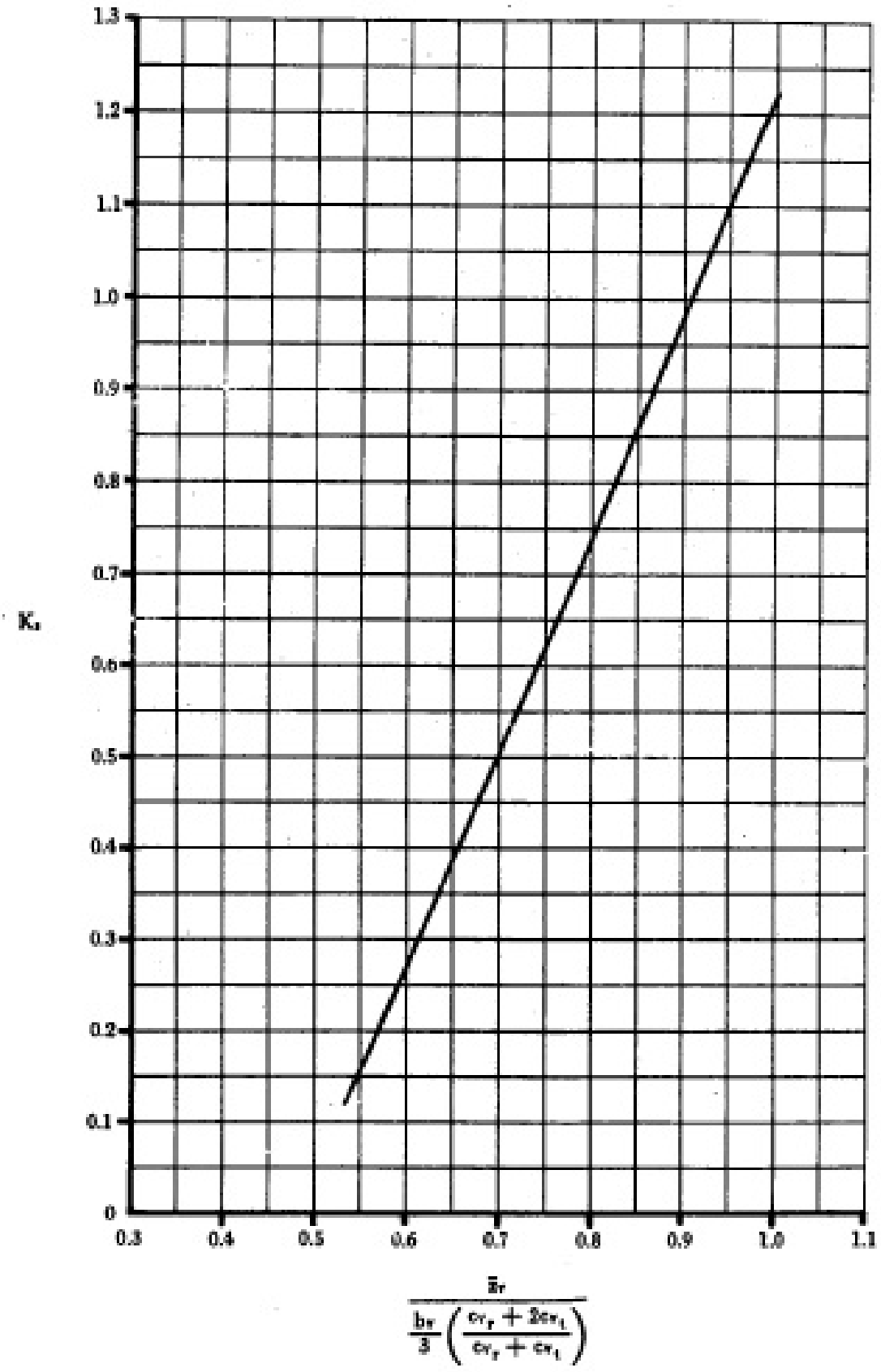

Figure B.2: Vertical stabilizer rolling inertia K factor, [5]